This is to certify that the

dissertation entitled

STRUCTURE FUNCTION RELATIONSHIPS OF METALLOPORPHYRINS

presented by

Brian Ward

has been accepted towards fulfillment
of the requirements for

Ph.D. degree in Chemistry

Chi K. Chang
Major professor

Date November 7, 1983

STRUCTURE FUNCTION RELATIONSHIPS OF METALLOPORPHYRINS

By

Brian Ward

A DISSERTATION

Submitted to
Michigan State University
in partial fulfillment of the requirements
for the degree of

Doctor of Philosophy

Department of Chemistry

1983

ABSTRACT

STRUCTURE FUNCTION RELATIONSHIPS OF METALLOPORPHYRINS

By

Brian Ward

The research presented here endeavors to shine light on specific questions in functional porphyrinoid biochemistry. There are three main topics of investigation:

Chromophore Selection: Comparative studies on CO kinetics and equilibrium constants have been carried out for iron porphyrins, chlorins and isobacteriochlorins. These studies in conjunction with ^{13}C NMR, N-methyl imidazole binding, autoxidation of Fe-O_2 and nitrite binding have lead to the conclusion that the iron hydroporphyrins are electron rich, and thus should be superior to iron porphyrin for the catalysis of substrate reductions.

Ligand Specificity: CO and O_2 binding to hemes with a steric encumbrance was studied (Chapter 2). The results indicate that if a steric effect can differentiate CO and O_2 it does so by association rate constant modulation. Studies of CO and O_2 bindings to Mb reconstituted with hemes lacking peripheral side groups (Chapter 3) suggest that peripheral methyl and vinyl groups play a cooperative role in orienting the heme in the protein and maintaining protein integrity. Synthetic hemes equipped with substituents of varying polarity on the ligand binding side were shown to have O_2

association and dissociation rates which correlated with a quadratic equation in the dipole moment of the local group (Chapter 4). Hydrogen bonding to oxy-heme was shown to affect only O_2 dissociation. CO kinetics did not correlate with distal polarity, but rather with the size of the distal substituent.

Chlorophyll optical shifts: The optical spectra of protonated Schiff's base porphyrin, chlorin and bacteriochlorin were characterized (Chapter 5). Related derivatives, solvent and counterion effects in conjunction with NMR and resonance Raman spectroscopies indicate that the spectral shifts associated with Schiff's base protonation are due to a combination of molecular symmetry and peripheral electron withdrawing effects.

To My Family and Friends

ACKNOWLEDGEMENTS

I would like to thank Professor C.K. Chang for his encouraging attitude which allowed me to pursue the work presented here. I am also very grateful to R. Young, C.B. Wang, S. Ebina and C.K. Chang for supplying synthetic materials and P.M. Callahan and G.T. Babcock for resonance Raman data and interpretation. I would also like to thank all of the above and M.A. Meador and P.J. Wagner for helpful discussions and friendship.

Appreciation is extended to the National Science Foundation, United States Department of Agriculture, Amway Corporation and Dow Chemical Company for financial support in the form of research assistantships.

TABLE OF CONTENTS

PAGE

PAGE

LIST OF TABLES

TABLE PAGE

LIST OF FIGURES

FIGURE PAGE

FIGURE PAGE

FIGURE PAGE

FIGURE PAGE

PART A

CHAPTER 1

COORDINATION REACTIONS OF IRON HYDROPORPHYRINS

Introduction

There are a number of heme proteins which do not utilize the ubiquitous protoheme as prosthetic group, and as such, the supposition is that nature chooses different hemes which are better than protoheme at providing a specific function. Among these are: cytochrome oxidase which contains two molecules of heme a per functional protein,[1] sulfite and assimilatory nitrite reductases which use siroheme as the prosthetic group[2] and a dissimilatory nitrite reductase which contains two heme c and two heme d[3] moieties. Cytochrome oxidase functions to reduce dioxygen to water,[1] sulfite and assimilatory nitrite reductases reduce sulfite to H_2S[4] and nitrite to ammonia,[2] while in the absence of O_2 dissimilatory nitrite reductase reduces NO_2^- to nitrous oxide or dinitrogen.[3b-d] In the presence of molecular oxygen dissimilitory nitrite reductase functions as an oxidase, reducing O_2 to H_2O. In all three systems there is substantial evidence that ligand binding and activation

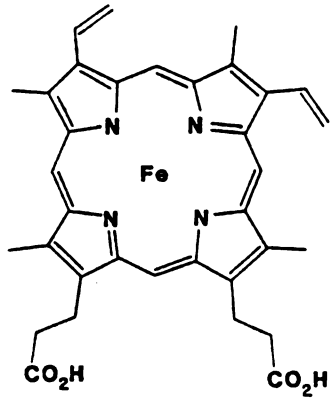

Protoheme

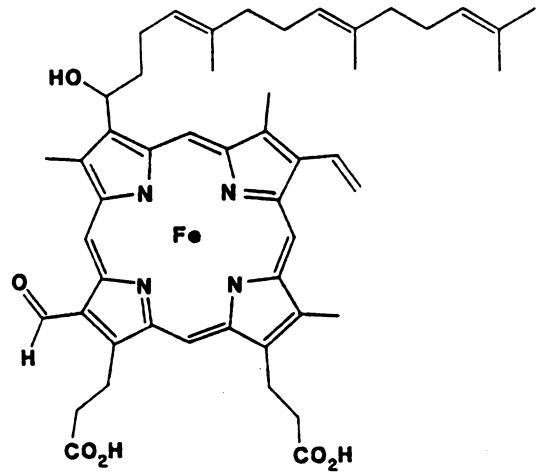

Heme a

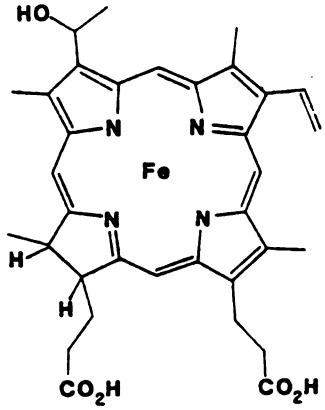

Heme d
(TENTATIVE STRUCTURE)

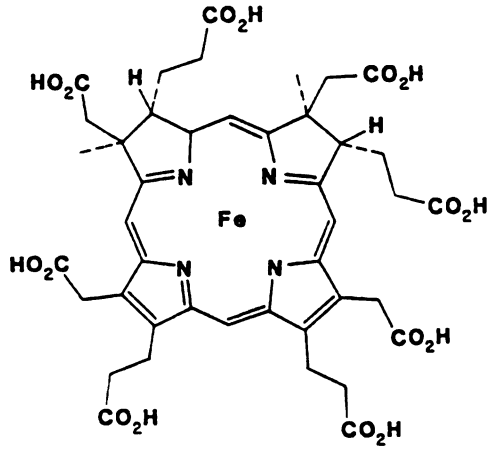

Siroheme

occur at the unique heme site. Since cytochrome oxidase is a much studied system further discussion of it are not presented.

An obvious method of investigation to probe what seems to be an obligatory role of these unique hemes is to synthesize model macrocycles (presented elsewhere[5,6]) and study the physicochemical properties of these in comparison with porphyrin model compounds.[7] Since iron chlorins (heme d analogs) and iron isobacteriochlorins (siroheme analogs) are β position reduced porphyrins, a better understanding of their properties should result from a comparison with porphyrins on ligand binding with various peripheral substituents. Therefore, this work centers on cis electronic effects of ligand binding to iron porphyrins and hydroporphyrins.

We and others[8] have encountered difficulty in reducing Fe^{III} chlorins to the ferrous state, as a result, a novel reduction method was developed.[9] This method and its implications to previous reports of hemeprotein photoreduction are given as a supplement to this chapter.

In view of the multielectron catalytic processes for which hydrohemes are employed in nature, investigations into the redox chemistry of these hemes is necessary and can be found elsewhere.[7,10]

Results and Discussion

A property of hydro-hemes which possibly makes them superior to iron porphyrins for the roles they play in nature is their coordination chemistry. To investigate this, the binding parameters of CO to four coordinate and five coordinate hydro-hemes have been investigated and compared with porphyrin models containing different peripheral substituents. The merits of this approach are twofold. It provides data for these hemes which might reveal any peculiarities in their binding behavior of CO (which may infer effects on substrate binding). Also, any variations in CO binding found for these hemes when compared to porphyrins with various peripheral substituents puts a perspective on the variation.

Four Coordinate Hemes:

Carbon monoxide binding to four coordinate ferrous heme was studied in toluene. Evidence for a four-coordinate heme under these conditions is provided by the optical spectrum of Fe^{II}Etioporphyrin I. As shown in Figure 1-1, the Soret region displays the splitting features typical of four-coordinate ferrous heme,[11] which are not present in coordinating solvents (i.e., THF Figure 1-1). This insures that CO association and dissociation occur by a direct pathway. This is of importance since in coordinating solvents (coordinating

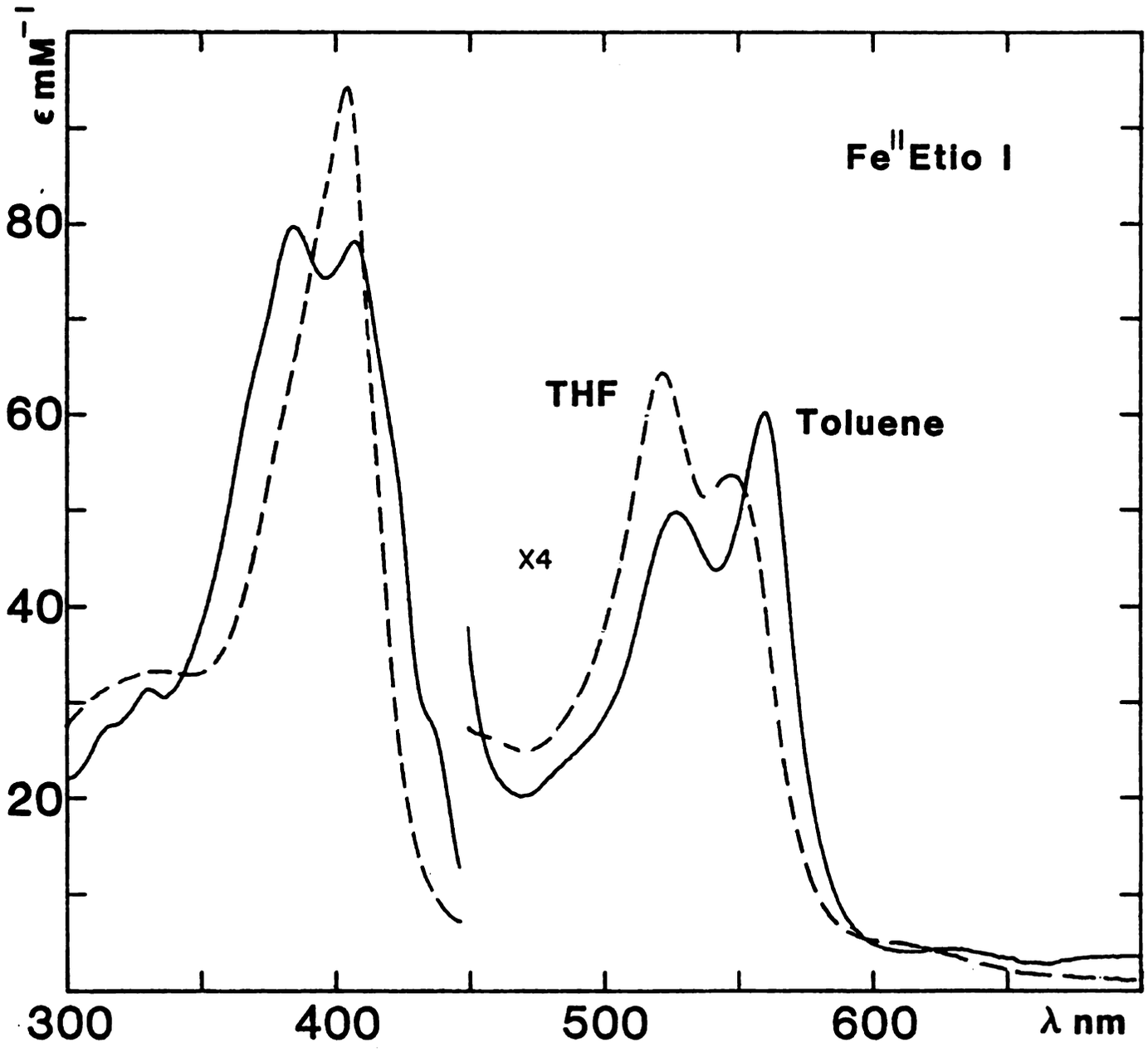

Figure 1-1. Absorption spectra of Fe^{II}etioporphyrin I.
Toluene ———; THF -----.

ligands) CO binding may be controlled by competing equilibria, which complicates binding data:

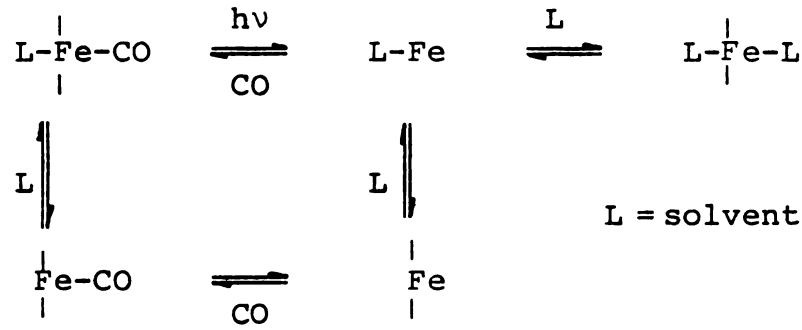

Four coordinate ferrous heme reacts with CO in two successive steps.[12] At moderate CO pressures (generally less than 200 torr) the five coordinate mono CO adduct predominates and at high pressures the bis adduct, according to:

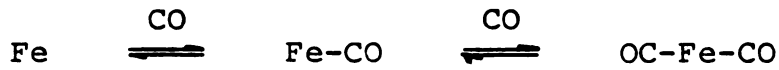

The kinetic and affinity constants for the first step and the affinity constant for the second step are contained in Table 1-1. To insure the observed CO recombination rates for all compounds were indeed due to mono carbonyl heme formation, CO pressures were used which should lead to little or no bis adduct. The reaction was monitored in the Soret region of the mono adduct (where mono and bis carbonyl heme are spectrally distinct, Table 1-2 and Figure 1-2). Formation of $Fe(CO)_2$ would have resulted in biphasic kinetic behavior. A slow phase was observed for Fe 2,3-DMeOEiBC which was more pronounced at higher CO

Table 1-1. CO Binding Constants to 4-Coordinate Hemes (20-22 °C).[a,b]

Heme	1' (M^{-1} s^{-1})	1 (s^{-1})	$P_{\frac{1}{2}}^{CO}$ (torr)	$P_{\frac{1}{2}}^{(CO)_2}$ (torr)
2,3-DMeOEiBc	14.0×10^8	1.1×10^4	0.8	80
MeOEC	7.6×10^8	1.2×10^4	1.6	450
Etio I	4.9×10^8	1.1×10^4	2.5	550
MeSO DME[e]	5.0×10^8[c]			
Deutero DME	5.7×10^8[c]	1.3×10^4[c]	2.2	540[d]
PPIX DME[e]	5.4×10^8	1.4×10^4	2.5[c,d]	580
2,4-Ac_2Deutero	7.6×10^8	1.2×10^4	1.6	550
T(p-OMe)PP	8.8×10^8	3.1×10^4	3.5	1270
TPP	6.1×10^8	2.7×10^4	4.5(1.6)[g]	1080(750)[g]
T(F_5)PP	0.7×10^8[f]	5.0×10^4[f]	71	650

[a]Toluene; [b]Measured a minimum of 2 times (estimated error ±10%); [c]Reference 12a; [d]Reference 12b; [e]Benzene; [f]Due to the low affinity, high CO concentrations were necessary resulting in pseudo-first order rate constants approaching detection limits; [g]Reference 14.

Table 1-2. Absorption Spectra of Hemes.[a]

Heme	λ_{max} (ε mM^{-1}) nm			
	$Fe^{III}Cl$	Fe^{II}	FeCO	OCFeCO
2,3-DMeOEiBC	380(58),601(26)	387(40),619(26)	377(41),591(28)	393(42),597(36)
MeOEC	378(89),605(17)	395(67),620(18)	393(77),615(23)	411(78),617(42)
Etio I	376(105),506(11) 534(12)	386(80),406(78) 527(13),559(15)	391(220),546(10)	408(152),537(8.6) 568(5.9)
PPIXDME	386(94),508(9) 540(9)	407(75),536(12) 567(15)	400(155),555(22)	418(130),545(16) 577(11)
2,4-Ac_2deutero	413(50),582(7)	417(59),540(10) 570(11)	413(69),561(16)	419(51),558(13)
T(p-OMe)PP	425(123),510(15)	421(120),445(70) 530(12)	413(230),520(14)	425(176),554(8) 594(6)
TPP	416(103),507(12)	418(100),442(54) 525(10)	409(205),517(13)	433(162),551(10) 590(5)
T(F_5)PP	410(100),500(11)	412(96),530(10) 560(9)	409(145),548(6)	417(192),544(7)

[a]Toluene.

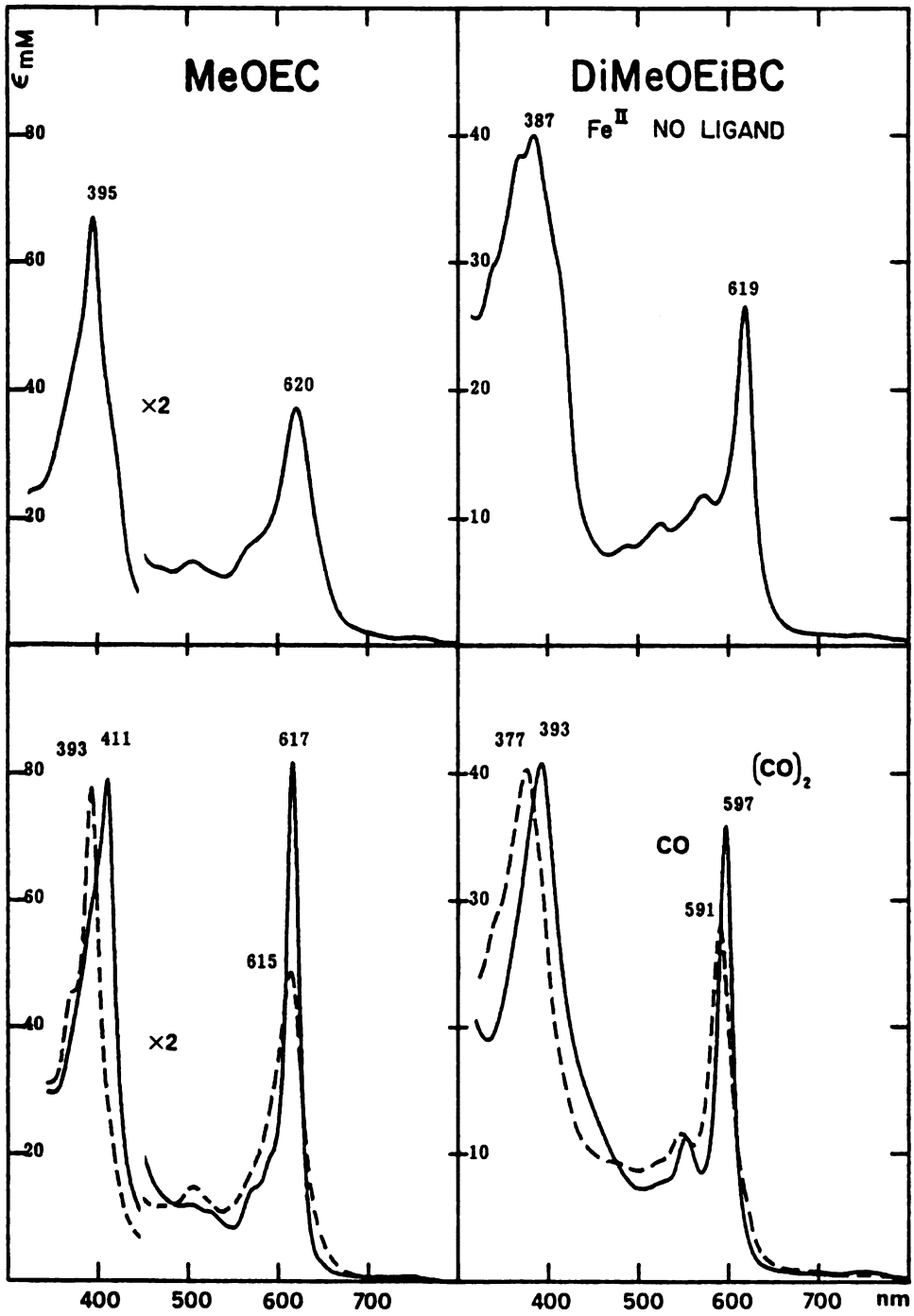

Figure 1-2. Absorption spectra of FeMeOEC (left) and FeDMeOEiBC (right). Fe^{II} (top), Fe-CO (——) and OC-Fe-CO (----).

concentrations. The observed rates of CO recombination were linear with CO concentration.

As shown in Table 1-1 variations in $P_{\frac{1}{2}}^{CO}$ are primarily the result of association rate constant modulation. In coordinating solvents Smith[13a] and Sono et al.[13b] found that ℓ' decreased with increasing electron withdrawing capability of the peripheral substituent (2,4-diformal < 2(4)-formal-4(2)-vinyl < proto < deutero < meso). These results are in direct contradiction to those presented here (2,4-diacetyl-deutero > deutero > proto > etio = meso). Since the rate constants measured by the above authors are approximately an order of magnitude less than those in toluene indicates that CO binding in coordinating solvents is controlled by solvent coordination processes. It is not known which of the equilibria is of major importance.

The trend that CO association rates increase with increased electron withdrawing capability of porphyrin β substituents is reversed for the porphyrin-chlorin-isobacteriochlorin series. The essential difference between these two series of compounds is that the substituted porphyrin's electronic effect is attributable to resonance while that of pyrrole saturation is inductive. Since the phenyl ring of tetraphenyl porphyrins is approximately perpendicular to the porphyrin plane, substituents on the phenyl ring should primarily exert an inductive electronic effect. Indeed, CO association rates increase with increasing electron donating ability of phenyl

substitution (T(p-OMe)PP > TPP > T(F_5)PP). These effects are summarized in Figure 1-3.

The trends observed for first CO binding do not apply to $Fe(CO)_2$ formation. For the porphyrin-chlorin-isobacteriochlorin series the second CO binds more strongly (affinity constant decreases) with pyrrole saturation. The TPP series shows the opposite behavior (T(F_5)PP > TPP > T(p-OMe)PP) and the β-substituted hemes show little or no effect. These results indicate either the trends observed for Fe-CO are coincidental or $Fe(CO)_2$ formation is dependent on a <u>trans</u> effect which is peculiar to the type of macrocycle. Further discussion of this is deferred to the section on imidazole binding.

Table 1-2 contains the infrared stretching frequencies of mono and bis adducts of the above hemes in CH_2Cl_2. The frequencies assigned to mono and bis CO complexes were shown by the dependence of the relative intensity of their absorption bands as a function of CO pressure. At low CO pressures a peak assigned to Fe-CO appeared at ca. 1950-1970 cm^{-1}. At higher CO pressures the monocarbonyl heme peak was replaced by an $Fe(CO)_2$ vibration at 2010-2040 cm^{-1}, in agreement with previously reported frequencies.[14]

The stretching frequency observed for CO bound heme results from populating COπ* orbitals with metal dπ electrons reducing ν_{CO} from the unbound value of 2143 cm^{-1}. ν_{CO} of the bis adduct is higher than FeCO due to

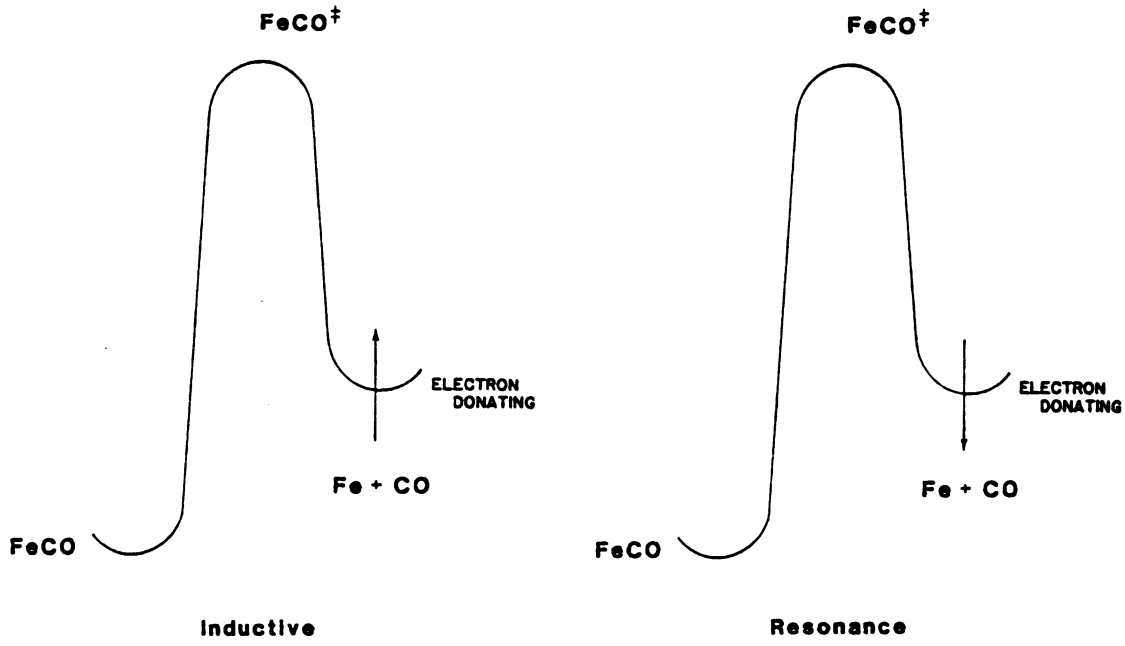

Figure 1-3. Reaction coordinates for reaction of CO with four coordinate hemes.

competition for metal $d\pi$ electrons. If competition for metal $d\pi$ electrons were independent of the ring system, then $\Delta\nu_{CO}$ should be constant throughout the 3 series. There is little variation (± 3 cm^{-1}) in $\Delta\nu_{CO}$ except for the TPP's. Previous work has revealed little correlation between ν_{CO} and CO binding data.[15] However, $\Delta\nu_{CO}$ for the TPP's stands alone, suggesting that this system may be subject to an electronic or trans effect not present in the others.

Five Coordinate Chelated Hemes

CO binding was studied in 2.5% aqueous myristyltrimethylammonium bromide (MTAB) and benzene at ambient temperature. Table 1-4 contains the binding parameters for CO binding to N-alkylimidazole chelated isobacteriochlorin (iBC), chlorin (Chl) and β-substituted hemes. (See Fig. 1-4 for structures of Chl and iBC.) Variations in the kinetic and affinity constants are relatively small for the chelated relative to the four coordinate hemes. In fact, in benzene ℓ' for β-substituted hemes is within experimental error of 1.1×10^7 M^{-1} s^{-1}.[15c] The association rate under similar conditions for the chelated chlorin is 2.0×10^7 M^{-1} s^{-1}. These results indicate that occupation of the fifth coordination site by imidazole far outweigh effects caused by substituents or ring saturation. This is evidenced by comparing the data of four-coordinate

Table 1-3. ^{13}C Chemical Shifts of CO and ν_{CO} of CO-Hemes.

Heme / Ligation	^{13}CO[a] (Hz rel.TMS) Im,CO	ν_{CO}[b] (cm^{-1}) Im,CO	$\Delta\nu_{IM-CO}$[c] (cm^{-1}) —,CO	ν_{CO}[c] (cm^{-1}) CO,CO	$\Delta\nu_{(CO)_2-(CO)}$
2,3-DMeOEiBC	4292	1957	1951	2012	61
MeOEC	4196.6	1956	1951	2012	61
Etio I	4113.9	1953	1949	2010	61
PPIX DME	4100.5[d]	1954	1948	2012	64
2,4-Ac_2Deutero	4081.0[d]	1959	1955	2018	63
T(p-OMe)PP	4090.5	1965	1960	2020	60
TPP	4087.0	1973	—[e]	—[e]	69[f,g]
T(F_5)PP	4016.3	1994	1972	2044	72

[a]0.1 M N-Methyl imidazole/$CDCl_3$; [b]0.1 M N-Methyl imidazole/CH_2Cl_2; [c]CH_2Cl_2; [d]Reference 15e; [e]insoluble; [f]in Nujol mull ν_{CO} 1973 (—,CO) and 2042 (CO,CO) [g]Reference 14.

Table 1-4. CO Binding Constants to Chelated Hemes (20-22°C).[a]

Chelated Heme	l' (M^{-1} s^{-1})	l (s^{-1})	$P_{\frac{1}{2}}^{CO}$ (torr)
iBC[b]	3.0×10^7	0.03[d]	0.00065
Chl[b]	2.0×10^7	0.025[d]	0.00093
Meso[c]	8.2×10^6	0.014[e]	0.0013
Proto[c]	3.6×10^6	0.005[e]	0.0010
2,4-Diacetyl[c]	5.6×10^6	0.0085[e]	0.0010

[a]2% aqueous MTAB.

[b]This work, pH 7.0 potassium phosphate (0.1 M).

[c]Reference 15c, pH 7.3 potassium phosphate (0.05-0.1 M).

[d]Calculated from $L = \ell'/\ell$.

[e]Measured by stopped flow.

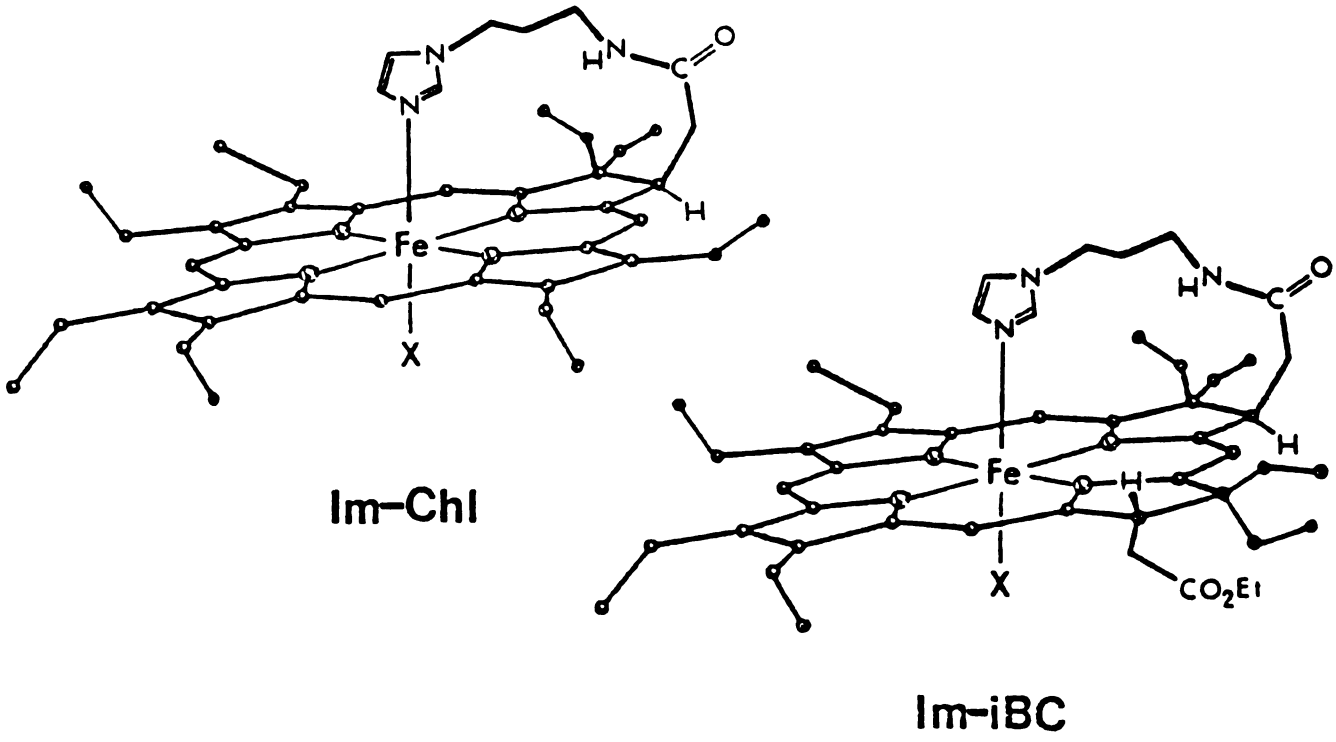

Figure 1-4. Structures of chelated chlorin and isobacteriochlorin.

(Table 1-1) to that in Table 1-4. Five coordinate imidazole hemes bind CO 10-100 times slower than four coordinate, while in general the cis effect allows for less than an order of magnitude variation. Similarly, CO dissociation decreases ca. 10^6 for the imidazole chelates vs. the vacant trans ligand CO complexes; which displayed little variation. Therefore, the presence of imidazole in the fifth coordination site has the effect of dampening out any electronic effect on CO binding.

The CO stretching frequencies of N-methyl imidazole-CO hemes are given in Table 1-3. As with CO binding to four-coordinate heme, there appears little correlation between ν_{CO} and CO binding behavior.[15] According to the synergistic interpretation of ν_{CO} on the binding nature of M-CO complexes the extent of π backbonding parallels the Fe-C bond strength predicting the order: Etio $\approx$ proto $\geq$ MeOEC $\approx$ 2,3-DMeOEiBC $\geq$ 2,4-Diacetyldeutero > T(p-OMe)PP > TPP > T(F_5)PP. Unfortunately, it is not possible to study CO binding to Im-FeTPP's, since covalently attached imidazoles are not available with these hemes and addition of external base results in competion between CO and base.

The chemical shift of a ^{13}C nucleus is approximated by the sum of a diamagnetic and paramagnetic screening tensor.[16] For diamagnetic screening an increase in electron density causes an upfield shift, while for paramagnetic screening increased electron density causes a downfield shift. In general, for transition metal

carbonyl complexes it has been found that electron donation to the metal results in a downfield shift of the carbonyl carbon resonance. Thus, from theoretical[17] and experimental[16] considerations paramagnetic screening dominates. Table 1-3 contains the ^{13}C NMR resonant frequencies relative to TMS for N-methyl imidazole ^{13}CO hemes. If as with other metal carbonyl complexes the paramagnetic screening tensor dominates, then the electron richness of the carbonyl carbon increases in the order: $T(F_5)PP$ < 2,4-diacetyldeutero < TPP < T(p-OMe)PP < proto < etio < MeOEC < 2,3-DMeOEiBC.

Gansow and others have found that ν_{CO} varies linearly with $\delta_{^{13}CO}$ for a variety of transition metal complexes.[16] These results are usually interpreted as indicating that the increased electron density on C is due to increased backbonding in M-CO. Figure 1-5 shows the orbital overlap for M-CO bonding. An empty metal d_σ orbital accepts electron density from the filled C_σ orbital and a filled metal $d\pi$ orbital donates electron density to a $CO\pi^*$ orbital. From Figure 1-6 (solid) there appears little correlation between ^{13}C resonant frequency and ν_{CO}. The dashed curve represents a correlation in which the extent of backbonding reaches a saturation point, that is, ν_{CO} varies linearly for the TPP's (squares), octa-alkyl hemes (triangles) are intermediate and the extent of backbonding no longer changes upon pyrrole saturation (circles). Whether one should expect compounds with

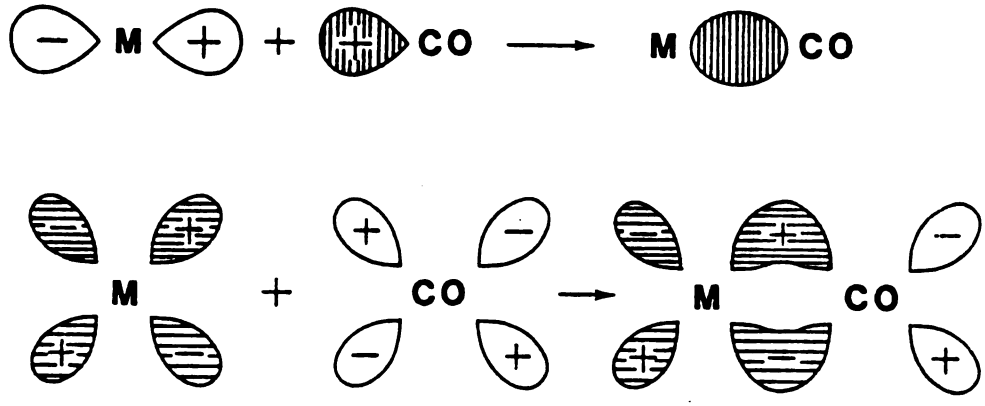

Figure 1-5. σ (upper) and π (lower) contributions to M-CO bonding.

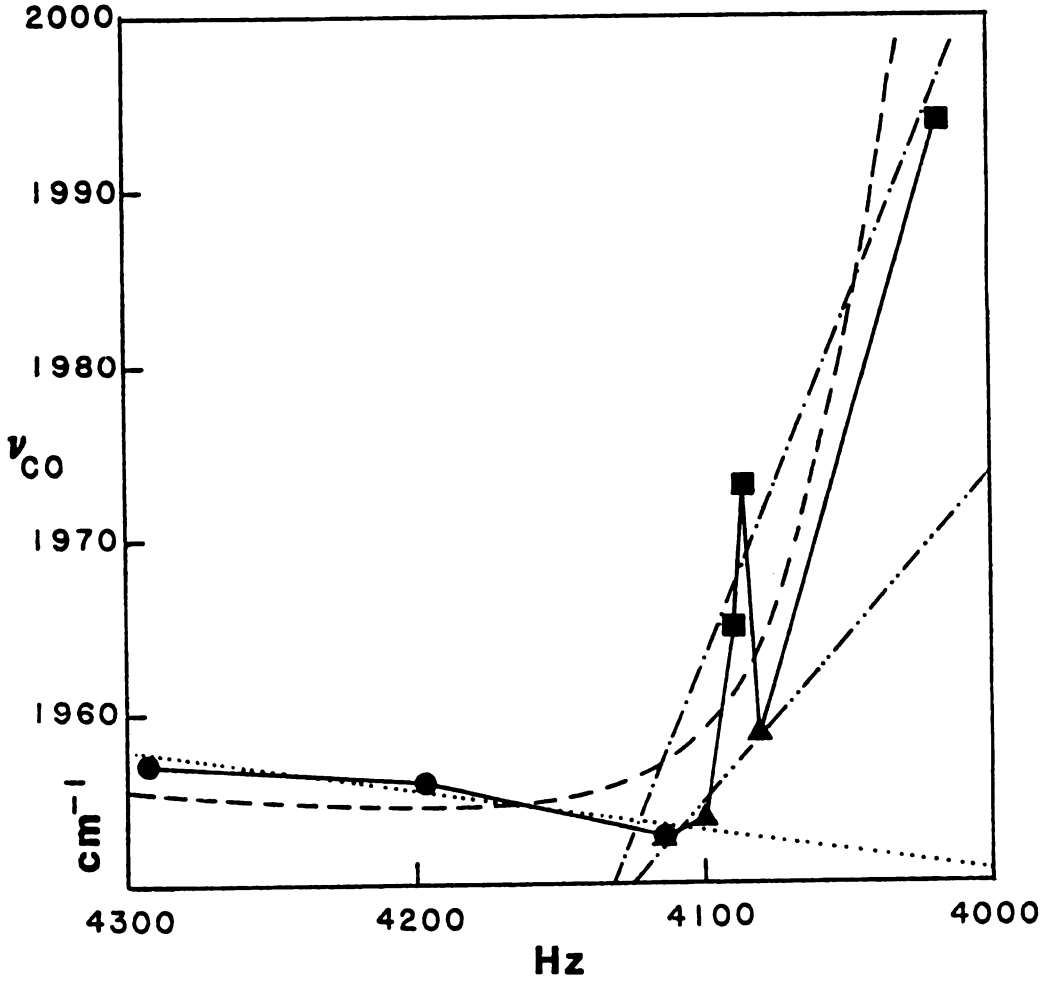

Figure 1-6. ^{13}C NMR resonant frequency vs. ν_{CO} for N-Methyl Imidazole-CO hemes; TPP's ; β-substituted porphyrins ; Hydrohemes . Solid line traces Fe-CO in order of decreasing electron density (left to right) from ^{13}C NMR data. Dashed curve represents a leveling of π-backbonding. (Possible) linear correlations dependent on macrocycle: TPP's -•-; OEP's -••-; and hydrohemes •••••.

inductive vs. resonance effects or TPP's vs. octa-alkyl hemes should lie on the same line is unclear. For the three classes of compounds Figure 1-6 also shows possible linear correlations between ν_{CO} and ^{13}C NMR data. The number of compounds studied here does not permit substantiation of either possibility. Mesomeric effects from N-methyl imidazole may also have pronounced effects. However, for the porphyrin-chlorin-isobacteriochlorin series the relatively insignificant variations in ν_{CO}, which should be most sensitive to π effects, and the large changes of the ^{13}C resonances imply the increased electron density on CO is primarily the result of σ effects.

From these results it should be of interest to determine if there is a correlation between ν_{CO} and ^{13}C chemical shift. This could be examined by characterizing a number of "OEP's" and TPP's with substituents which primarily influence electron densities through resonance and inductive effects. Such studies should also include the use of pyridine as axial base so as to offset any mesomeric effects which might be caused by imidazole.

Imidazole Binding

Ferrous hemes bind nitrogenous bases (e.g. imidazole, pyridine) in two successive steps according to:[18]

$$\begin{array}{c}|\\ Fe\\ |\end{array} \xrightleftharpoons{K_1} \begin{array}{c}|\\ Fe\text{-}B\\ |\end{array} \xrightleftharpoons{K_2} B\text{-}Fe\text{-}B$$

Table 1-5. N-Methyl Imidazole Binding Constants to Ferrous Hemes (20-22°C).

Heme	K_1 (M^{-1})	K_2 (M^{-1})
Deuteroheme[a,b]	5×10^3	7×10^4
FeMeOEC[c,d]	2.5×10^4	6×10^4
Fe-2,3-DMeOEiBC[c,d]	3.5×10^4	2×10^3

[a]Reference 12a; [b]Benzene; [c]This work; [d]Toluene.

Table 1-5 contains the binding constants to Fe^{II}deuteroporphyrin, MeOEC and 2,3-DMeOiBC. Deuteroheme was measured in benzene,[15c] the chlorin and iBC in toluene and reduced from the ferric chloride by the photochemical method.[9] K_1 and K_2 were measured by titration of the ferrous chlorin and iBC. K_2 for the chlorin was further verified by CO vs. N-methyl imidazole competition kinetics with the chelated compound according to:

$$\text{Im-Fe-CO} \underset{\text{CO}}{\overset{h\nu}{\rightleftharpoons}} \text{Im-Fe} \overset{K_2}{\rightleftharpoons} \text{Im-Fe-Im}$$

K_2 was calculated from:

$$1/R = 1/k_{off} + K_2[\text{Im}]/\ell'[\text{CO}]$$

where R is the carbonylated heme regeneration rate, k_{off} (not given) is the imidazole dissociation rate constant and $\ell'[\text{CO}]$ was the pseudo-first order CO recombination rate before introduction of base. K_2 measured by both methods

were within ±5%. K_2 for the iBC could not be similarly verified since the heme was photochemically unstable in the presence of excess N-methyl imidazole.

For ferrous porphyrins K_2 is generally larger than K_1; hence, Fe-B cannot accumulate in solution. As is apparent from Table 1-5 pyrrole ring saturation results in increasing K_1 and decreasing K_2. For the isobacteriochlorin it is possible to prepare a pentacoordinate imidazole complex with externally added base. The reason for this imidazole binding behavior is believed to be the result of the electron richness of the hydroheme iron. When imidazole binds to ferrous heme the iron becomes more electron rich from a combination of σ and π effects (Figure 1-7). Apparently a saturation point is reached for the hydrohemes and binding a second imidazole becomes less favorable. Similar arguments have been used to explain the inability of ferrous heme to form six-coordinate bis thiolate complexes.[15b,19] The opposite situation can be envisaged as occurring for CO binding to Fe^{II}TPP's. The inductive effect of the phenyl ring makes them electron deficient relative to octa-alkyl type porphyrins.[20] Thus, as the TPP becomes more electron withdrawing the first CO is bound more difficultly (T(p-OMe)PP > TPP > T(F_5)PP). Sigma donation from the first CO then increases the electron donating ability of the iron and allows the second CO to bind more easily (T(F_5)PP > TPP > T(p-OMe)PP). The inherent electron

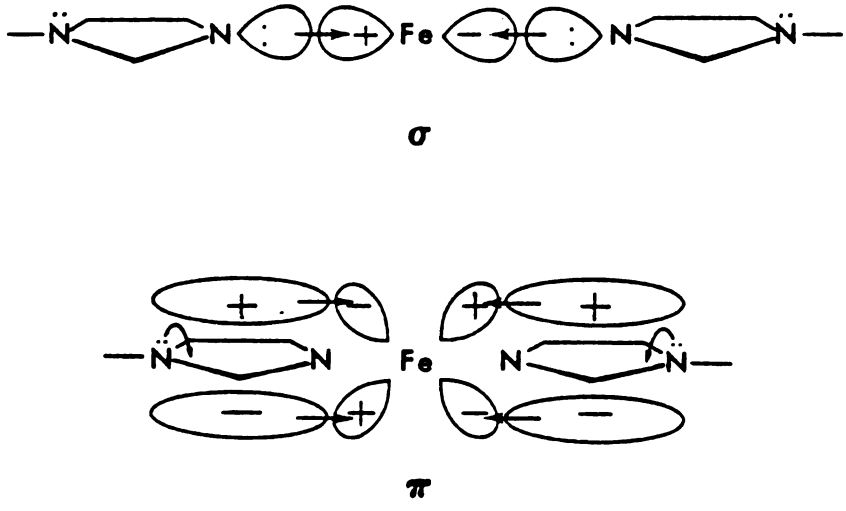

Figure 1-7. σ (upper) and π (lower) donation to Fe from coordinated imidazole.

richness of hydrohemes allow the second CO to bind more easily. It would seem that octa-alkyl type hemes are electronically neutral. That is, $Fe(CO)_2$ formation is not altered by either <u>cis</u> electronic effects or <u>trans</u> CO effects.

Oxygen Binding

Oxygen binding to unprotected hemes can be conveniently studied by kinetic CO replacement[21] (below) or at low temperatures.[22]

$$\text{B-Fe}^{II}\text{-CO} \underset{\text{CO}}{\overset{h\nu}{\rightleftharpoons}} \text{B-Fe}^{II} \underset{-O_2}{\overset{O_2}{\rightleftharpoons}} \text{B-Fe}^{II}\text{-}O_2$$

Reliable O_2 binding constants have not been obtained for either the chelated chlorin or iBC. Flashing off CO in the presence of O_2 resulted in facile oxidation of the heme. The hemes were found to be completely oxidized within a relatively few flashes. Thus, it was not possible to determine whether the observed kinetic traces were due to O_2 binding or oxidation.

At -45°C in 5% H_2O/DMF, N-methyl imidazole Fe^{II}-O_2 porphyrins are almost indefinitely stable.[22] Under the same conditions oxy MeOEC had a half life of approximately 10 minutes (spectrum of MeIm-Fe-O_2MeOEC, Figure 1-8). Autoxidation of oxy-iBC was so rapid that attempts at measuring the optical spectrum were unsuccessful. These

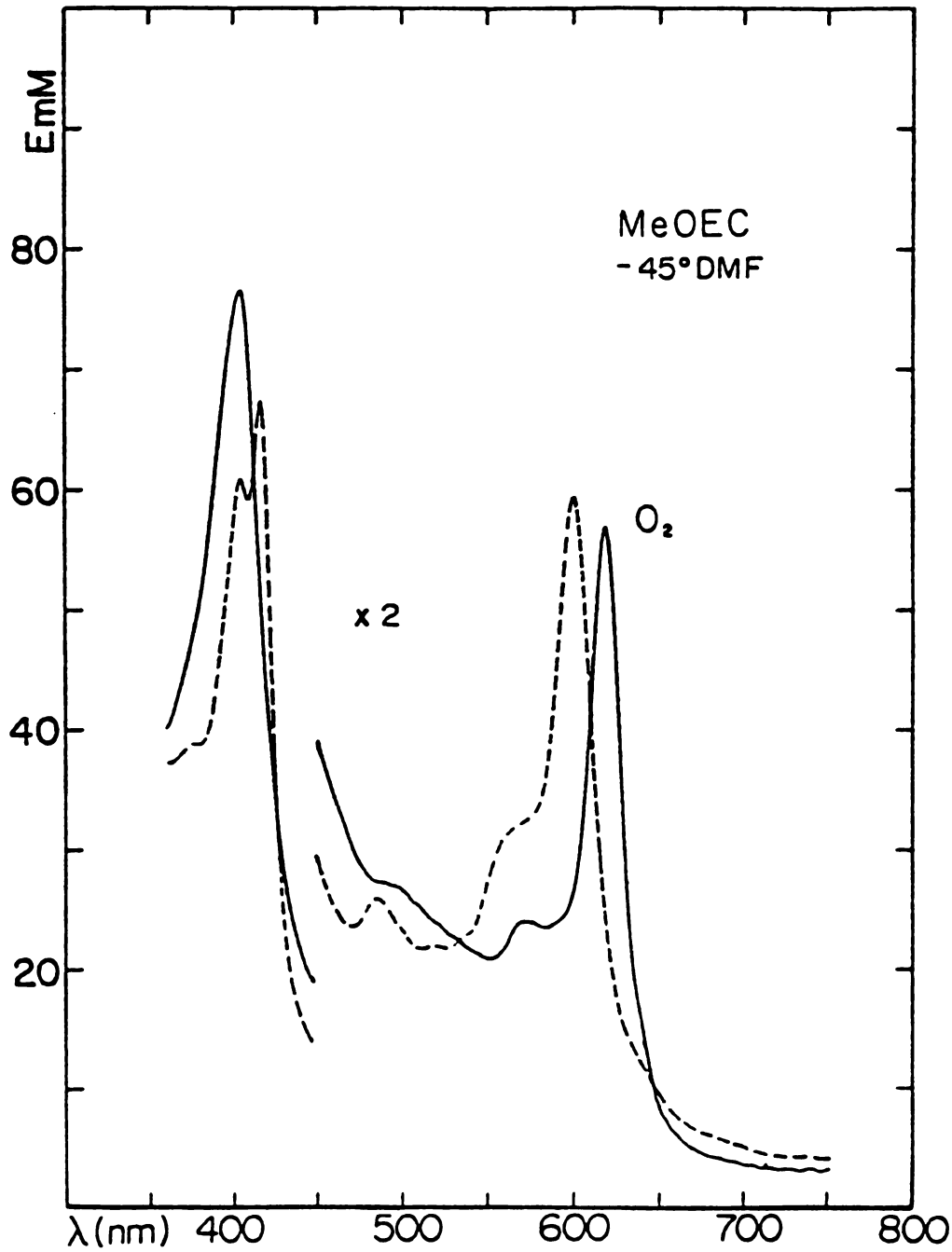

Figure 1-8. Absorption spectra of Fe^{II}MeOEC in 5% H_2O/DMF containing excess N-Methyl Imidazole (-45°C); Im-Fe-Im ----, Im-Fe-O_2 ——. The oxyheme has a half life of approximately 10 min.

results are not totally surprising since stability of oxy-heme decreases as the macrocycle becomes electron rich.[23]

Nitrite Binding

Of principal importance in assessing the obligatory role of hydrohemes in denitrification reactions is their comparative nitrite binding. Table 1-6 contains the formation constants of nitrite ferric hemes in THF.

Table 1-6. Formation Constants of Hemin Nitrites.[a,b]

Ferric Heme	K_f (M^{-1})
Etio	770
MeOEC	830
2,3-DMeOEiBC	1600

[a]Reaction of hemin chloride and tetrabutylammonium nitrite.
[b]In THF.

$$Fe^{III}Cl + nBu_4NNO_2 \overset{K_f}{\rightleftharpoons} Fe^{III}(NO_2)$$

Figures 1-9 and 1-10 show the optical spectral changes upon titration of Fe^{III}MeOEC·Cl and Fe^{III}-2,3-DMeOEiBC·Cl with tetrabutylammonium nitrite. Hill plot slopes for Fe^{III}Etio I, MeOEC and 2,3-DMeOEiBC were 0.95, 0.95 and 0.93, respectively. Etioheme nitrite was also prepared by refluxing the hemin chloride with one equivalent of

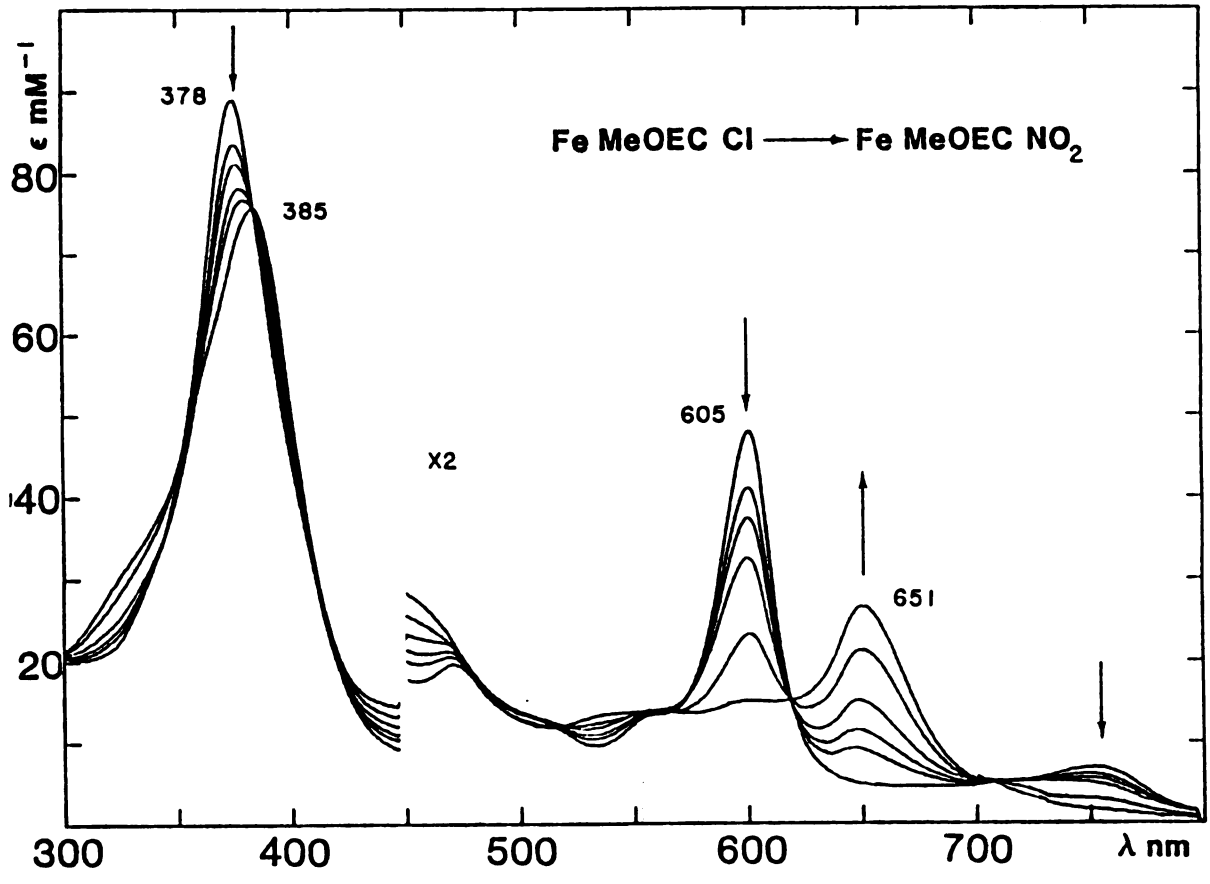

Figure 1-9. Absorption spectra monitoring the titration of Fe^{III}MeOEC·Cl with tetrabutylammonium nitrite in THF. Arrows indicate spectral shifts with increased nitrite concentration.

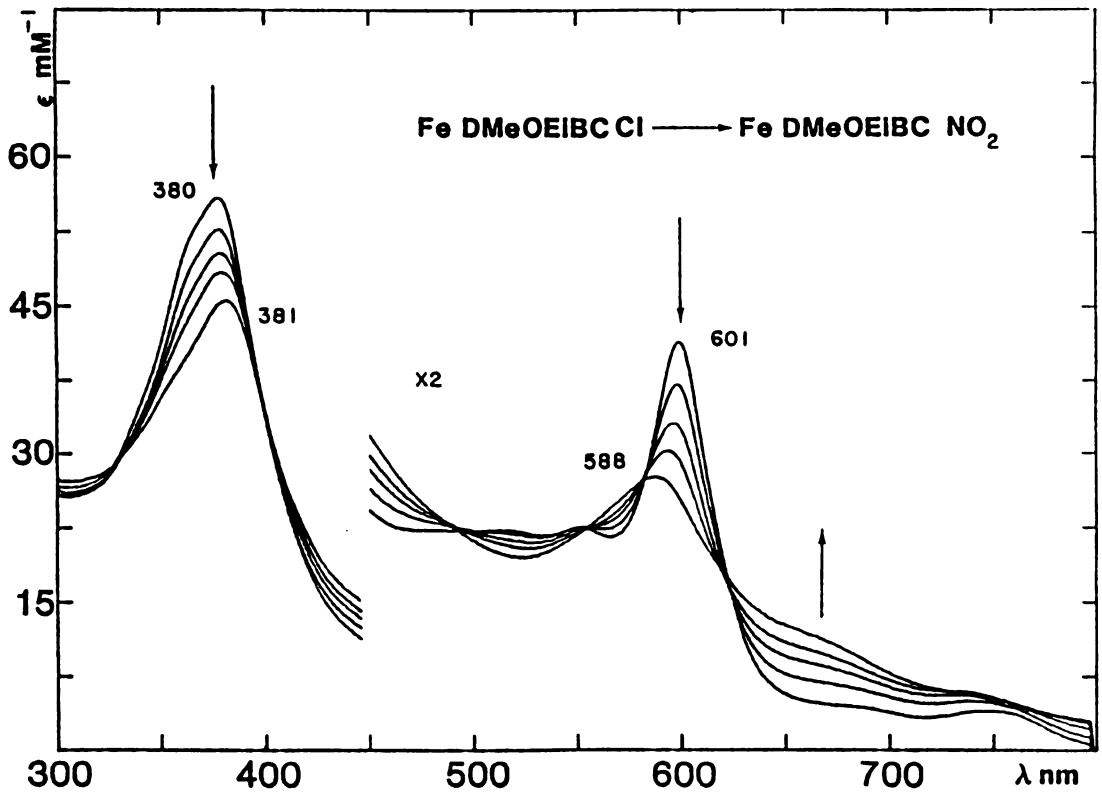

Figure 1-10. Absorption spectra monitoring the titration of Fe^{III}2,3-DMeOEiBC·Cl in THF. The arrows indicate the spectral shifts associated with increased tetrabutylammonium nitrite concentrations.

$AgNO_2$ in butyronitrile. The products from both reactions were spectrally identical. As evident from Table 1-6 displacement of chloride by nitrite increases in the order porphyrin < chlorin < isobacteriochlorin. This result is similar to CO and first imidazole binding to the ferrous species. It is expected that an electron rich iron should stabilize resonance structure II, hence enhance binding.

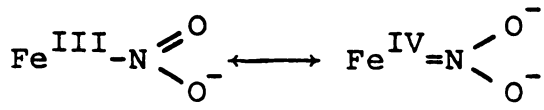

I II

where the N-bonded form is assumed (see IR data below).

The EPR spectrum of etioheme nitrite had a principal g value at 5.25. Signals in the g = 2 region were persistently obscured by a contamination (<10%) of $Fe^{II}NO$. ^1H NMR confirmed hemin nitrites are high spin.

Coordination of nitrite may occur through the nitrogen (nitro form) or an oxygen (nitrido form). Preliminary IR results suggest the nitro form. This assignment is based upon the apparent lack of ν_{N-O}, which typically appears between 1000 and 1250 cm^{-1} for transition metal nitrido-complexes.[24] There was essentially no difference between the IR spectra of etioheme chloride and nitrite in this region. As well, there was a weak absorbance of the heme nitrite vs. chloride in the 620 cm^{-1} region. This band is assigned to a rocking vibration of $M-NO_2$, which is

absent in nitrido complexes.[24] The bands in the 1250-1550 cm^{-1} region (Figure 1-11), though indicative of nitrite, do not confirm a nitro or nitrido form, as there is significant overlap between absorbances of either structure.[24]

Figure 1-12 shows the cyclic voltammograms (CV) of etiohemin chloride, perchlorate, nitrite and ferrous nitrosyl. As evident from the CV's of the chloride and perchlorate, measuring the redox parameters under argon vs. CO provides a diagnostic probe for metal centered redox reactions. For $Fe^{III}Cl$ the anodic Fe^{II}/Fe^{III} wave shifts from ca. -280 mV (argon) to +680 mV (CO). Similarly, for $Fe^{III}ClO_4$ the anodic Fe^{II}/Fe^{III} wave shifts ca. 550 mV positive with a concomitant 150 mV anodic shift of the cathodic wave. Likewise, the Fe^{II}/Fe^{I} waves shift to more negative potentials in the presence of CO. These reactions are summarized as:

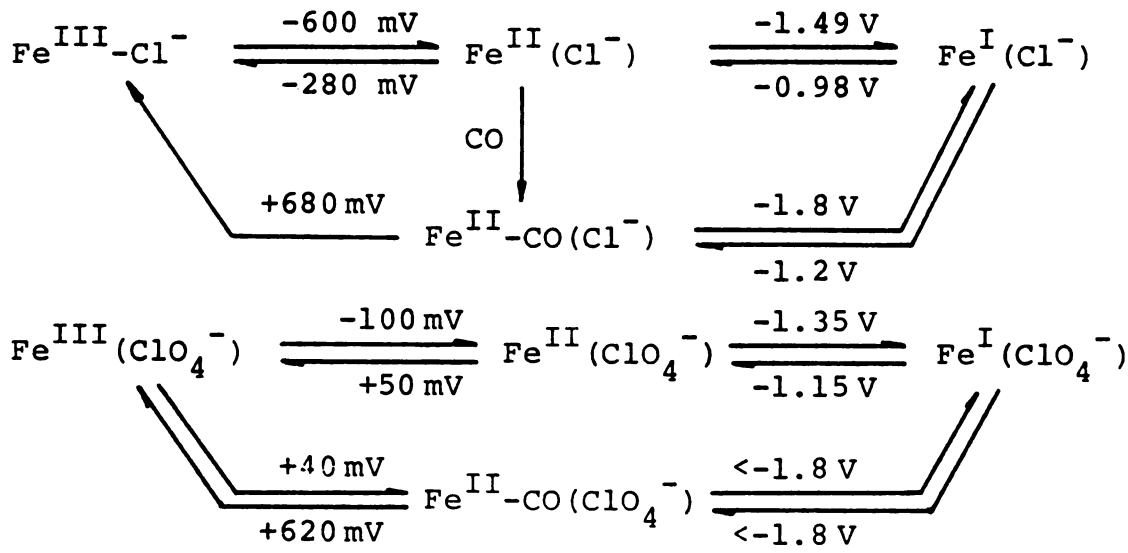

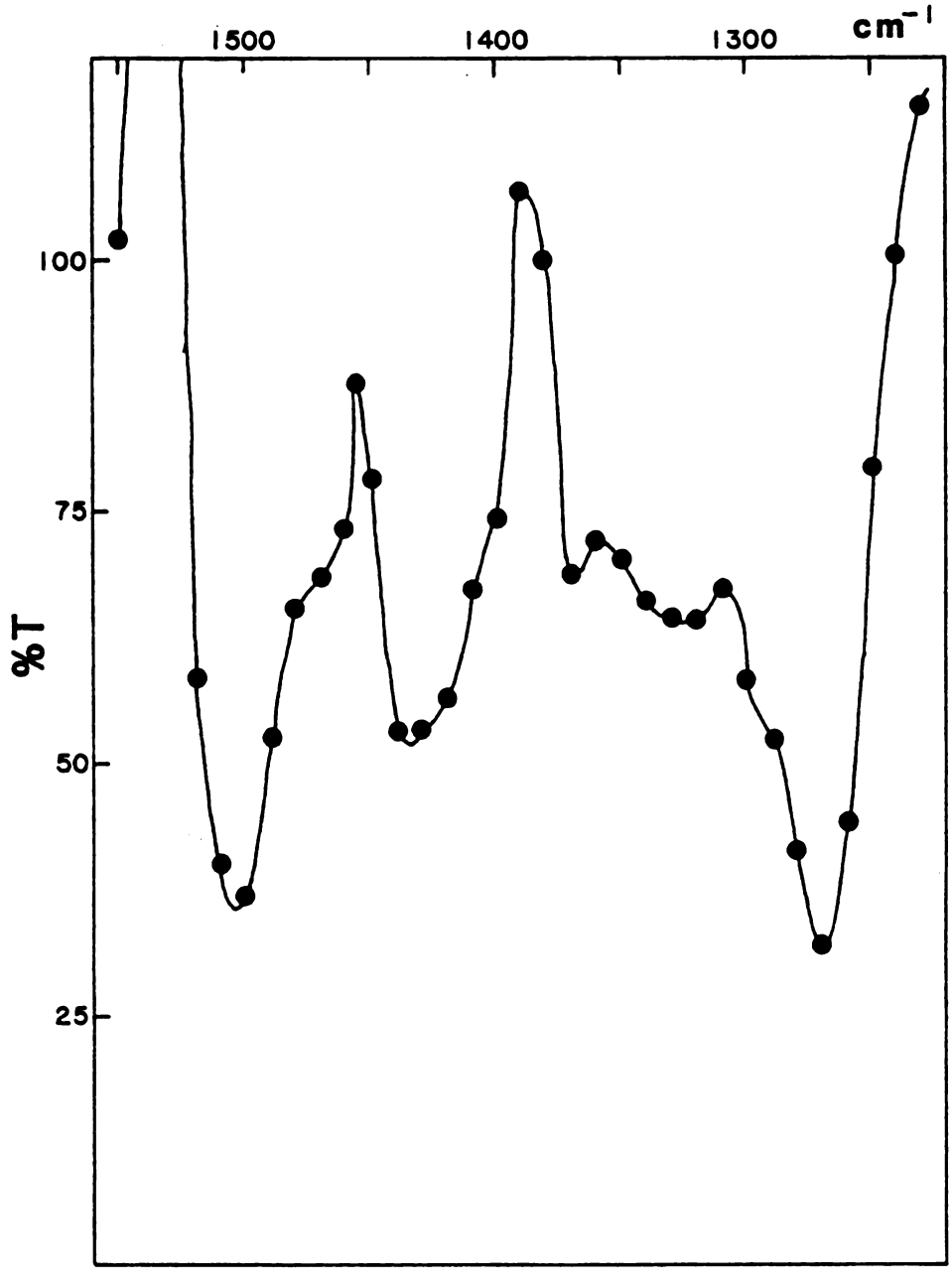

Figure 1-11. Difference infrared spectrum ($FeNO_2$/FeCl) of Etioheme nitrite in AgCl pellet.

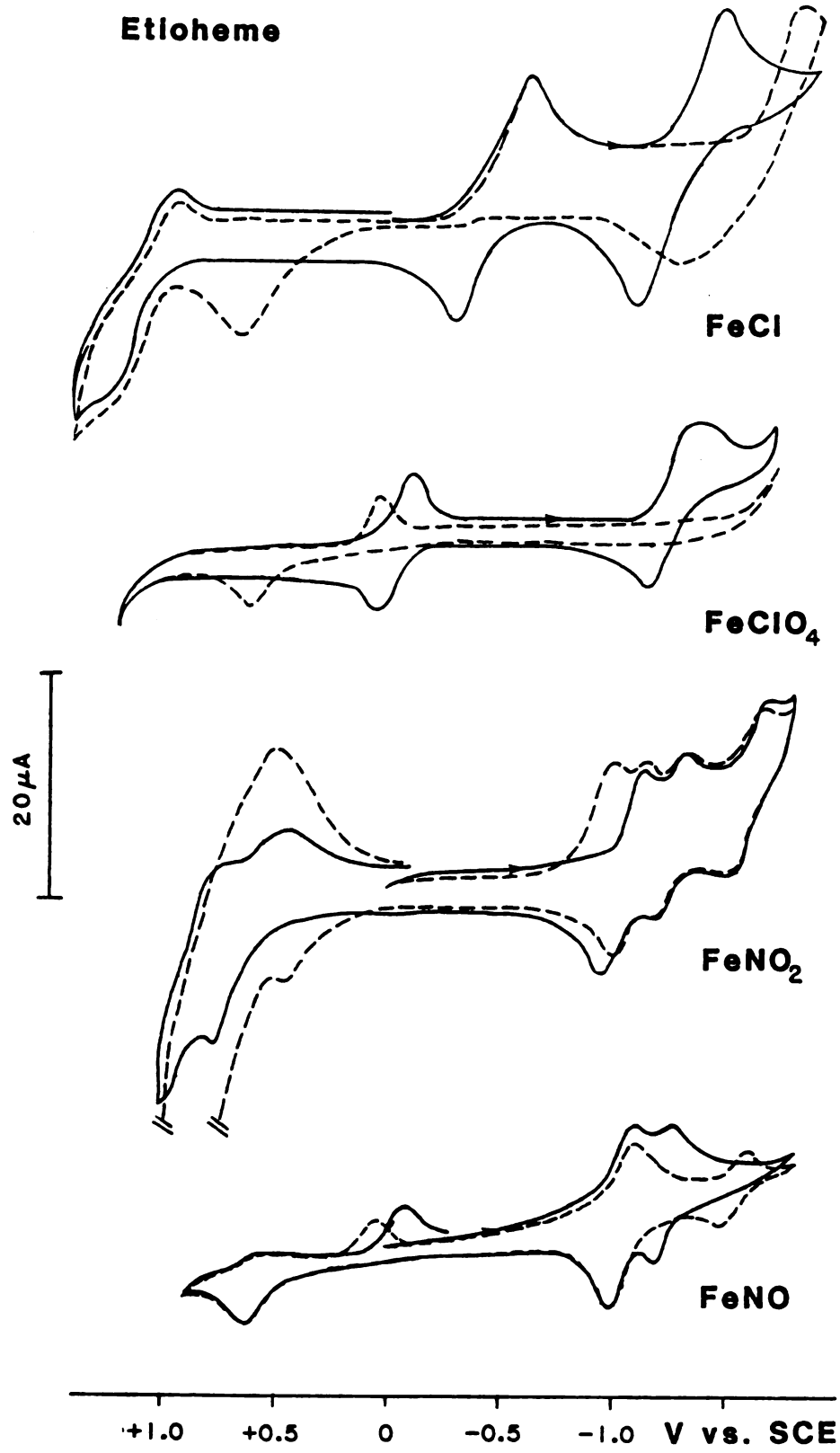

Figure 1-12. Cyclic voltammograms of Etioheme species under argon (——); CO (-----) in THF containing 0.1 M TBAP at a scan rate of 100 mV/sec.

where the potentials are vs. SCE and (X^-) indicates a non-bonded heme-anion interaction. Thus, under CO the Fe^{II}/Fe^{III} couples become irreversible with the anodic and cathodic waves being separated by greater than 500 mV and the Fe^{I}/Fe^{II} couples shift to more negative potentials relative to measurements in inert atmosphere.

Under argon the CV of etioheme nitrite had three quasireversible redox couples centered at -1.05, -1.25 and -1.58 V vs. SCE. Addition of CO caused the appearance of a redox couple with a cathodic wave at -1.0 V and anodic wave at +480 mV. The other waves were little perturbed by the presence of CO. These results suggest the redox reactions of etioheme nitrite are not primarily metal centered. The couple at -1.05 V (argon) appears to possibly be a two electron process. This is evident since under CO the cathodic wave splits into two waves and the anodic wave shifts to more negative potentials. It would seem one electron provides the Fe^{II}/Fe^{III} couple. Whether the other electron and redox couples are nitrite or porphyrin centered is unclear.

Under argon ferrous nitrosyl etioporphyrin has two reversible waves centered at -1.04 and -1.10 V vs. SCE. Oxidation of Fe^{II}-NO occurs at +640 mV with a rereduction wave at -100 mV. These are assigned so since: a. the -100 mV wave does not appear unless scanning is continued past ca. +700 mV; b. the -100 mV wave corresponds to the $Fe^{III} \rightarrow Fe^{II}$ wave of $Fe^{III}ClO_4^-$; c. the -100 mV wave shifts

to +50 mV under CO. These observations are consistent with:

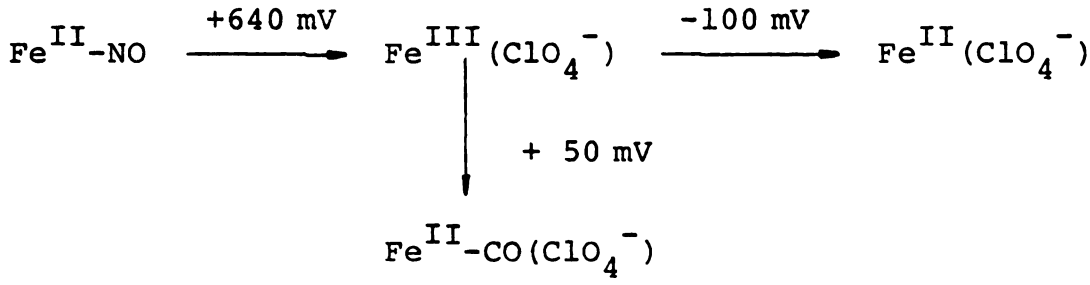

Under Co the redox couple at -1.04 V is unaltered. Reduction of Fe^{II}-NO should place the electron in the iron-N bonding orbital, with substantial localization on the ligand.[25] Thus, this couple is assigned to Fe^{II}-NO /Fe^{II}-NO^-. The second redox couple shifts from -1.10 V (argon) to -1.52 V (CO). This behavior is consistent with the shifting to more negative potentials of Fe^{II}/Fe^{I} couples in the presence of CO. Thus, it is assigned as Fe^{II}-NO^-/Fe^{I}-NO^-. The redox reactions on the reducing side for nitrosyl heme are summarized as:

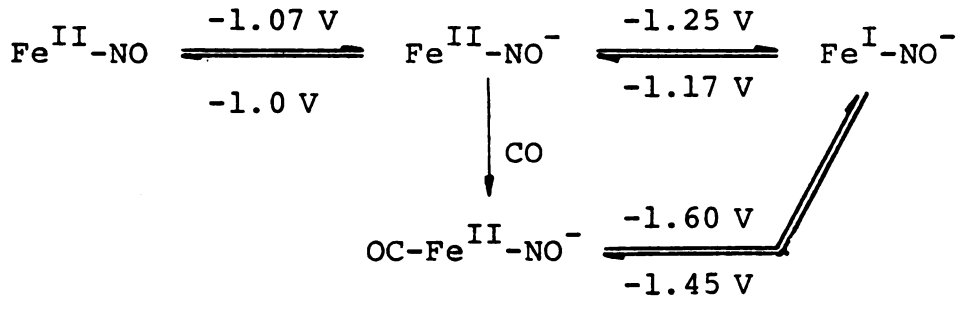

Conclusion

The results presented here show the iron of hydrohemes is electron rich relative to iron porphyrins. Although the kinetic rates and binding constants of pseudo-substrates such as CO and N-methyl imidazole do not significanlty differ from iron porphyrin to make them superior at substrate binding, the electron richness of iron should make them superior toward substrate reduction. The oxidative instability of oxy-hydrohemes is in strong support of this view.

Although the IR results are not totally conclusive, an N-bonded heme nitrite should be catalytically advantageous. During nitrite reduction a nitrito-heme may require a dissociation-reassociation step. This would seem to be the case since NO-heme has been detected during the catalytic cycle of nitrite reductases.[26] A dissociation/association step in the catalytic cycle is expected to decrease the efficiency of nitrite reduction.

Materials and Methods

Materials:

Porphyrins, chlorins, isobacteriochlorins and their iron salts were prepared as described elsewhere.[5,6,27] Toluene was stirred with several changes of conc. H_2SO_4 at 0°C followed by washing with water, drying over anhydrous

Na_2CO_3 and distillation from lithium aluminum hydride. Methylene chloride was distilled from CaH. N-Methyl imidazole was vacuum distilled from CaH. All other reagents were of highest purity commercially available.

Reduction of Fe(III) hemes:

Hemin chlorides were reduced to the ferrous state by the previously described photochemical method[9] in toluene for kinetic and equilibrium measurements. Isosbestic points for $Fe^{III}Cl$ to four coordinate Fe^{II} reduction for the various hemes are provided in Table 1-7. For IR experiments heme reduction was accomplished by addition of a couple of crystals of tetrabutylammonium borohydride to the hemin solution before introduction into the cavity cell under a blanket of argon. A biphasic reduction technique ($H_2O/CDCl_3$) using $Na_2S_2O_4$ or N_2H_4 was used for ^{13}C NMR experiments. Reductions were carried out in the NMR tube in an argon atmosphere.

Kinetic and Equilibrium Measurements:

Carbon monoxide association rates and affinity constants were measured in toluene at ambient temperature (20-22°C) by flash photolysis[28] and direct titration, respectively. The flash source was a Phase-R DL2100 flash lamp pumped dye laser using rhodamine 6G dye ($\lambda = 590$ nm) in 95% EtOH. The PMT output was recorded on an oscilloscope as %T and the screen photographed. The

Table 1-7. Isosbestic Points for Photochemical Heme Reduction[a] in Toluene.

Heme	Isosbestic Points (nm)
2,3-DMeOEiBC	659,582,543,440,395
MeOEC	679,612,581,496,440,381
Etio I	583,515,452,402
PPIX DME	592,521,459,401
2,4-Ac_2Deutero DME	587,499,455,390
T(p-OMe)PP	580,525,461,441,422,388
TPP	569,521,459,435,414,384
T(F_5)PP	573,518,450,426,410,380

[a]Reference 9.

pseudo-first order rate constants were plotted vs. CO concentration (1×10^{-5} M/torr for toluene[15d]); the resulting line had slope 1'. CO association rates were measured a minimum of 2 times which typically were within ±5% between runs. CO dissociation rates were calculated from $L = 1'/1$. To provide the high CO pressures necessary for bis CO-heme formation the side arm of the tonometer was placed in liquid nitrogen to condense CO, a known volume of CO was then introduced. After warming to room temperature the resulting CO pressure was calculated assuming ideal gas behavior.

N-methyl imidazole and nitrite binding constants were determined as described in the text.

IR:

Infrared spectra were recorded on a Perkin-Elmer 283B spectrometer in a NaCl cavity cell in solvents as described in Table 1-3. Samples were prepared as shown in Figure 1-13 under argon atmosphere. The 2100-1800 cm^{-1} region was recorded before introduction of CO. CO was introduced by pressurizing the sealed cavity cell with CO via a gas-tight syringe.

The infrared spectra of etioheme chloride and nitrite were measured in AgCl pellets. 3 mg heme was ground with 60 mg AgCl which was then compressed into a pellet.

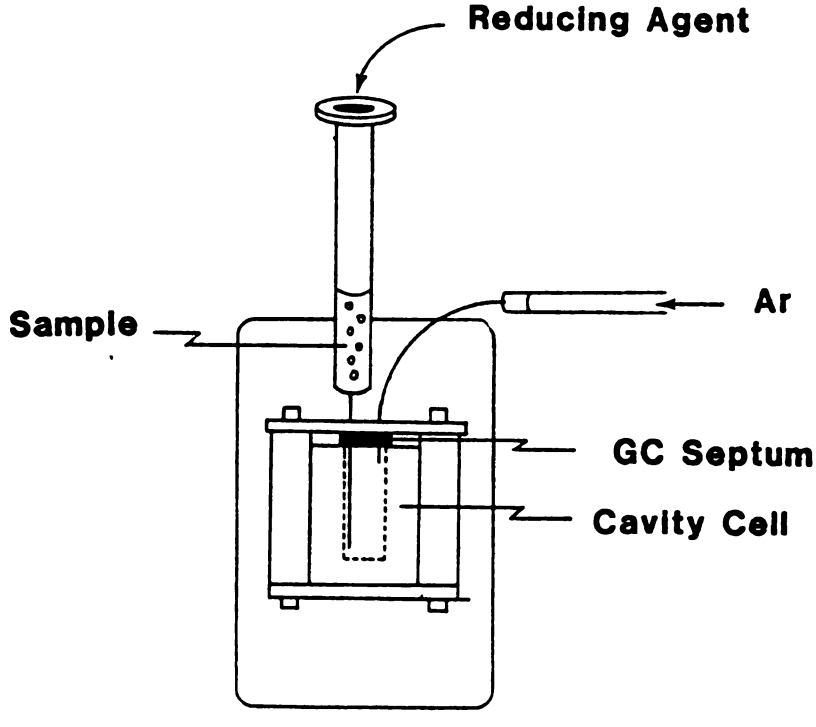

Figure 1-13. Experimental technique for generation of ferrous hemes.

Carbon-13 NMR:

^{13}C NMR spectra were recorded on a Varian Associates CFT-20 spectrometer in 0.1 M N-methyl imidazole/$CDCl_3$ at -15°C. Temperatures were regulated by the V-4360 temperature controller and monitored with a copper-constantan thermocouple. 8 K of memory was used to cover 4500 Hz spectrum width with no transmitter offset. Pulse angle was set at 4 μsec (15 degree tip angle). About 10,000 transients were collected. Chemical shifts were referenced to internal TMS in Hz and output with a digital printer. ^{13}CO was 92.1 atom% enriched. A typical spectrum is shown in Figure 1-14.

Cyclic Voltammetry:

Cyclic voltammetry was performed using a Bioanalytical Systems CV-1A unit in a specially constructed glass cell which contains two platinum spherical electrodes sealed through the cell wall. All measurements were carried out in THF containing 0.1 M tetrabutylammonium perchlorate as supporting electrolyte at a scan rate of 100 mV/sec.

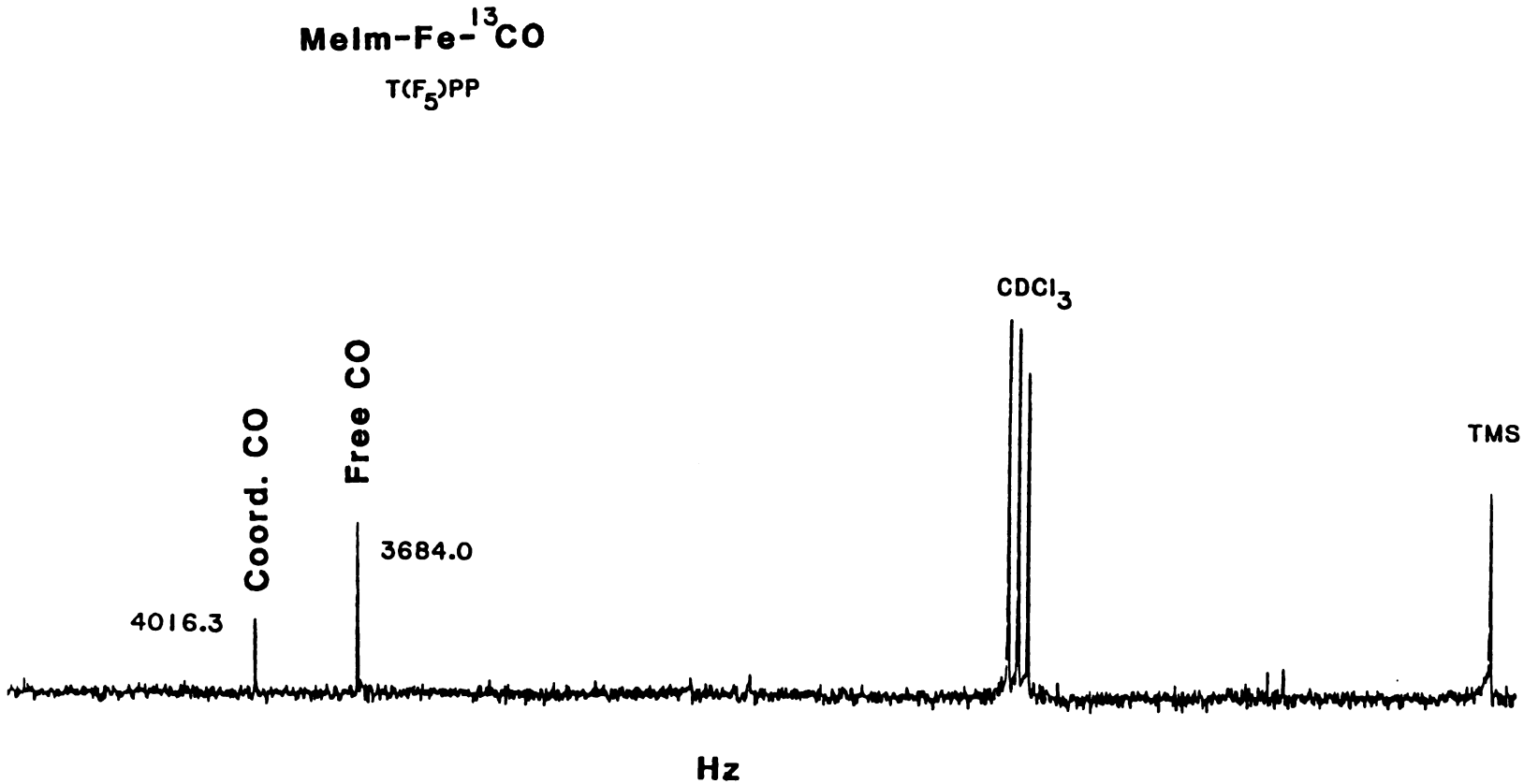

Figure 1-14. ^{13}C NMR spectrum of $Fe^{II}T(F_5)PP$ in 0.1 M N-methyl imidazole/$CDCl_3$ and excess ^{13}CO (90%)

CHAPTER 1: SUPPLEMENT

A CONVENIENT PHOTOCHEMICAL METHOD FOR REDUCTION OF FERRIC HEMES

Introduction

Ferric hemes and hemoproteins in dilute solution have been shown to be reduced to the ferrous form by α-hydroxyalkyl (ketyl) radicals generated by pulse radiolysis.[29] The ketyl radicals, being strong reducing agents and soluble in organic solvents, compare favorably with conventional heme reducing agents such as aqueous dithionite. However, the method by which the ketyl radicals are generated is not easily adaptable to routine use. We wish to report a method based on radical oxidation by ferric heme during the course of the well-known ketone photoreduction.[30] Using this technique one can easily and cleanly reduce ferric hemes to the ferrous form even in anhydrous organic solvents without introducing extra (contaminating) ligands.

Results and Discussion

Figures 1S-1A and 1S-1B show the progress of reduction with Fe(III) etioporphyrin chloride in toluene and THF,

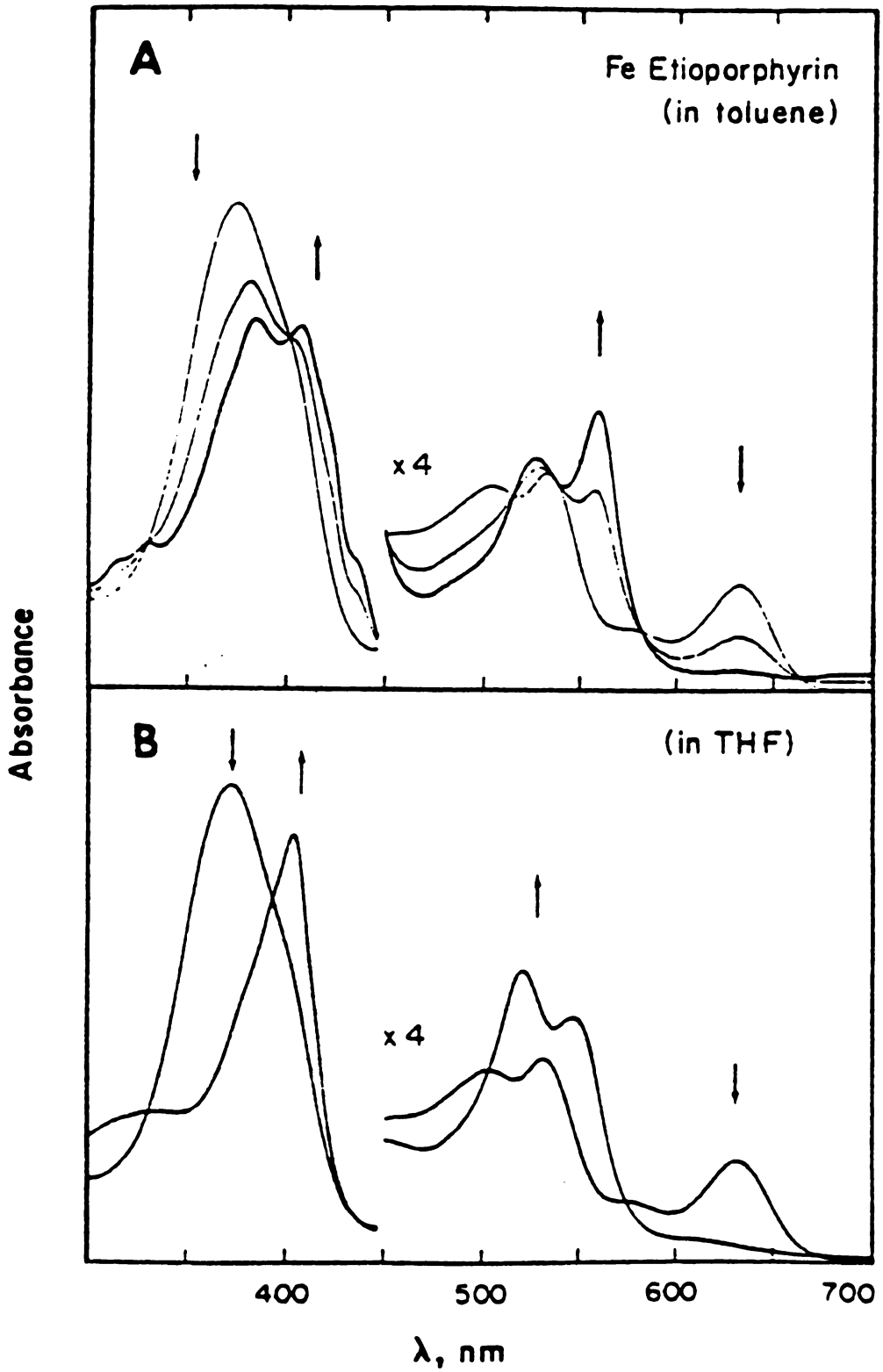

Figure 1S-1. Photoreduction of Etioheme chloride.
A: 0.1 mM benzophenone/toluene; irradiation time = 0, 3, 10 sec.
B: 0.1 mM benzophenone/TFH; irradiation time = 0, 5 sec. Arrows indicate progress of reduction.

respectively. The final spectrum in Figure 1S-1A exhibts the unique multiple peaks in the Soret region, characteristic of an uncoordinated (four-coordinate) ferrous heme.[11] Upon addition of CO, the corresponding mono-CO and bis-CO complexes can be observed. The reduced heme in THF is the high-spin bis-THF adduct.[31]

Figure 1S-2 shows the photolytic reduction of (Fe Etiochlorin)$_2$O in 0.2 M pyridine/toluene. The resulting bis pyridine hemochrome has a spectrum identical with that obtained by reduction of the ferric chlorin in pyridine with aqueous dithionite or hydrazine hydrate.

The photoreduction of horse heart myoglobin is illustrated in Figure 1S-3. Oxygenation of the reduced form yielded stable oxy Mb; addition of CO then readily displaced O_2, in accordance with the known reactions of ferrous myoglobin.

The photoreduction of ferric heme is represented by Scheme 1, which shows the photochemical reduction of ketones[30] followed by Fe(III) mediated radical oxidation.[29,32] While both R• and the ketyl radical seem capable of reducing Fe(III), examination of the redox potentials (Table 1S-1) suggests that only those radicals which oxidize at more negative potentials than the Fe(II)/Fe(III) couple (0 ~400 mV) would be the effective reducing species. Indeed, gas chromatographic analyses of the photoreaction products in our hemin chloride /benzophenone/toluene system revealed no trace of benzyl

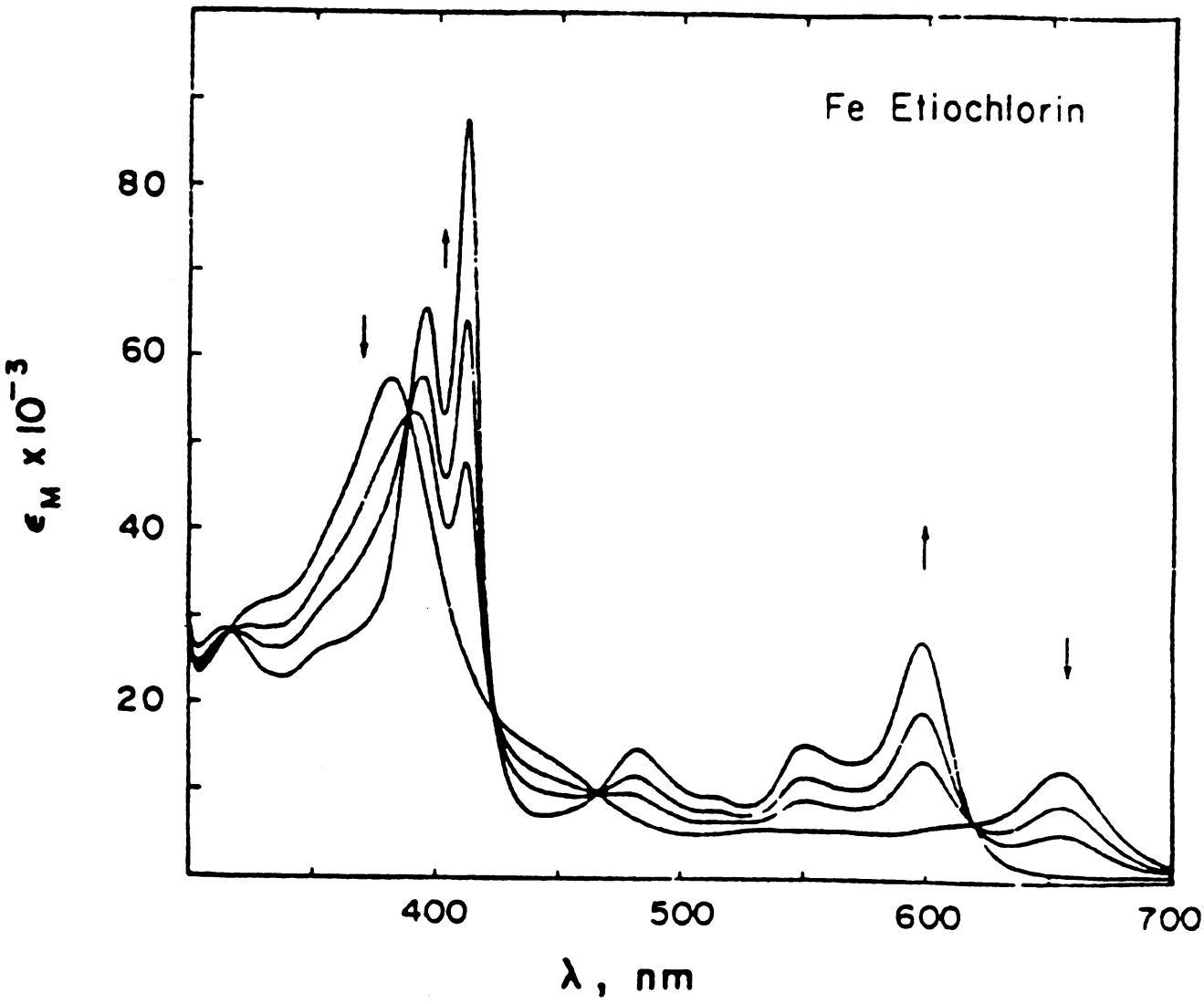

Figure 1S-2. Photoreduction of Fe^{III}etiochlorin$_2$O in 0.2 M pyridine/toluene containing 0.2 mM benzophenone. Irradiation time = 0, 5, 10, 20 sec.

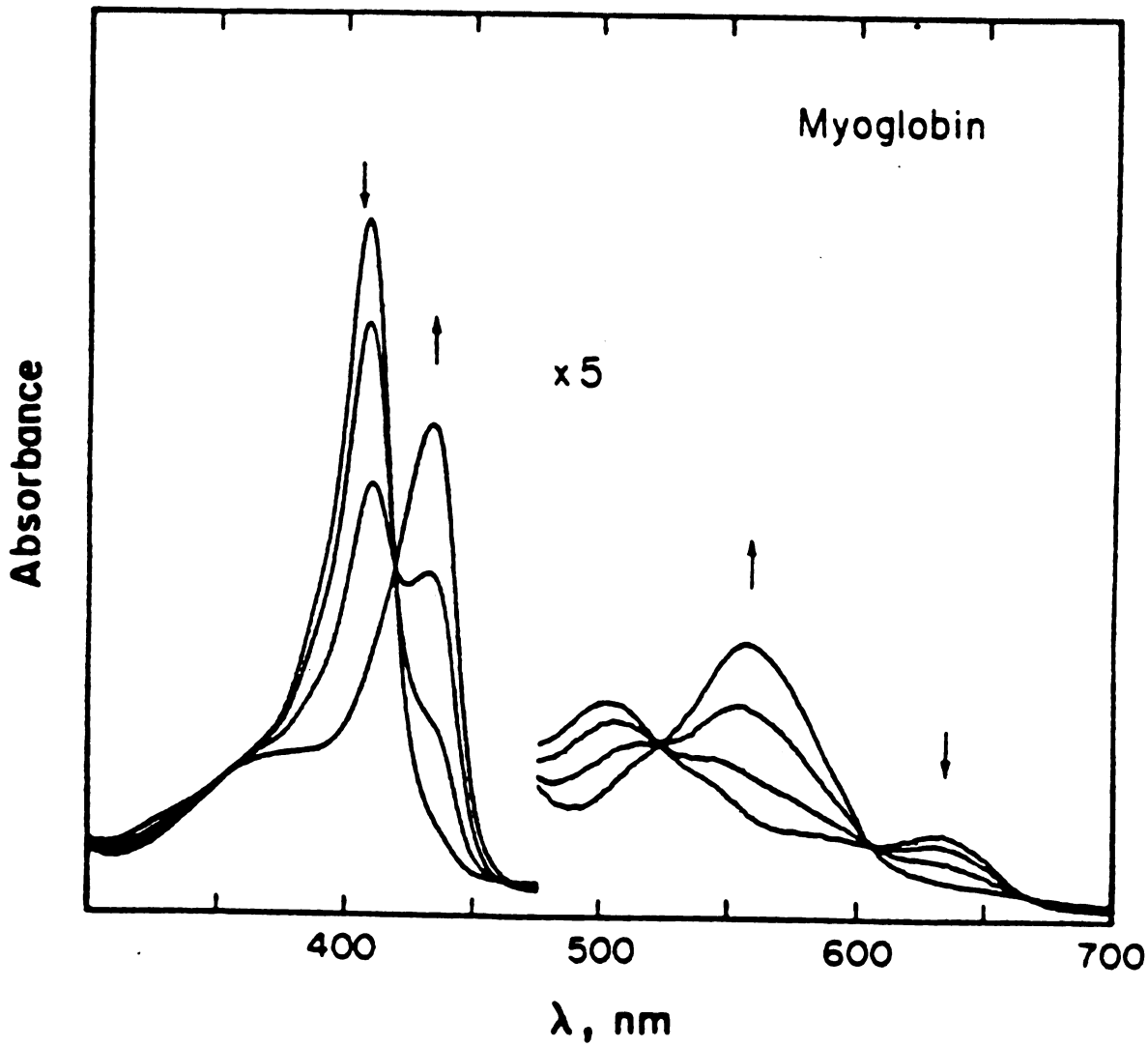

Figure 1S-3. Photoreduction of metmyoglobin in 0.1 M potassium phosphate buffer (pH 7.0) containing 0.008% acetophenone and 2% isopropyl alcohol. Irradiation time = 0, 5, 10, 25 sec.

Table 1S-1. Oxidation Potentials vs. SCE of Organic Free Radicals in H_2O.

RH	$R^{\bullet}$	$E_{\frac{1}{2}}$ (V)	Ref.
	$\phi_2\dot{C}OH$	-1.242^{a}	33a
	$\phi\dot{C}OH(CH_3)$	-1.532^{a}	33a
ϕCH_3	$\phi CH_2\cdot$	$\sim-0.2^{b,d}$	33b
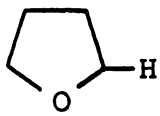	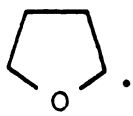	$\sim-0.8^{c,d}$	33c
$(CH_3)_2\,C(OH)-H$	$(CH_3)_2\,C(OH)\cdot$	-1.29^{a}	33a

[a] pH 7.
[b] pH 14.
[c] pH independent.
[d] Estimated from polarograms in references.

chloride but only the dibenzyl ($\phi CH_2CH_2\phi$) coupling product, indicating that the benzyl radical did not participate in the reduction of hemin chloride.

Scheme 1

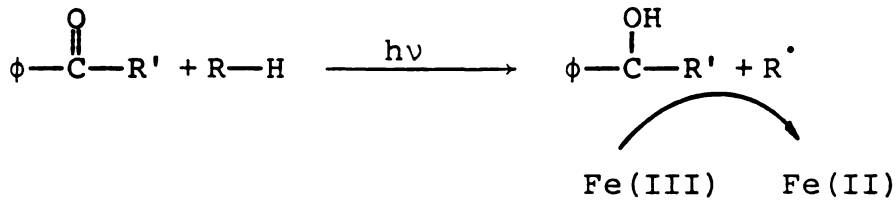

R' = ϕ,CH_3 RH and R as shown in Table 1S-1.

Heme photoreduction has previously been observed for a number of proteins. Among these are: cytochrome oxidase,[34] horse heart cytochrome c,[35] cytochrome b,[36] T-state hemoglobin[37] and cytochrome c_{552}.[38] Furthermore, heme photoreduction has purposefully been demonstrated with cyt P450 using a proflavin/EDTA system[39a] and cyt c using flavin/EDTA.[39b] The reduction presumably involved the prior photoreduction of a chromophore (e.g. flavin) followed by heme reduction.[34b,38,40] In fact cyt b and cyt c_{552} do not photoreduce in the absence of flavin.[38,40] Therefore, the mechanism of hemoprotein photoreduction apparently is akin to scheme 1. One common feature to all of the protein photoreductions, as well as to our system, is a wavelength dependence. For instance, cytochrome c oxidase is not photoreduced with visible excitation[41] but is reduced in the UV region,[34] cytochrome c photoreduces 8 times faster at 410 nm than at 535 nm,[35]

as well T-state Hb displays a photoreductive wavelength dependence.[37] In our system, irradiation through pyrex vs. quartz results in a very sluggish reduction, attributable to the low absorptivity above 310 nm of benzophenone or acetophenone.

It is also the experience of many workers in the field that ferric hemes in pyridine under CO atmosphere can be photoreduced to the carbon monoxide complex. We have observed, however, that the rate of this reaction is related to pyridine purity. Using highly purified pyridine this photoreduction, in fact, did not proceed to completion; but addition of trace amounts of ϕ_2CO/i-PrOH resulted in completed reduction. Therefore, it seems there are impurity chromophores present in commercial grade pyridine which are responsible for initiating the photoreduction.

In conclusion, we have developed a simple and reliable technique for reducing ferric heme under a variety of conditions. This method is especially suitable for studies carried out in organic solvents as well as aqueous protein work. One advantage of this method is that tedius reductant titration may be avoided when excess reducing agents may be deleterious (i.e. O_2 binding). The fact that the ketyl radicals are more powerful reducing agents than dithionite also suggests that some hemoproteins, e.g. cytochrome $\underline{c}_3$, which cannot be completely reduced by dithionite may do so with this technique.

Materials and Methods

Solvents:

Toluene was purified by stirring with several changes of concentrated sulfuric acid followed by distillation from lithium aluminum hydride. Tetrahydrofuran (THF) was distilled from lithium aluminum hydride. Pyridine was distilled from calcium hydride.

Hemes:

Etioporphyrin and etiochlorin were prepared by standard procedures.[27b] Iron insertion was accomplished by the $FeSO_4$ method. Horse heart myoglobin (Sigma, type III) was used as received.

Photoreduction in Non-Aqueous Systems:

Ferric hemes either in the chloride or μ-oxo dimer form ($\sim 10^{-5}$ M) and benzophenone ($\sim 10^{-4}$ M) were dissolved in dry toluene, THF, or 0.2 M pyridine/toluene mixture. The solution was rendered oxygen-free by either flushing with argon gas for 30 minutes using a syringe needle or by freeze-thaw cycles under vacuum. The deoxygenated solution was then irradiated with a Hg lamp (Hanovia "Utility" UV lamp, 140 W). In general, reduction was complete within 20 s. Spectral changes were monitored using a Cary 219 spectrophotometer. In all experiments

further irradiation after the heme reduction was complete resulted in no spectral change.

Photoreduction in Aqueous System:

Myoglobin was dissolved in 0.1 M potassium phosphate buffer (pH 7.0) containing 2% isopropanol and 0.008% acetophenone. The solution was degassed and irradiated as above.

PART B

ENVIRONMENTAL INFLUENCES ON CO AND O_2 BINDING TO HEME

CHAPTER 2

KINETICS OF CO AND O_2 BINDING TO IRON-COPPER COFACIAL DIPORPHYRINS AND STRAPPED HEMES

Introduction

X-ray crystallography showed that the structures of carbon monoxide liganded hemoglobins (Hb) and myoglobins (Mb) exhibit a bent or tilted FeCO linkage with respect to the porphyrin ring,[42-46] whereas in heme model compounds the FeCO bond is linear and perpendicular to the heme plane.[47,48] The origin of the distorted configuration in the proteins is attributed primarily to nonbonding steric interactions of the axial ligand with residues at the distal side. An assumption is made that ligands such as O_2 and NO, which preferentially form bent complexes, should encounter less steric hindrance when bound in the heme pocket.[49,50] It has been proposed that in Hb and Mb, the distal steric effect would decrease the affinity ratio of CO vs. O_2, and is responsible for the detoxification of CO poisoning in respiratory systems.[51-54] A comparison of ligand binding constants of proteins and model compounds often shows that many heme models have a larger CO vs. O_2

affinity ratio (M value) than the proteins. However, such a comparison does not necessarily constitute a correlation between the distal steric effect and affinity as the ligand binding constants of heme models can be drastically altered by medium effects.[28b,55] Indeed, Traylor and coworkers have shown that a five-coordinate protoheme-imidazole model binds both O_2 and CO in aqueous suspensions with equilibrium and kinetic parameters almost identical to R-state isolated hemoglobin chains.[15c,28,55,56] In other cases, for example, T-state hemoglobin and notably myoglobins have very small M values which cannot be duplicated with simple heme compounds.

It is therefore of importance to examine the steric effects on ligand affinity using synthetic models equipped with varying degrees of steric hindrance at the distal side. Several porphyrin models of this kind have been prepared[57-60] and recently an iron complex with a bent CO has been shown.[61] Here is presented the equilibria and kinetic rates of CO and O_2 binding to two hindered heme systems. One is mixed metal cofacial diporphyrins in which an inert copper porphyrin[62] is tightly linked to the heme thereby providing a compression from above to the coordinating ligand. The second system is iron cyclophane porphyrins where a hydrocarbon chain is strapped across one face of the heme. Depending on the chain length, the strap would mostly exert a side-way shearing strain to the gaseous ligand.

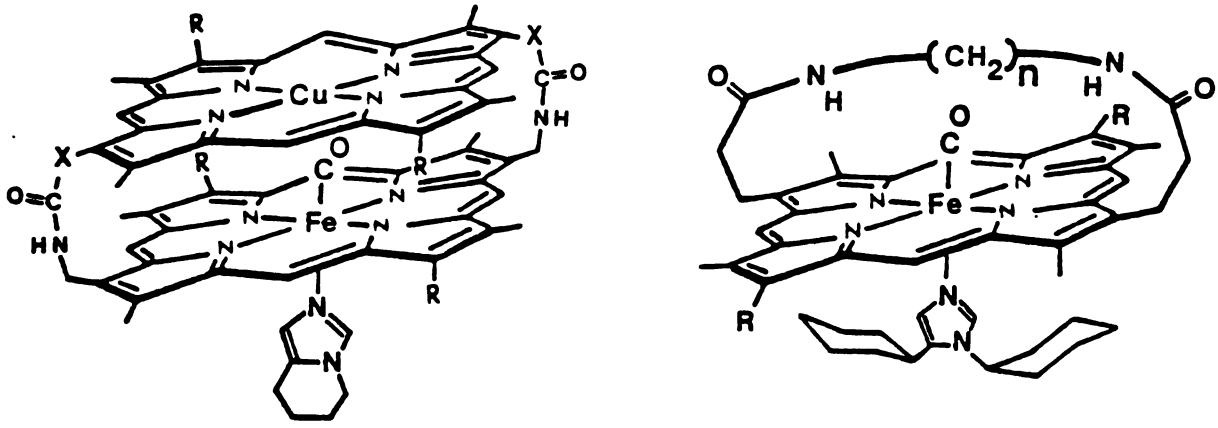

R = n-pentyl

Fe-Cu-4	$X=(CH_2)$	FeSP-13	n=5
Fe-Cu-5	$X=(CH_2)_2$	FeSP-14	n=6
		FeSP-15	n=7

Figure 2-1. Structural formula of sterically hindered hemes.

CO and O_2 binding to the ferrous hemes were studied in benzene solution containing excess N-alkyl imidazoles. The nitrogen base was chosen such that it can only form five-coordinate heme. N-Methylimidazole was bulky enough to meet this criterium only with the very tightly gapped Cu-Fe-4 and FeSP-13 but was not satisfactory for Cu-Fe-5 nor FeSP-15 as considerable competition of CO binding at the hindered site by a second imidazole can be observed. We therefore used a "tall" bicyclic imidazole[63a] for the dimers and a "fat" dicyclohexyl-imidazole[63b] for the strapped hemes; using these bases no competition was observed.[64] Typical relaxation curves along with the corresponding absorption spectra of different complexes are shown in Figure 2-2. The CO and O_2 association rates were obtained under pseudo-first order conditions. The oxyheme complex formed in the Cu-Fe dimers was so stable (no oxidation detectable even after 12 hrs at room temperature) that the $P_{\frac{1}{2}}^{O_2}$ values can be measured directly by gas titration and as such, they provided an independent check on the O_2 off rates derived from the kinetic equations.[28,65] All rates and equilibrium constants for models and relevant heme proteins are tablulated in Table 2-1.

The most striking result shown by Table 2-1 is that indeed, distal steric hindrance can affect ligand binding but this effect is manifested only in the ligand association rate constants and has almost no effect on

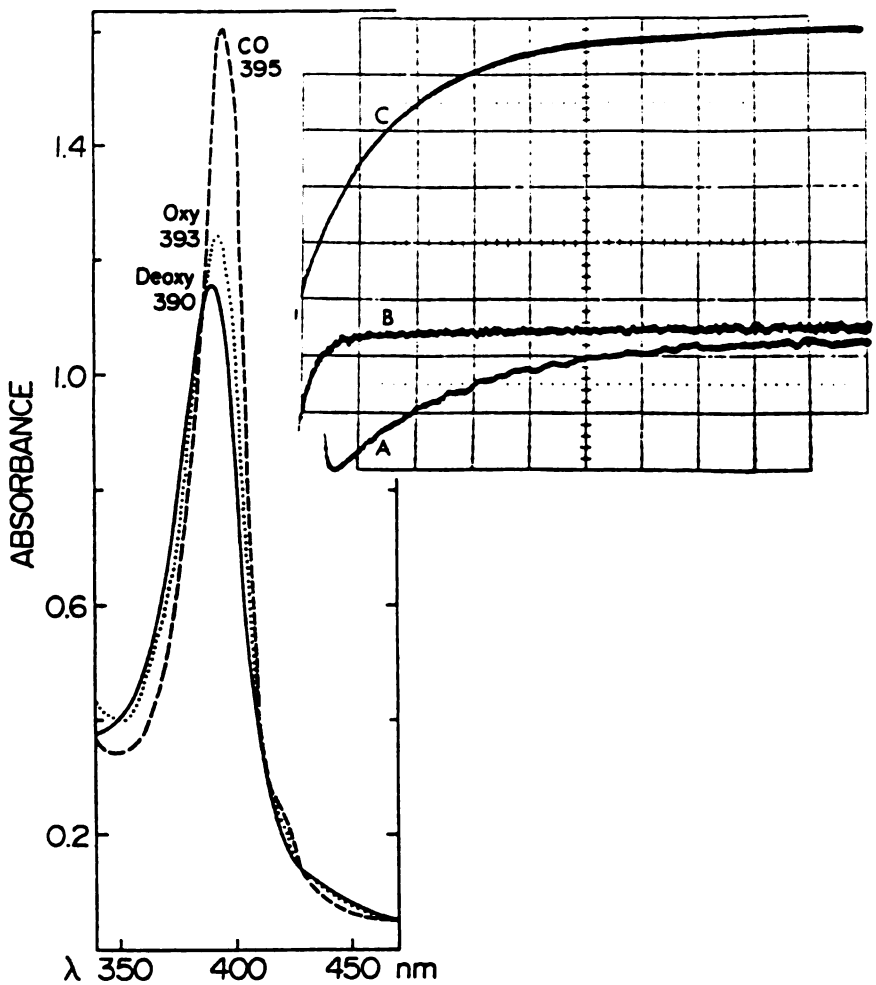

Figure 2-2. Absorption spectra of the various forms of FeCu-d_4 and the corresponding oscilloscope traces for regeneration of Fe-O_2 (A. 0.2 ms/div.; B. 2 ms/div.) and Fe-CO (C. 2s/division).

Table 2-1. Kinetic and Equilibrium Constants for Binding of CO and O_2 to Sterically Hindered Hemes (20-22°C).[a]

Compound	Solvent	l' (M^{-1} s^{-1})	l (sec^{-1})	$P_{\frac{1}{2}}^{CO}$ (torr)	k' (M^{-1} s^{-1})	k (sec^{-1})	$P_{\frac{1}{2}}^{O_2}$	(M)	Ref.
Mb	H_2O	$3\text{-}5 \times 10^5$	0.02-0.04	0.014 ~0.025	$1 \sim 2 \times 10^7$	$10 \sim 30$	$0.5 \sim 1$	$20 \sim 40$	27
Hb, isolated α^{SH}	H_2O	4×10^6	0.013	0.0024	5.0×10^7	28	0.3	130	8
chelated protoheme	H_2O[b]	3.6×10^6	0.009	0.0018	2.6×10^7	47	1.0	560	14
chelated mesoheme	H_2O[b]	11×10^6	0.019	0.0013	2.2×10^7	23	0.58	450	15a, 14
chelated mesoheme	toluene	8×10^6	0.03	0.0004	5.3×10^7	1700	3.2	8×10^3	15a, 14
deuteroheme + *N*-MeIm	benzene	12×10^6	0.028	0.0002					
Fe-Cu-4 + 0.2 M *N*-MeIm	benzene	2.0×10^4	0.02	0.1	5.2×10^5	160	31[e]	310	this work
Fe-Cu-4 + 1.0 M THPIm[c]	benzene	2.2×10^4	0.03	0.13	5.0×10^5				this work
Fe-Cu-5 + 0.2 M THPIm[c]	benzene	9.0×10^4	0.02	0.02	1.8×10^6	91	5[e]	250	this work
FeSP-13 + 0.2 M *N*-MeIm	benzene	6×10^2	0.07	12					this work
FeSP-14 + 1.0 M DCHIm[d]	benzene	8×10^3	0.04	0.5	3×10^5				this work
FeSP-15 + 0.2 M DCHIm[d]	benzene	9.1×10^4	0.04	0.05	1.7×10^6	250	15	300	this work

Notes for Table 2-1 on following page.

Notes for Table 2-1.

[a]Rates were calculated using the following solubilities: 1 torr of CO = 1×10^{-5} M (benzene, toluene), 1.35×10^{-6} M (H_2O); 1 torr of O_2 = 1×10^{-5} M (benzene, toluene), 1.8×10^{-6} M (H_2O).

[b]Suspended in 2% CTAB or MTAB.

[c]THPIm: 5,6,7,8-tetrahydroimidazo[1,5-*a*]-pyridine.

[d]DCHIm: 1,5-dicyclohexylimidazole.

[e]$P_{\frac{1}{2}}O_2$ obtained from direct titrations and from kinetic measurements agreed within 20%.

the off rates, in agreement with the predictions made earlier by Moffat et al.[49] and consistent with the isocyanide binding results of Traylor.[66] Since it has previously been shown that the CO and O_2 association rates are nearly independent of medium and heme electronic effects and that the O_2 off rates are very much affected by the local polarity of the ligand binding site,[67,68] it is futile to directly compare the O_2/CO affinity ratio, M, of different model compounds. However, when we compare only the association rate data we find, relative to chelated mesoheme, FeCu-5 or FeSP-15 a CO reduction of 90-fold while an O_2 of 30 (a reduction ratio of 3) and for Fe-Cu-4 a CO reduction of 400-fold with O_2 being reduced by 100 (a reduction ratio of 4). This unequal reduction of CO and O_2 association rates may be considered as an evidence for the steric differentiation of O_2 and CO. This steric selectivity nonetheless does not explain why we cannot obtain the degree of differentiation observed for Mb, i.e., chelated protoheme or R-Hb vs. Mb has a reduction ratio of at least 5, even though our model compounds have more steric hindrance built into them than does Mb, as reflected by the CO on rates. Neither can we reconcile the fact that there is essentially no change in the on rate reduction ratio nor the M value going from Fe-Cu5 to FeCu-4 while the structural data as well as the CO on rates indicate clearly that the FeCu-4 has a tighter gap than FeCu-5. If the bending of CO is responsible for

the differentiation, it would have to show in the 4 to 5 comparison. One possibility is that the differentiation is not proportional to the steric hindrance; it reaches a maximum then decreases as the steric effect becomes too great. Unfortunately, in the present study we found it is difficult to have a system whose CO on rate is in the neighborhood of 5×10^5 M^{-1} s^{-1}, to compare with Mb. Cofacial diporphyrins with longer linkages, e.g., FeCu-6 and FeCu-7, exhibit kinetic rates similar to FeCu-5 since the two porphyrin rings have a tendency to assume a slipped conformation and maintain a tight gap, as shown by X-ray studies,[69] thus these compounds offered no insight. On the other hand, hemes equipped with longer straps tend to form six-coordinate hemochromes with the excess base.

Although the present study does not provide a definitive answer as to whether or not steric bulk at the ligand binding site can selectively reduce the <u>affinity</u> of CO vs. O_2, surely the kinetic results imply that models which bind CO 2 to 3 orders of magnitude slower than Mb should decisively indicate whether there is any relation between ligand affinity and ν_{CO}. Table 2-2 summarizes the ν_{CO} of some of the synthetic compounds measured in different solvents. It is evident that the influence of medium is far greater than the steric effect. That is, the variation in ν_{CO} observed for the strapped hemes in 0.1 M N-Methyl imidazole/CH_2Cl_2 can be completely removed in neat N-Methyl imidazole. Thus, it would be dangerous to

Table 2-2. ν_{CO} of Sterically Hindered Hemes.

Compound	Medium	$\nu_{^{12}CO}$ (cm^{-1})	$\nu_{^{13}CO}$ (cm^{-1})
FeCu d_4	N-MeIm[a]	1960	1915
	0.1 M TIm[b]/ CH_2Br_2	1967	1924
FeSP-13	N-MeIm[a]	1962	
	0.1 M TIm[b]/ CH_2Br_2	1967	
	0.1 M N-MeIm/ Ch_2Cl_2	1932	1888
FeSP-14	0.1 M N-MeIm/ CH_2Cl_2	1939	1894
FeSP-15	0.1 M N-MeIm/ CH_2Cl_2	1945	1901
Heme 5[c]	N-MeIm[a]	1955	1910
	0.1 M N-MeIm CH_2Cl_2	1954	1910

[a]Neat N-Methyl imidazole.

[b]N-(triphenylmethyl)imidazole.

[c]Iron 2,6-di-n-pentyl-1,3,5,7-tetramethyl-4,8-[d]dimethacetamido porphine.

use ν_{CO} as an indication of CO affinity for comparison between different systems, i.e. comparing proteins and model systems. The unequal reduction of the CO and O_2 association rates by the steric bulk implies that such differentiations must be related to the bond forming processes. Szabo[70] has suggested that CO-heme transition state resembles product while O_2-heme has a more reactant-like transition state. That is to say since the Fe-CO bond formation requires shorter contact, the CO molecules must be in closer proximity than O_2 to attain transition state. Any steric barricade at the heme binding site therefore would hinder CO coordination more than O_2 coordination.

The present study also indicates that it would be a unique synthetic challenge to prepare heme models[71] that match Mb's kinetic behavior. So long as we showed that bending of CO cannot be solely responsible for the large differentiation observed in Mb, other factors such as the basicity of the proximal base, pre-equilibrium of the heme conformation inside the protein pocket, etc. have to be taken into consideration.[72] The synthesis of other sterically hindered, five-coordinate hemes is underway.

Summary

The work presented does not provide definitive evidence either for or against a steric effect

differentiating CO vs. O_2. It does suggest that if a steric effect can differentiate small ligands (CO, O_2) it does so primarily by ligand association rate modulation. This work also shows that ν_{CO} is not a reliable indicator of ligand affinities.

Materials and Methods

Strapped and cofacial diporphyrins were synthesized by previously described methods[73] and characterized by UV-visible, NMR and mass spectroscopies. Iron insertions were accomplished by the ferrous sulfate method.[27b] Benzene was purified by stirring with several changes of conc. H_2SO_4 followed by washing with water, drying over anhydrous Na_2CO_3 and distillation from lithium aluminum hydride. 5,6,7,8-tetrahydroimidazo[1,5-a]pyridine was prepared by hydrogenation of 2,3a diazaindene,[63a] and purified by vacuum distillation from KOH. N-methyl imidazole was vacuum distilled from CaH. 1,2 dimethyl imidazole was vacuum distilled from Na. All other reagents were of purest commercial grade and used as received.

Kinetic rates were measured in benzene containing 0.1 M base by flash photolysis[28] according to:

$$\text{B-Fe-CO} \underset{l'(CO)}{\overset{h\nu}{\rightleftharpoons}} \text{B-Fe} \underset{k}{\overset{k'(O_2)}{\rightleftharpoons}} \text{B-Fe-O}_2$$

Under pseudo-first order conditions l'CO was monitored spectrally at 398 nm. A plot of l'CO vs. CO yielded a straight line with slope l'. CO dissociation rates were calculated from $L = l'/l$, which was determined by direct titration of the ferrous heme with CO. Oxygen dissociation rates were measured directly as shown in trace A of Figure 2-2. Oxygen dissociation was calculated from $K = k'/k$ which was determined from the Gibson equation:[65]

$$1/R = 1/k + K(O_2)/l'(CO)$$

where R is the observed rate of heme-CO formation in the presence of O_2; l'(CO) was the pseudo-first order rate constant before introduction of O_2. When possible (see results and discussion) K was measured by direct titration of the ferrous heme with O_2. The results of each method were in excellent agreement. $Fe^{III}Cl$ porphyrins were reduced to the ferroheme by addition of a slight excess of Vitride (sodium bis-(2-methoxyethoxy)aluminum hydride). Use of this reagent for heme reduction requires that solutions be absolutely dry since reaction with water can produce hydroxide, which can compete with ligand binding to ferroheme.[15b]

Infra-red spectra were recorded on a Perkin-Elmer 283B spectrometer in a NaCl cavity cell in solvents as described in Table 2-2. Samples of Fe^{II}-^{12}CO porphyrins were prepared anaerobically as shown in Figure 2-3. ^{13}CO bound samples were prepared by exchange with ^{12}CO. 0.3-0.5 ml 92.1 atom

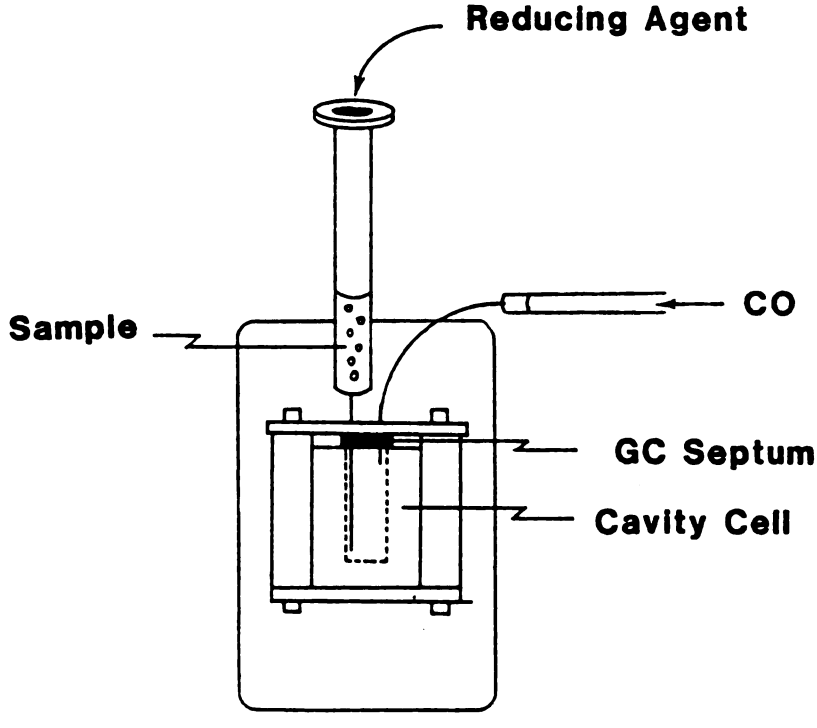

Figure 2-3. I.R. cell for anaerobic generation of Fe^{II}-CO porphyrins.

percent ^{13}CO was bubbled through the solution using a gas tight syringe and an outlet needle to allow excess gases to escape. As shown in Figure 2-4 this method allows ^{13}CO to completely replace ^{12}CO. Iron reduction was accomplished by addition of a couple of crystals of tetrabutyl ammonium borohydride to the sample before allowing it to flow into the cell.

Optical spectra were recorded on a Cary 219 spectrometer.

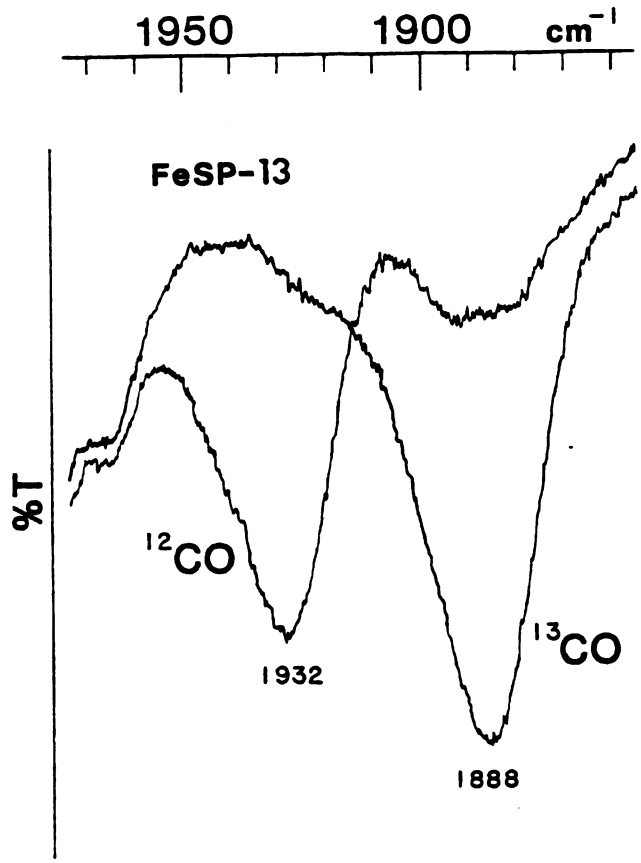

Figure 2-4. Infrared spectrum of $Fe^{II}SP-13(CO)$ in 0.1 M N-methyl imidazole/CH_2Cl_2.

CHAPTER 3

KINETIC STUDY OF CO AND O_2 BINDING TO HORSE HEART MYOGLOBIN RECONSTITUTED WITH SYNTHETIC HEMES LACKING METHYL AND VINYL SIDE CHAINS

Introduction

Variations in heme function among hemoproteins often arise from specific interactions between the heme prosthetic group and the apoprotein. An obvious method of probing the heme-protein relationship is to investigate structural modifications in the heme moiety and relate these to alterations of the functional properties of reconstituted hemoproteins. Indeed, reconstitutions with protohemes modified at the 2,3 positions[67,73,74] and iron chlorophyllides[75] have revealed significant changes in the ligand binding or oxidative stabilities of hemeglobins and myoglobins. While the variation in properties can often be attributed to electronic[73] and/or steric[67,74,75] effects, precise interpretation of these results is often difficult for there is a very limited number of modified hemes capable of distinguishing between a steric and electronic effect.[67,74] As part of an effort to probe structure function relationships of oxygen binding hemoproteins, we

report here the oxygen and carbon monoxide binding behavior of horse heart myoglobin reconstituted with hemes deprived of peripheral side chains. As shown in Figure 3-1, the hemes employed were 2,4-dimethyl deuteroheme; deuteroheme; 1,3-didemethyl deuteroheme ("bald" heme); and iron-6,7-dipropionic acid porphine ("stripped" heme). These synthetic hemes all possess the two propionic acid groups necessary for specific binding to the protein heme pocket but they differ from each other in the number of ring methyl groups. In the absence of large variations in their electronic properties, this series of hemes should allow a more accurate assessment on the effect brought about by structural and shape perturbations of the heme group.

Results and Discussion

The basic supposition of hemoprotein reconstitution is that after reconstitution the protein tertiary structure regains its native form. Indeed, the ligand binding properties of protoheme reconstituted Mb's and Hb's are essentially identical to the native proteins.[67,73-75] Table 3-1 summarizes the kinetic and equilibrium constants for CO and O_2 binding to the reconstituted Mb's of this study. Comparison of our results with those of Sono et al.[73g] for deuteroheme-reconstituted horse heart Mb are in good agreement. As well, 2,4-dimethyl deuteroheme Mb has similar CO and O_2 binding properties to mesoheme

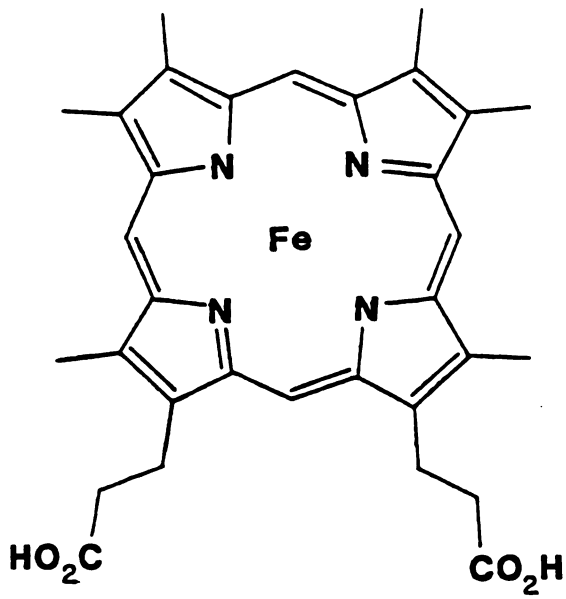

2,4 Dimethyl deutero

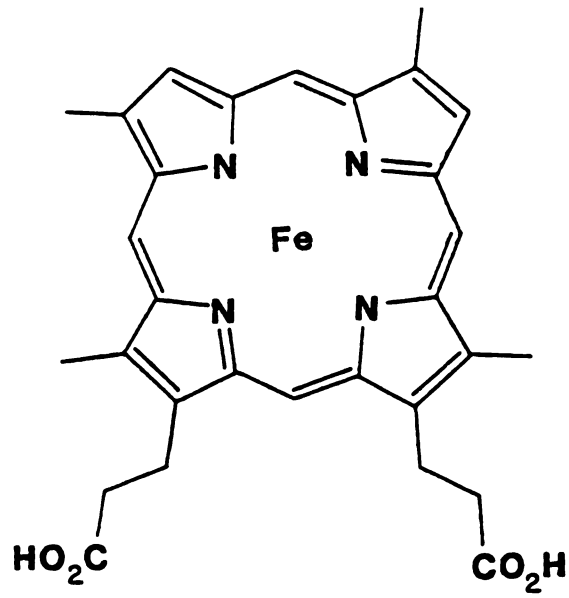

Deutero

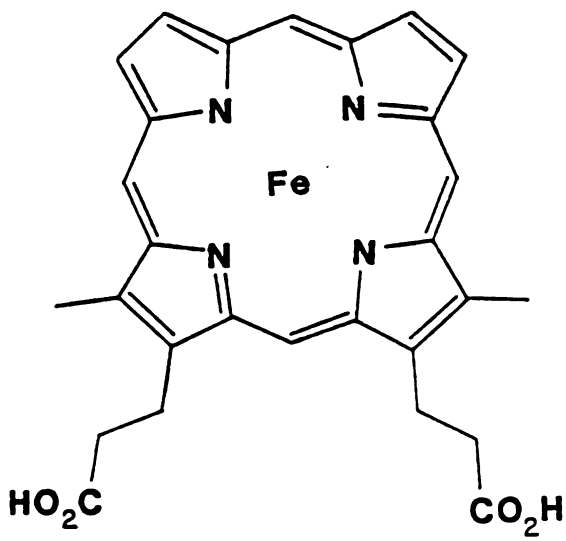

1,3 Didemethyl deutero

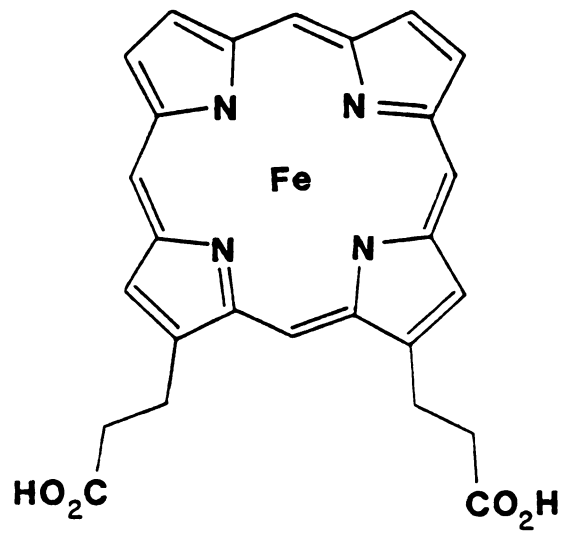

6,7 Dipropionic acid porphine

Figure 3-1. Structural formula of synthetic hemes used for myoglobin reconstitutions.

Table 3-1. Kinetic and Equilibrium Constants for CO and O_2 Binding.[a]

Myoglobins	Reaction with Co				Reaction with O_2			
	pK_3[b]	$P_{\frac{1}{2}}$ (torr)	l' (M^{-1} s^{-1})	l (s^{-1})	$P_{\frac{1}{2}}$ (torr)	k' (M^{-1} s^{-1})	k (s^{-1})	M
Protoheme (native and reconst.)	4.8	0.025	6.4×10^5	0.022	0.40	2.4×10^7	15	16
2,4-Dimethyl Deuteroheme	5.9	0.026	6.7×10^5	0.022	0.40	3.0×10^7	3.7	8
Deuteroheme	5.5	0.0074	1.9×10^6	0.019	0.23	3.2×10^7	13	31
"Bald" heme	5.2	0.0041	3.3×10^6	0.018	0.40	3.7×10^7	31	98
"Stripped" heme	5.0	0.020	6.5×10^5	0.017	0.26	1.9×10^7	21	13

[a] In phosphate buffer, pH 7.0, 20-22°C.

[b] In 2.5% SDS.

Mb, as obtained by the same authors.[73g] The results of the present study clearly indicate that the removal of peripheral methyl and vinyl groups of heme can change the ligand binding constants, particularly the carbon monoxide association of reconstituted myoglobins. As shown in Table 3-1, carbon monoxide association rates underwent a five-fold increase upon removal of peripheral methyl groups on going from 2,4-dimethyl deuteroheme Mb to the "bald" heme myoglobin, while O_2 association rates, for the same MB's increased only 20%. The behavior of "stripped" heme Mb, however, does not fit any trend.

That the ligand binding behavior of dealkylated heme reconstituted Mb's is not primarily caused by an electronic effect is evidenced by a comparison with the work of Sono et al.[73g] These workers have shown that ligand dissociation rates (CO and O_2) correlate with pk_3 of the porphyrin for horse heart Mb reconstituted with protoheme derivatives modified at positions 2 and 4. Also, with the exception of deuteroheme Mb, a similar correlation exists for ligand association (k' and l') rates and equilibrium constants (K and L). Their results predict that k, k', l, l' and L decrease and K increases with increasing pK_3 of the free base porphyrin. Since porphyrin dealkylation resulted in a slight decrease in pK_3 (see Table 3-1), from an electronic perspective, changing from "stripped" heme Mb to 2,4-dimethyl deuteroheme Mb, nearly all parameters (k, k', $P_{\frac{1}{2}}^{O_2}$, l and l') would decrease. From Table 3-1

only l seems to follow this prediction, even so, the very small decrease in l does not support such a correlation without question. The inability of electronic effects to account for the anomalous behavior of deuteroheme previously nor the results in Table 3-1 argues strongly that the modified ligand binding properties of our reconstituted Mb's are due to effects other than electronic.

Previously we[15d] and others[60] have shown that steric crowdedness near the ligand binding site in heme models greatly modifies the ligand association rate. For myoglobin, the steric hindrance from residues at the distal side has been postulated to cause a geometric distortion of the bound CO and therefore is responsible for differentiating CO and O_2 binding.[49] Mb reconstitution with dealkylated hemes which have a smaller bulk than protoheme would result in a looser fit of the heme into the heme pocket. This could result in a relaxing of the steric constraints surrounding the heme group. As noted earlier, any steric effect affecting CO and O_2 binding should principally be reflected in ligand association rate data. With the exception of "stripped" heme Mb, Table 3-1 reveals an apparent correlation between heme steric bulk and l' and to a much lesser degree, k'. Thus, if one assumes that the native tertiary structure remains intact for Mb's reconstituted with 2,4-dimethyldeutero, deutero, and "bald" hemes, then these results allow for the possibility of a steric effect differentiating CO and O_2 binding.

With the exception of the CO dissociation rate, the ligand binding properties of "stripped" heme Mb are anomalous when compared with the other dealkylated heme-containing myoglobins. It seems certain that the heme in the protein is still bound to the proximal imidazole since its CO dissociation is consistent with the other hemes (l is known to be dependent on the trans ligand effects[12a,15b]) and the spectral shifts upon ligation and oxidation are similar to the other myoglobins (Table 3-2 and Figure 3-2). However, the absorption spectrum of this Mb is remarkable in that all absorption maxima shift bathochromically relative to the "bald" heme Mb. In contrast, visible absorption peaks of pyridine hemochrome of both hemes are essentially identical. This can only be attributed to modulations by local environment. A similar case reported by Sono et al.[73a] noticed that Mb's reconstituted with spirographis and isospirographis hemes exhibit different absorption maxima even though the two hemes have the same spectrum outside the protein. In view of the fact that the association rates are slow in comparison with the other demethylated systems, it would appear that the lack of position 5 and 8 methyl groups would allow a protein conformational change producing a more crowded ligand binding site.

To probe this heme substituent effect further, the stability of the various oxymyoglobins was examined and their autoxidation kinetics are presented in Figure 3-3.

Table 3-2. Absorption Spectral Maxima of Synthetic Hemes and Myoglobins.[a]

Mb/Heme	Soret (nm)	Visible Bands (nm)		
2,4-Didemethyl deuteroheme				
met Mb	395	495		623
deoxy Mb	422		544	
O_2 Mb	403	532		567
CO Mb	409	530		556
pyridine hemochrome[b]	406	515		545
Deuteroheme				
met Mb	393	495		623
deoxy Mb	421		543	
O_2 Mb	402	530		565
CO Mb	409	529		555
pyridine hemochrome[b]	405	513		543
"Bald" heme				
met Mb	389	492		620
deoxy Mb	417		538	
O_2 Mb	401	528		559
CO Mb	406	525		550
pyridine hemochrome[b]	403	509		538
"Stripped" heme				
met Mb	395	495		623
deoxy Mb	422		545	
O_2 Mb	403	533		568
CO Mb	409	529		555
pyridine hemochrome[b]	401	509		538

[a]In phosphate buffer, pH 7.0; [b]In pyridine — CH_2Cl_2.

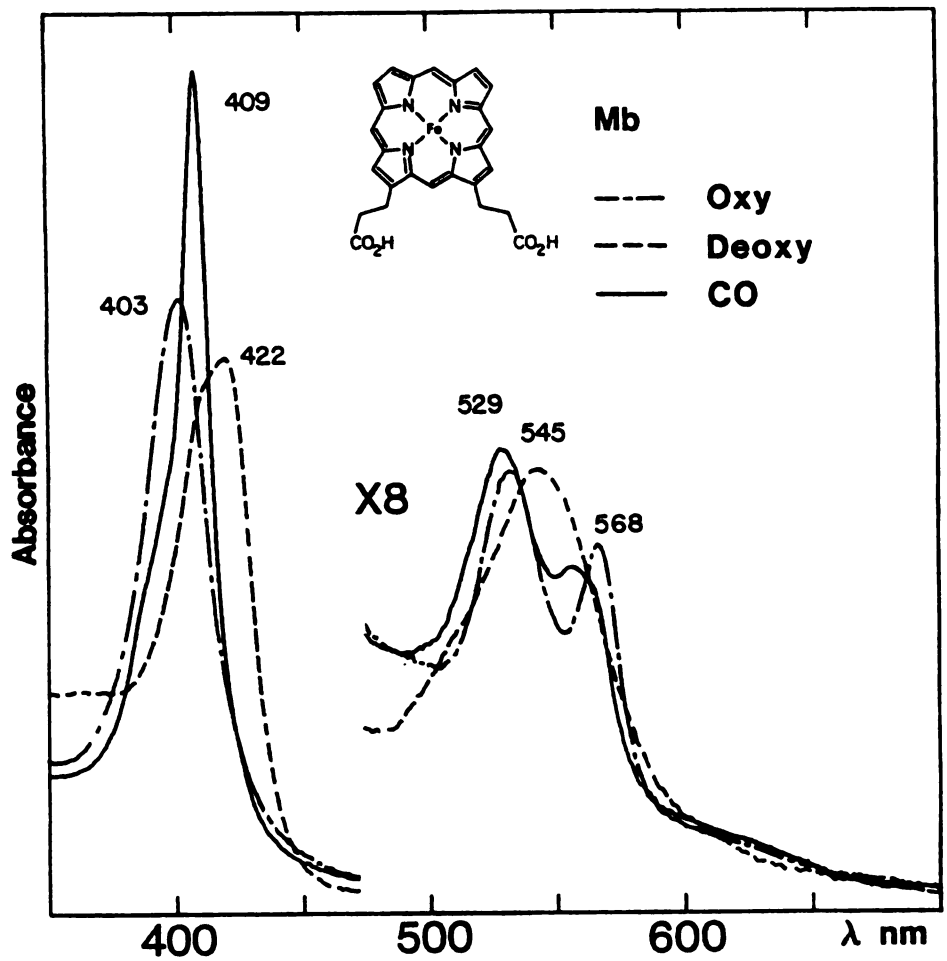

Figure 3-2. Optical spectra of "stripped" heme myoglobin; Oxy (—•—), Deoxy (— — —), CO (——), in 0.1 M (pH 7.0) potassium phosphate buffer.

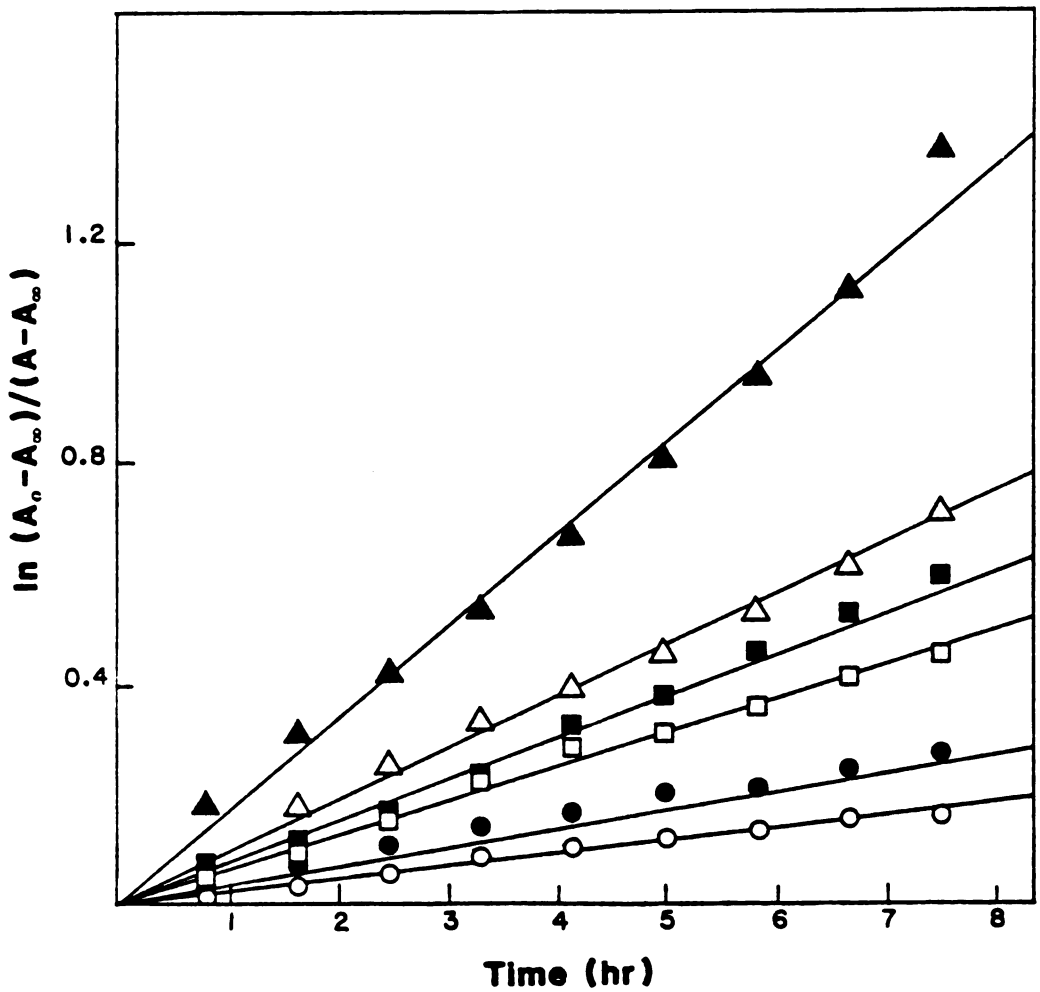

Figure 3-3. Autoxidation of reconstituted myoglobins.

Protoheme (native)	slope: 0.39×10^{-3} s^{-1}	corr. coef.: 0.996
Proto (reconst.)	0.56×10^{-3} s^{-1}	0.995
2,4 Me_2	1.25×10^{-3} s^{-1}	0.981
Deutero	1.04×10^{-3} s^{-1}	0.997
"Bald"	1.56×10^{-3} s^{-1}	0.997
"Stripped"	2.79×10^{-3} s^{-1}	0.994

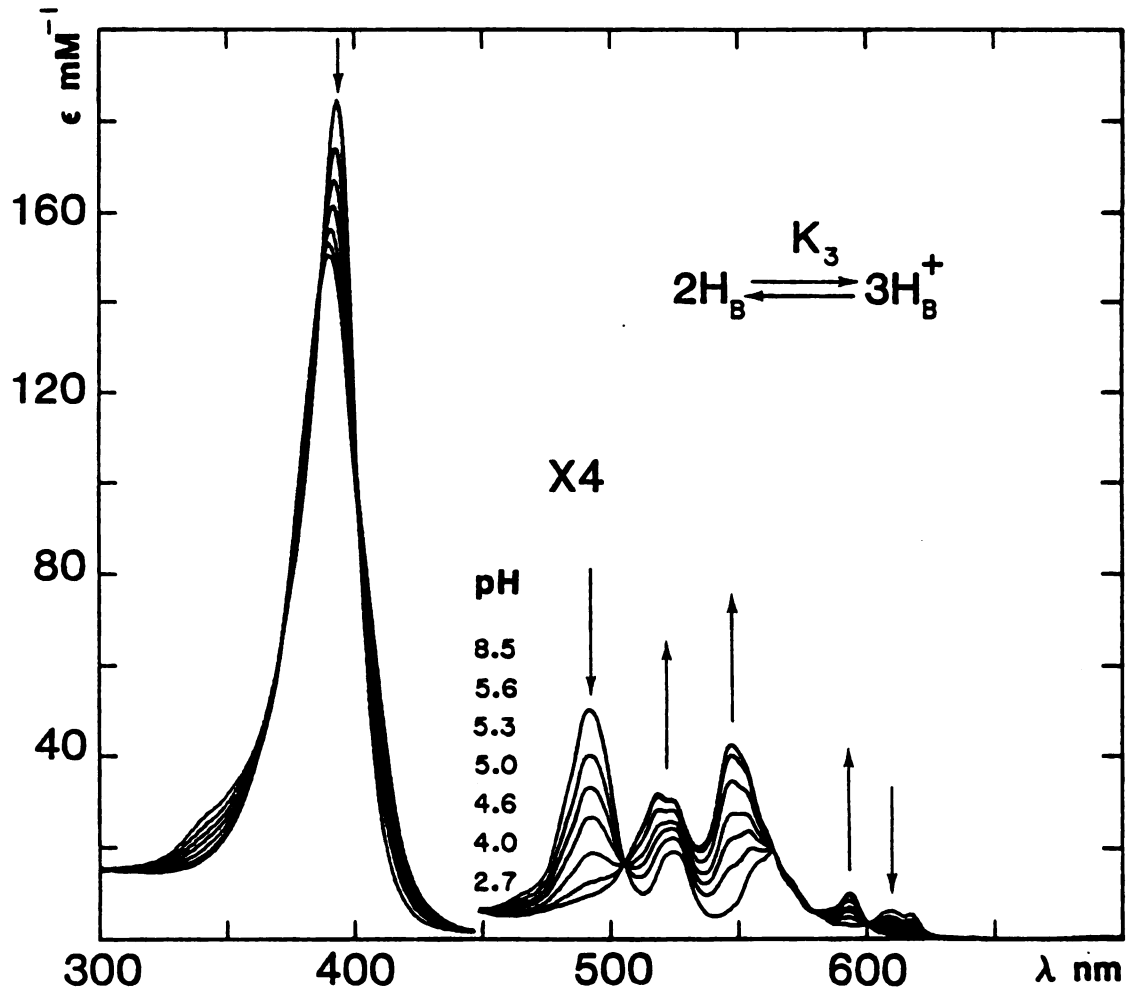

Figure 3-4. pH titration of "bald" porphyrin in 2.5% sodium dodecyl sulphate.

As is apparent, the "stripped" heme Mb stands alone in that the other myoglobins (2,4-dimethyl deutero, deutero and "bald") are approximately within experimental error of one another. The rapid oxidation of the "stripped" Mb cannot be attributed to electronic effects; on the contrary, autoxidation rate is usually slowest in acidic (electron deficient) hemes.[23] In a recent communication LaMar[76] has shown by ^{1}H NMR that myoglobin reconstituted with protohemin or carbonylheme results immediately in a statistical (1:1) heterogeneous Mb mixture, which slowly equilibrates to a ratio of 12:1. The heterogeneity is believed to be from a rotational disorder of the holoprotein. The equilibration (heme reorientation) probably occurs via a heme-protein dissociation-association pathway, during which the proximal imidazole-heme iron bond must rupture. This finding provides for the possibility that one pathway of myoglobin autoxidation[77] may involve heme-protein dissociation. Thus, a heme pocket conformational change could result in a faster heme-protein dissociation and hence accelerated autoxidation. In any event that the "stripped" Mb stands alone with regard to autoxidation lends support to our speculation that Mb reconstitution with this particular heme produced a holoprotein comprising a modified heme environment which is at variance with the native myoglobin.

Conclusion

If one assumes that the protein tertiary structure of various reconstituted Mb's retains their native conformation, our results suggest that there is an apparent ligand specificity associated with heme size. To a first approximation, this may be interpreted as evidence for the operation of a steric effect regulating ligand specificity since if the above assumption is true then the dealkylated hemes should fit the heme crevice in a looser manner, allowing residues near the oxygen binding site to become less constrained and thereby decreasing distal steric controls on ligand binding. However, this cannot be considered as a general rule in Mb reconstitution experiments since it is not known to what extent structural modifications of the prosthetic groups would cause functionally significant alterations on the protein. It is indeed unexpected that the removal of the 5 and 8 methyl groups should bring about a sudden turn in the trend. If the anomalous behavior of the "stripped" heme Mb is due to a protein conformational effect, it would suggest that the 5 and/or 8 methyl groups are critical for maintaining the nativeness of the protein. This result opens the question as to what effect side chain positions have on protein function. Previous reconstitution studies on b-type hemoproteins invariably centered on variations in the 2,4 positions of protoheme. The present

work reveals a seemingly obligatory role of the other methyl groups in determining the properties of the protein.

Materials and Methods

Myoglobins:

Horse heart myoglobin (Sigma, type III) was used as received. Heme extraction and myoglobin reconstitution were carried out using standard procedures.[78] 2,4-dimethyl deuteroporphyrin IX,[67] deuteroporphyrin IX,[79a] 1,3-didemethyl deuteroporphyrin IX,[79b] and porphine 6,7-dipropionic acid[79b] were synthesized according to previously described methods. Iron was inserted by the ferrous sulfate method.[80] For kinetic and equilibrium measurements, metMb's in pH 7.0, 0.1 M potassium phosphate buffer were reduced with a minimum amount of aqueous sodium dithionite in an argon atmosphere. The previously described photochemical reduction method was employed for spectral characterization.[9]

Kinetic Measurements:

The flash photolysis technique was used to measure CO and O_2 association rates. The laser/xenon flash photolysis apparatus, the tonometer, and procedures for sample preparations have been previously described.[28] $P_{\frac{1}{2}}^{CO}$ was determined by titrating deoxyMb's with a 0.82% CO in

argon gas mixture. The M values were measured by titrating oxyMb's with CO which were previously equilibrated with 500 torr O_2. $P_{\frac{1}{2}}^{O_2}$ was calculated by $P_{\frac{1}{2}}^{O_2} = M \times P_{\frac{1}{2}}^{CO}$, which were in excellent agreement with $P_{\frac{1}{2}}^{O_2}$ values obtained by direct titration and obtained from kinetic measurements according to the Gibson equation:[65]

$$1/R = 1/k + K[O_2]/'[CO] ,$$

where l'[CO] is the pseudo-first order rate constant measured before introducing O_2, R is the displacement rate of oxyMb by CO, k is the O_2 dissociation rate constant and K is the O_2 equilibrium constant. The dissociation rate constants l[CO] and k[O_2] were calculated from $L = l'/l$ and $K = k'/k$, respectively where $L = (P_{\frac{1}{2}}^{CO} \times 1.35 \times 10^{-6}$ M /torr$)^{-1}$ and $K = (P_{\frac{1}{2}}^{O_2} \times 1.80 \times 10^{-6}$ M/torr$)^{-1}$. In all experiments, the myoglobin concentration was approximately 10^{-5} M.

pK_3 Titrations:

A small amount of free base porphyrin was dissolved in 0.2-0.3 ml glacial acetic acid which was then added dropwise to an unbuffered 2.5% SDS solution to a Soret absorbance of ca. 1.9. The pH was adjusted to 8-10 followed by acidification with conc. HCl. The optical spectra were measured as a function of pH (Figure 3-4 shows the spectra of "bald" porphyrin as a function of pH). The pK_3 value obtained for deuteroporphyrin

dimethyl ester was within 0.1 pH units of that reported in reference 80.

CHAPTER 4

POLARITY CONTROL OVER LIGAND BINDING TO HEMOPROTEINS. KINETICS OF OXYGEN AND CARBON MONOXIDE BINDING TO HEME MODELS EQUIPPED WITH POLAR GROUPS NEAR THE COORDINATE SITE

Introduction

Heme protein ligand specificity is a topic of current interest.[49,50,52,65,70,81-85] Judging by the various functions heme proteins must perform it seems logical to conclude that the way a protein interacts with the heme determines the specificity of function for that protein. A vivid example can be seen in the oxygen transport and storage proteins hemoglobin (Hb) and myoglobin (Mb). For various Hb's and Mb's, that O_2 vs. CO affinity ratios (M-values) are variable[49,70,84,85] and that these values in general are reduced in magnitude relative to simple heme model compounds[28,55,56,86] exemplifies the protein influence. This ligand binding specificity is probably not caused by a single dominant steric effect, although some have proposed so, but rather by a combination of several effects which optimize O_2 binding. One such effect is the polarity surrounding the heme group. In previous model systems it

has been shown that O_2 binding to hemes is very sensitive to solvent polarity, owing to the dipolar nature of bound O_2, whereas CO is relatively insensitive.[28,55] However, solvent effects alone cannot mimic the action of a protein in that the protein acts as an "ordered solvent" which maximizes the efficiency of its function. For instance, recent neutron diffraction studies on oxyHb[87] and oxyMb[88] have revealed that the terminal oxygen of FeO_2 is within hydrogen binding distance of the distal imidazole proton, yet kinetics of oxygen binding to model hemes in protic solvents[28,55] did not show large differences from those in polar aprotic media. In order to investigate the distal polarity effect, synthetic heme models having a wide range of polar groups situated at different positions from the heme center are required. Here we report the kinetics of O_2 and CO binding to hemes equipped with groups of varying dipole moments at various distances from the heme center as well as compounds capable of providing a hydrogen bond to the bound ligand. By studying the O_2 and CO binding of these compounds in identical environments (i.e. in toluene) we can quantify a distal polarity effect where the heme cavity may be viewed as containing a dominant dipole and/or H-bond donor in a hydrophobic environment.

Results and Discussion

Oxygenation Kinetics:

In an effort to quantify distal polarity and hydrogen bonding effects, compounds 1a-g and 2a,b (Figure 4-1) were synthesized.[89] We chose not to directly compare the compounds in Table 4-1 with those in Table 4-2 since 1) the proximities of the dipoles to heme center are very different; and 2) the size of the distal substituents may result in very different solvation. For compounds 1b-g 3,5-disubstitutions on benazmide were chosen so that the orientation of the m-substituent would be inconsequential. The use of monosubstituted benzene dipole moments[90] in fitting the ligand binding data in Table 4-1 seems reasonable for two reasons. First, the dipole used is the closest to the heme center, thus it should dominate any other dipoles. Secondly, the benzamide-porphyrin linkage is constant throughout the series; thus its contributions should be nearly constant.

Table 4-1 contains the kinetic and binding parameters of O_2 and CO for a series of compounds differing principally in the dipole moment of the phenyl substituent above the O_2 binding site. Fitting the oxygen binding data as described in the theoretical section, results in the following dependence of k' and k on dipole moments, where μ_g is the dipole moment of the substituent.

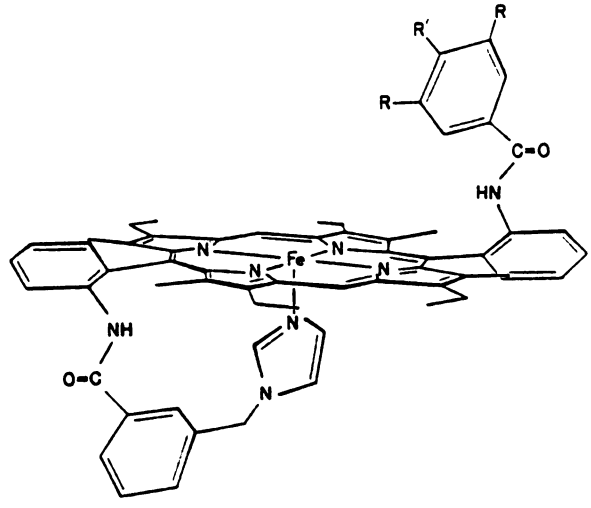

1a R = H R' = t-Bu
b R = CH_2OMe R' = H
c R = CH_2OH R' = H
d R = $CO_2C_4H_9$ R' = H
e R = $CONHC_4H_9$ R' = H
f R = $CONEt_2$ R' = H
g R = CONi-Pr_2 R' = H

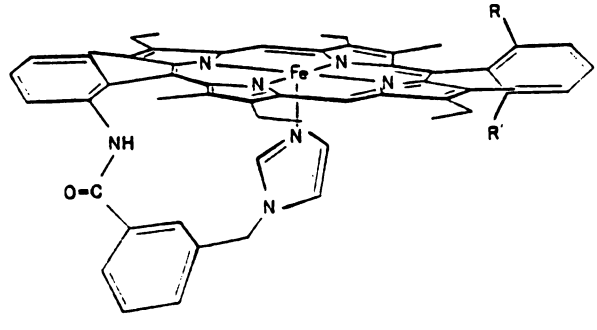

2a R = H R' = $NHCOCH_3$
b R = $NHCOCH_3$ R = H

Figure 4-1. Structural formula of diphenyl hemes.

Table 4-1. CO and O_2 Binding Constants of Diphenyl Hemes with Groups of Varying Polarity Situated Near the Ligand Binding Site (20-22°C).[a]

Compound	μ_g[b]	k' (M^{-1} s^{-1})	k (s^{-1})	$P_{\frac{1}{2}}^{O_2}$ (torr)	l' (M^{-1} s^{-1})	l (s^{-1})	$P_{\frac{1}{2}}^{CO}$ (torr)	M[c]
1a 4-t-Butyl	0.52	4.7×10^7	15,500	33	2.5×10^6	0.14	0.0057	5,800
1b 3,5-CH_2OMe	1.3	2.6×10^7	9,900	38	1.1×10^6	0.028	0.0075	15,000
1c 3,5-CH_2OH	1.7	2.3×10^7	2,900	13	1.2×10^6	0.090	0.0075	1,700
1d 3,5-CO_2nBu	1.9	2.2×10^7	11,000	48	1.5×10^6	0.13	0.0086	5,600
1e 3,5-CONHnBu	3.6	1.3×10^7	300	2.3	1.3×10^6	0.042	0.0032	720
1f 3,5-$CONEt_2$	3.8-3.9	1.4×10^7	4,750	34	0.59×10^6	0.048	0.0081	4,200
1g 3,5-$CONiPr_2$	3.8-3.9	1.3×10^7	9,300	72	0.47×10^6	0.053	0.011	6,500

[a]Toluene.
[b]Reference 20.
[c]$P_{\frac{1}{2}}^{O_2}/P_{\frac{1}{2}}^{CO}$.

Table 4-2. CO and O_2 Binding Constants of Diphenyl Hemes with Remote Polar Groups (20-22°C).[a]

Compound	k' (M^{-1} s^{-1})	k (s^{-1})	$P_{\frac{1}{2}}^{O_2}$ (torr)	l' (M^{-1} s^{-1})	l (s^{-1})	$P_{\frac{1}{2}}^{CO}$ (torr)	M[e]
2a *cis* acetamide	3×10^7[b]	38,000	126	2.3×10^6	0.12	0.0054	23,000
2b *trans* acetamide	2.6×10^7	4,100	16	1.6×10^6	0.072	0.0045	3,550
ether strap[c,d]	3.0×10^8	40,000	18.6	6.8×10^7			
amide strap[c,d]	3.6×10^8	5,000	2	3.5×10^7			

[a] In toluene.

[b] Due to the low O_2 affinity high oxygen concentrations were necessary leading to pseudo-first order rate constants approaching the limits of detection.

[c] Axial base was a covalently attached pyridine.

[d] Reference 21.

[e] $P_{\frac{1}{2}}^{O_2}/P_{\frac{1}{2}}^{CO}$.

$$\ln k'_{calc} = 0.0925\mu_g^2 - 0.748\mu_g + 18.0$$

$$\ln k_{calc} = -0.0148\mu_g^2 - 0.263\mu_g + 9.73$$

Figures 4-2 and 4-3 show plots of the calculated rate constants vs. the observed rate constants. The dipole moments used were those of unsubstituted phenyl models or reasonably close approximations.[90] The striking linearity of Figure 4-2 (correlation coefficient 0.994, slope 1.06) shows that oxygenation behavior can be affected in a predictable manner by the magnitude of a nearby dipole. The linearity of Figure 4-3 (correlation coefficient 0.967, slope 0.995) is not quite as ideal as Figure 4-2, however, the most striking feature is the very large deviations from the calculated line of the compounds capable of hydrogen bonding, namely the 3,5-CONHnBu and 3,5-CH_2OH.

Prior to 1940 quadratic equations correlating reaction rates and acidity constants with dipole moment data were emperically developed.[91] These equations have the same form as Equations 7 and 9 (see theoretical section). Concurrent with the earlier work, the Hammett free energy relationships were being developed. Since little work has appeared after about 1940, it seems as though the success of the Hammett correlations left such dipole moment correlations by the wayside. Thus, there appears to be no theoretical explanation for the observed quadratic dependence of reaction rates on substituent dipole moments.

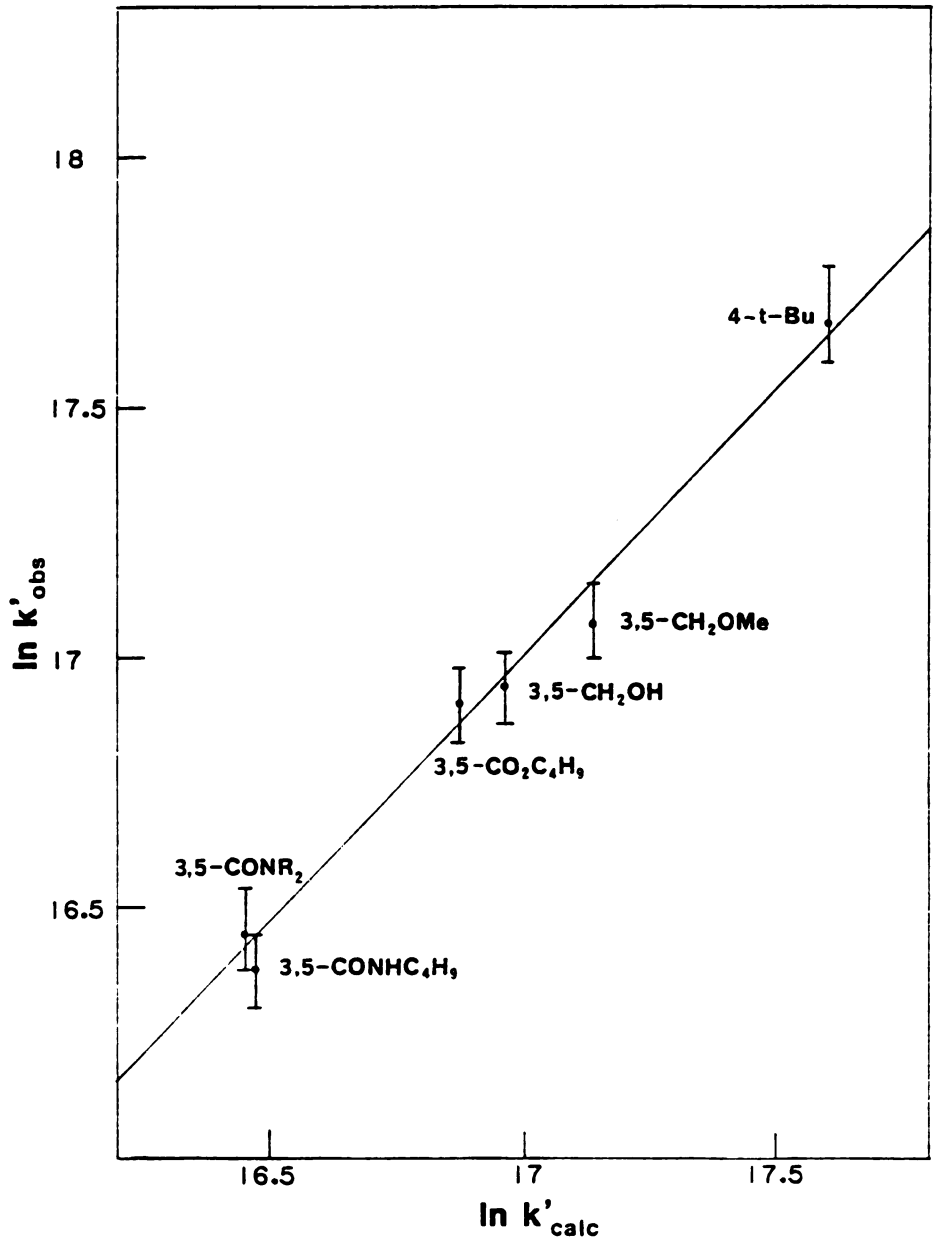

Figure 4-2. Correlation between $\ln k'_{calc}$ and $\ln k'_{obs}$.
$\ln k'_{calc} = 0.0925\mu_g^2 - 0.748\mu_g + 18.0$.
Correlation coefficient: 0.994. Slope: 1.06.

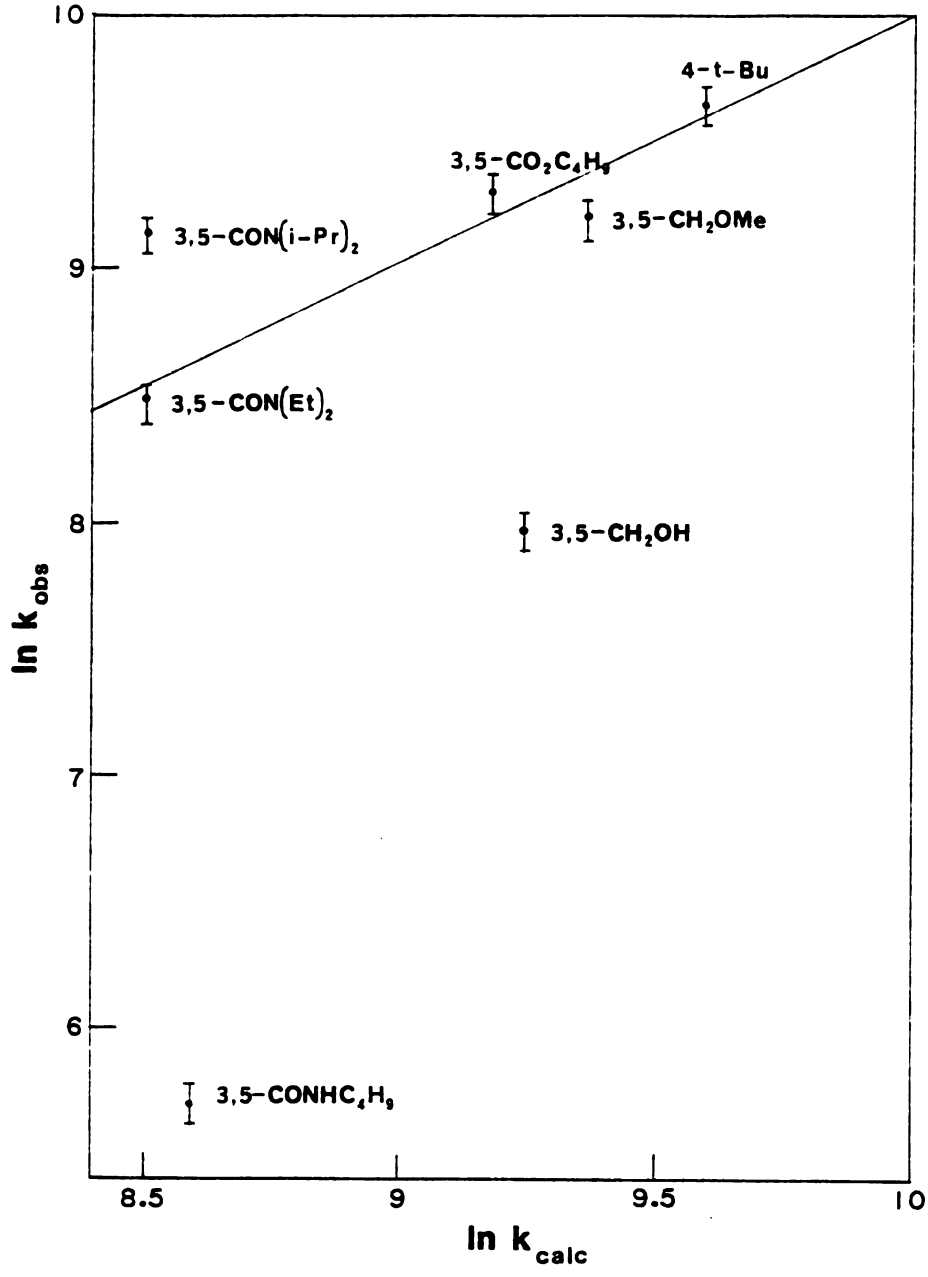

Figure 4-3. Correlation between $\ln k_{calc}$ and $\ln k_{obs}$.
$\ln k_{calc} = -0.0148\mu_g^2 - 0.263\mu_g + 9.73$.
Correlation coefficient: 0.994.
Slope: 0.995 (calculated without 1c,1e).

The quadratic functional form for the dependence of ln k (k') on a local dipole moment can be obtained without including dipole-dipole polarization terms. In effect, replacing the polarization scalers by unity and the polarization vectors by zero in Equations 6 and 8 (theoretical section) yields such equations. However, the "unpolarized" equations are not intuitively satisfying. The signs of the coefficients on μ_g^2 obtained from fitting Equations 7 and 9 to the observed O_2 rate data dictate that the radius of the deoxyheme (r_D) is greater than the transition state ($r_\ddagger$) which is greater than the oxyheme complex (r_B). This does not constitute a proof that the model presented in the theoretical section is necessarily complete, it does suggest that the interaction between FeO_2 and a local dipole is more than the vector sum of their respective dipoles. Unfortunately, the large number of parameters in Equations 6 and 8 makes physical interpretation of them difficult. The dipole-dipole interaction thought to occur in the oxyheme complexes is shown pictorially in Figure 4-4.

The unmistakable linearity in Figure 4-1 indicates that dipole-dipole interactions, interpreted here as polarization, in the transition state plays a dominant role in O_2 binding to the models studied. Assuming an early transition state,[70] the increased scatter in Figure 4-3 is not surprising since oxygen dissociation should be more dependent on orientation parameters than

Figure 4-4. Relative orientation of FeO_2 dipole and dipole of a 3,5 disubstituted benzamide (A). Scale drawing[a] of the relative orientations and distances of an FeO_2 dipole and an unconstrained o-phenyl amide dipole[b] (B).

[a]From ref. 94b; [b]For acetanilide ref. 105.

association. Comparison of the O_2 rate data for diethyl amide (1e) with that of diisopropyl amide (1f) indicates that the difference in O_2 binding is primarily in O_2 dissociation. It is rationalized that the bulkier diisopropyl amide may not be able to assume an orientation in which the amide dipole and FeO_2 dipole achieve maximal head-to-tail alignment. As well, it may also restrict the distance at which the two dipoles approach one another. Indeed CPK models predict that such a situation might exist. The electrostatic potential relationship[92] (Equation i) predicts that both processes should result in a lower O_2 affinity for 3,5-diisopropyl benzamide substituted heme relative to the diethyl amide.

$$\psi = \mu \cos \theta / r^2 \ , \qquad \text{(i)}$$

where ψ is the electrical potential; μ, the dipole moment; r, the distance between dipoles; and θ, the angle between dipoles.

In addition, the 4-t-butyl benzamide heme deviates from a simple rule of thumb relationship consisting of "the more polar, the higher the affinity". This could be rationalized as a dipole-dipole orientation and/or distance effect as above. However the unmistakable linearity of Figure 4-2 as well as the congruence to the trend in Figure 4-3 argue against this rationalization and suggest that oxygen affinity need not adhere to such a simple relationship. This is understandable since O_2 association

is dependent on the dipolar forces in the transition state while dissociation is dependent in both the transition state and oxyheme complex. Thus the O_2 affinities in Table 4-1 reveal that $P_{\frac{1}{2}}$ reaches a maximum for the 3,5-dibutyl ester (neglecting the di-isopropyl amide). In fact a TPP based capped porphyrin in which the cap was linked to the porphyrin via ether and ester linkages actually discriminates against oxygen.[60b,93] From this then the polarization of the transition state and the oxyheme complex seem to be unequal, i.e. $\alpha \neq \alpha_{\ddagger}$ (see theoretical section).

Somewhat disconcerting is that upon increasing the polarity of the distal side results in slower O_2 association. This too is consistent with an early oxyheme transition state. Increased polarization of O_2 in the transition state results in a more product-like activated complex, hence decreasing O_2 dissociation rates. If this is indeed the case then by microscopic reversibility O_2 association would also be reduced.

The results obtained here indicate that placing a dipole at close proximity to the heme center produces kinetic and thermodynamic control of the reaction between O_2 and ferroheme. That this control is due to polarization of FeO_2 is further evidenced by the data in Table 4-2 which shows the binding parameters of O_2 and CO to hemes equipped with groups of differing dipole moments at greater than 4 Å[94] from the heme center on one face and covalently linked

bases on the other. In order to assure no electronic effects, cis-trans rotomers were chosen, in which the polar acetamido group is on the same (trans) and opposite (cis) of the O_2/CO binding site. The other two entries in Table 4-2 are of Momenteau and Lavalette[95] in which amide and ether linkages were used to supply an alkyl strap across the distal heme face. The results are essentially identical.

These data suggest that the enhanced O_2 affinity of the trans-amides relative to the cis-acetamide or ether would be due to a head-to-tail alignment of the Fe-OO and amide dipoles. That this may be the case is evidenced by the strong dependence of k which increases by 8-900% on going from the same side amide system to the cis-acetamide or ether strap. Furthermore, we believe that this enhanced affinity is derived from a constructive dipole-dipole interaction and not a direct interaction such as hydrogen bonding. In the crystal structure of FeO_2 (TpivPP) (1 MeIm)[94] there exists a four way statistical disorder of the terminal oxygen atom which bisects the N_{PYR}*Fe*N_{PYR} angle and thus points toward the amide "picket" moieties. The crystallographic structure shows the terminal oxygen to N_{AMIDE} distance to be approximately 4 Å, which is too far for effective H-bonding. Assuming in solution the structure remains for the oxyheme complex as in the crystal than an Fe-OO dipole would align in a constructive mode with the amide dipole (see Figure 4-4B)

resulting in a net increase of the FeO_2 dipole moment. Thus, it seems reasonable to conclude that the stabilization is the result of increased polarization of FeO_2 producing a more ferric superoxide-like compound rather than an $Fe(II)O_2$. In this regard, deviations between experimental[96,97] and theoretical[98] considerations may become unified since calculations do not consider the effects of the local environment resulting in polarization of the FeO_2 moiety.

In the absence of other model heme-O_2 complexes of known structure, a dipole-dipole alignment mechanism provides an alternative rationale for O_2 orientation relative to the heme axis. We notice that in oxy hemoglobin[49,87,99] and oxy myoglobin[88,100] the 0-0 axis eclipses an N_{PYROLE}-Fe bond whereas in picket fence heme[94] it bisects the N_{PYR}-Fe-N_{PYR} angle. Inspection of stereoviews of the active sites for oxy Hb[88] and oxy Mb[89] reveals that an FeO_2 dipole may be somewhat aligned with the distal histidine dipole in a head-to-tail fashion besides being hydrogen bonded.

The most striking feature in Figure 4-3 is the large deviations from the calculated line of the 3,5-di-n-butyl amide and 3,5-dibenzylic alcohol substituted hemes. These deviations are accounted for in terms of hydrogen bonding to iron bound O_2. Comparison of Figures 4-2 and 4-3 reveals that the primary amide and alcohol lie on the calculated line for O_2 association whereas significant deviations occur in oxygen dissociation. This is the

result of hydrogen bond formation occurring subsequent to a rate limiting process.

Estimated hydrogen bond strengths for the n-butyl amide (1d) and benzyl alcohol (1c) are 1.6 and 0.6-0.8 Kcal/mole, respectively. These are the $\Delta\Delta G$ values for the n-butyl vs. diethyl amide and benzyl alcohol vs. benzyl methyl ether or butyl ester where $\Delta G = -RT \ln K$. Such a calculation should be regarded as qualitative since these calculations assume that the magnitude of the local dipole moment and that the FeO_2 dipole and local dipole orientation are independent of hydrogen bonding. Figure 4-5 shows the effect of dipole-dipole interactions and hydrogen bonding on a simple reaction coordinate for heme oxygenation.

Carbonylation Kinetics:

Since free carbon monoxide has a dipole moment ($\mu_{CO} = -0.112$ D[101]) and bond formation between Fe and CO increases the dipole moment of CO,[85] it would be expected that dipole-dipole interactions should play some role in carbonylation kinetics. Consistent with previous solvent studies[28,55] we find little correlation between CO kinetics and the magnitude of a local dipole moment. The lack of correlation is explainable from Equation 1 in the theoretical section. It would appear that electrostatic perturbations on carbonylation are outweighed by non-electrostatic

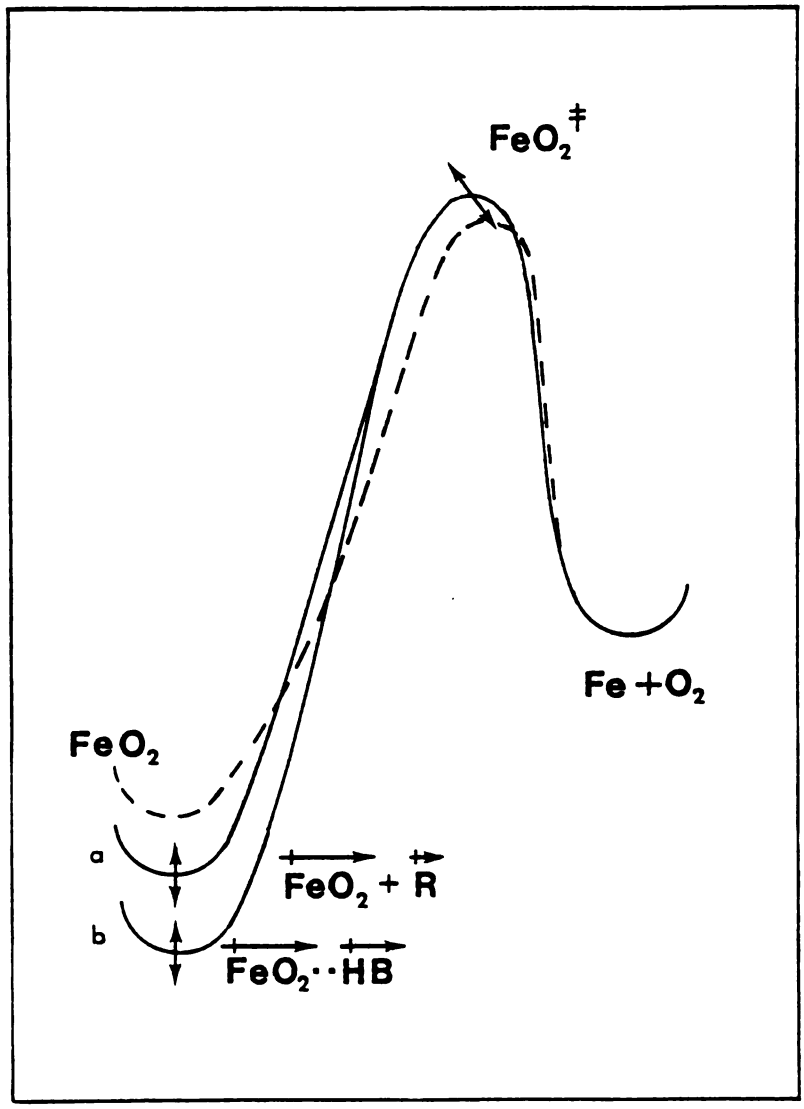

Figure 4-5. Schematic representation of a proposed simplified reaction coordinate of heme oxygenation. Hypothetical unperturbed coordinate (---), plus an interacting dipole ([a]——) and hydrogen bonded oxyheme complex ([b]——).

factors. This dependence could be explained in terms of the size and position of the phenyl substituent.

Previously we[15d] and others[60] have shown that a distal steric effect differentiating CO and O_2 binding will be most pronounced in the association rate constants. Indeed, a comparison of the 3 amides in Table 4-1 shows that increasing the size of N substitution regularly decreases 1' with almost no effect on 1. Oxygenation however remains almost constant. Furthermore, compounds 1b-d have very similar CO association rates which differ significantly from 1a. This may be attributed to the position of substitution on the benzamide distal substituent. CPK models reveal that at the heme center compounds 1b-d have similar steric bulk which is not present in 1a. Although this does not constitute a proof for the existence of a steric effect differentiating CO and O_2, it is noteworthy that with the exception of the O_2 dissociation rate, the 3,5-diisopropyl amide (1g) has CO and O_2 kinetic rate constants very similar to Mb ($1' = 3\text{-}5 \times 10^5\ M^{-1}\ s^{-1}$, $1 = 0.0015\text{-}0.04\ s^{-1}$, $k' = 1\text{-}2 \times 10^7\ M^{-1}\ s^{-1}$, $k' = 10\text{-}30\ s^{-1}$.[65] The possibility of hydrogen bonding to carbonylated hemoproteins has previously been discussed.[102] It is evident that compounds 1c and 1e can provide a hydrogen bond to FeO_2 yet the possibility of hydrogen bonding has no effect on carbon monoxide kinetics. That is to say, if hydrogen bonding is occurring in our models is has no effect on carbonylation kinetics.

Distal Steric Effect:

Recently much effort has been put forth in the synthesis and characterization[15d,60,93] of models aimed to test the distal steric effect hypothesis.[49,50,95,103] It is well-established that a distal steric effect does modify oxygen and carbon monoxide association rates[15d,60] but the effect on dissociation rates, primarily oxygen, is in question. Conflicting results have been obtained for oxygen dissociation rates as a function of steric encumbrance.[15d,60] From the work presented here it becomes evident that the lack of a clear cut answer to steric differentiation could mainly be due to dipole-dipole and/or hydrogen bonding variability within a seemingly congruent series of compounds.

Collman's picket fence-based compounds showed marked decreases in O_2 dissociation rates upon shrinking the cavity of the ligand binding site. The reported oxygen dissociation rates are, respectively, 2900, 71, and 9 s^{-1} for $FePiv_3$5ClIm, FeMedPoc(1 MeIm) and FePocPiv (1 MeIm).[60b] From CPK models it appears that the introduction of the phenyl cap on top of the heme face (pocket hemes) results in a pulling of the amide moieties toward the heme center (Figure 4-6). This would bring about a closer head-to-tail dipole-dipole interaction between the amides and FeO_2, relative to Fe picket fence. In fact for FePocPivP it appears that the amide proton may come close enough for hydrogen bonding.

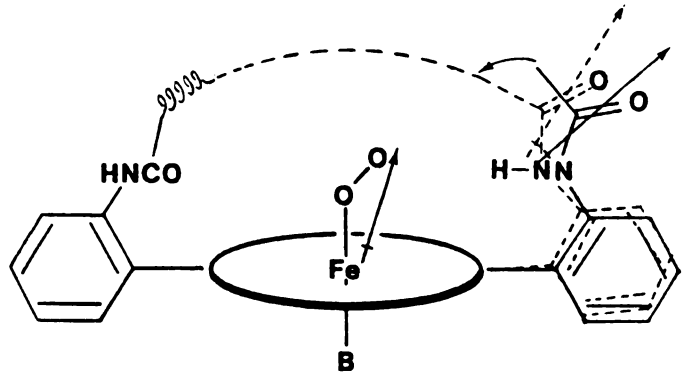

Figure 4-6. The change in dipole orientation upon introduction of a tight strap across the heme face. (——) unconstrained o-phenyl amide. (---) sterically encumbered model.

The alkyl amide linkages of Traylor's cyclophane hemes[602] should be flexible enough to rotate and it is not difficult to find conformations in which the amide dipole may align itself in a head-to-tail manner with FeO_2. On expanding the length of the anthracenyl strap, the amide dipole would become more distant from the heme center. Oxygen dissociation rates for Fe 6,6-cyclophane heme ($k = 800\ s^{-1}$) and Fe 7,7-cyclophane heme ($k = 1000\ s^{-1}$) are consistent with this interpretation. Our linear chain strapped hemes also showed this correlation;[15d] on increasing the strap length we obtained an increase in oxygen dissociation rate: 250, 175, 130 s^{-1} for FeSP-15, -14, and -13 respectively.

Among all sterically hindered models which contain amide linkages, the only inconsistency is the O_2 dissociation rate data for our Fe-Cu cofacial diporphyrins where k for Fe-Cu-4 and Fe-Cu-5 is 160 and 91 s^{-1}, respectively.[15d] We believe that this is due to the relatively large distance between the amide group and the heme center, which renders the dipole interaction relatively insignificant. Expanding the diporphyrin gap may also result in an increased accessibility to FeO_2 by polar molecules present in the system, i.e. imidazoles. This is not the case with the strapped hemes since the linear hydrocarbon chain provides much less shielding than does the Cu porphyrin cap.

Our contention is that with models so far available, it is still not possible to judge the steric differentiation

between CO and O_2 based upon the affinity ratio M since one cannot ascertain how much change in O_2 dissociation rates comes from pure ligand distortion and how much is due to dipolar effects, let alone the effects of bending and ruffling of the porphyrin plane introduced by the encumbrance.

Summary

Our work presented definitive evidence showing that both short and long range dipolar forces as well as hydrogen bonding can play a significant role in regulating oxygen affinities to heme proteins. While this general conclusion is consistent with previous solvent studies,[28,55] the use of covalently attached polar groups offered much greater advantages in probing the micro-environment of the heme coordination site. We have demonstrated that while dipolar forces can produce kinetic and thermodynamic control, hydrogen bonding provides an additional path for thermodynamic control of heme oxygenation. In contrast, CO binding to hemes is little affected by distal polarity effects.

Theoretical Section

In general[92] the reaction constant between two dipolar molecules in a medium of dielectric constant ε is related to an unperturbed rate constant (k_0) by

$$\ln k = \ln k_0 - (\varepsilon-1)/kT(2\varepsilon-1)\left[\frac{\mu_A^2}{r_a^3} + \frac{\mu_B^2}{r_B^3} - \frac{\mu_\ddagger^2}{r_\ddagger^3}\right] + \Sigma\Phi/kT \qquad (1)$$

where μ_A, μ_B and $\mu_\ddagger$ are dipole moments of the reacting species and transition state respectively, r_A, r_B and $r_\ddagger$ are molecular radii, $\Sigma\Phi$ is the perturbation due to non-electrostatic forces (i.e. H-bonding, steric effects, etc.) and kT has its usual meaning. Equation 1 is usually used to investigate solvent effects of a particular reaction (ε is a variable and μ_i's are constants). If Equation 1 is taken to be valid, then it seems reasonable that ε could be held constant and μ_i's varied. For this approach it is necessary that a series of compounds be used in which the varying dipoles location, relative to the point of reaction, is essentially constant. It is felt that most of the compounds in Table 4-1 meet this requirement. Thus, setting $(\varepsilon-1)/kT(2\varepsilon+1)$ equal to a constant (c) for reaction rates measured under conditions of constant temperature and solvent composition, the electrostatic perturbation (E_{-L} from Equation 1) may be written for unimolecular ligand dissociation as:

$$\frac{E_{-L}}{c} = \frac{\mu_B^2}{r_B^3} - \frac{\mu_{B\ddagger}^2}{r_{B\ddagger}^3} \tag{2}$$

where the subscript B refers to the ligand bound state.

It is assumed that the net dipole interacting with solvent is a dipole aggregate of the liganded heme and transition state and is represented as the vector sum of the individual dipoles of the complex, that is, the Fe-L dipole (μ_c) and the interacting dipole (μ_1). Equation 2 is rewritten as:

$$\frac{E_{-L}}{c} = \frac{\left(\mu_c + \mu_1\right)^2}{r_B^3} - \frac{\left(\mu_c + \mu_{1\ddagger}\right)^2}{r_{B\ddagger}^3} \tag{3}$$

Since the ligand does not chemically react with the local dipole it seems reasonable that the dipole moment of the local group in the activated complex may become polarized, changing its magnitude and direction in the extreme. The local groups intrinsic dipole moment in the activated complex is related to the unpolarized dipole moment (μ_g) as:

$$\mu_{g\ddagger} = a\mu_g + b \tag{4}$$

where a is a magnitude scaler and b is an orientation vector. Similarly, it is expected that the interaction between the

Fe-L and local dipoles results in polarization of the respective intrinsic dipoles:

$$\mu_c = \alpha\mu_i + \beta \tag{5a}$$

$$\mu^{\ddagger} = \alpha_{\ddagger}\mu_{i\ddagger} + \beta_{\ddagger} \tag{5b}$$

$$\mu_l = \gamma\mu_g + \delta \tag{5c}$$

$$\mu_{l\ddagger} = \gamma_{\ddagger}\mu_{g\ddagger} + \delta_{\ddagger} \tag{5d}$$

where μ_i is the unpolarized intrinsic dipole moment of Fe-L, α's and γ's are polarization scalers due to changes in dipole magnitude and β's, γ's are polarization vectors due to changes in dipole direction. Substitution of Equations 4 and 5 into Equation 3 yields the electrostatic perturbation term for ligand dissociation (Equation 6).

$$\begin{aligned}\frac{E_{-L}}{c} = &\left[\frac{\gamma^2}{r_B^3} - \frac{\gamma_{\ddagger}^2 a^2}{r_{B\ddagger}^3}\right]\mu_g^2 + \left[\frac{2\gamma(\delta+\alpha\mu_i+\beta)}{r_B^3} - \frac{2a\gamma_{\ddagger}(\gamma_{\ddagger}b+\delta_{\ddagger}+\alpha_{\ddagger}\mu_{i\ddagger}+\beta_{\ddagger})}{r_{B\ddagger}^3}\right]\mu_g \\ &+ \frac{(\delta+\beta)^2 + \alpha(\delta+\beta)\mu_i + \alpha^2\mu_i^2}{r_B^3} \\ &- \frac{\gamma_{\ddagger}^2 b^2 + 2\gamma_{\ddagger}b(\delta_{\ddagger}+\alpha_{\ddagger}\mu_{i\ddagger}+\beta_{\ddagger}) + (\delta_{\ddagger}+\beta_{\ddagger})^2 + 2\alpha_{\ddagger}(\delta_{\ddagger}+\beta_{\ddagger})\mu_{i\ddagger} + \alpha_{\ddagger}^2\mu_{i\ddagger}^2}{r_{B\ddagger}^3}\end{aligned} \tag{6}$$

For a series of closely related compounds (as in Table 4-1) it is conceivable that the polarization sum terms

(coefficients of μ_g in Equation 6) approximate constants. The kinetic expression for ligand dissociation as a function of a local dipole moment is then simply a quadratic in the local groups dipole moment.

$$\ln k_{-L} = A\mu_g^2 + B\mu_g + C \tag{7}$$

Equation 7 could be made more general by including dipole-dipole interaction energy terms (Equation i in results and discussion), however for the models studied it is assumed that the distance and angles between Fe-L and the local dipole are essentially constant. A more complete theoretical treatment will be presented elsewhere.[104]

Identical treatment of ligand association results in the following expression for the dipole-dipole perturbation term.

$$\frac{E_L}{c} = \frac{\mu_L^2}{r_L^3} + \left[\frac{1}{r_D^3} - \frac{\gamma_\ddagger^2 a_\ddagger'^2}{r_{B\ddagger}^3}\right]\mu_g^2 - \frac{2a'\gamma_\ddagger(\gamma_\ddagger b' + \delta_\ddagger + \alpha_\ddagger\mu_{i\ddagger} + \beta_\ddagger)}{r_{B\ddagger}^3}\mu_g$$
$$- \frac{\gamma^2 b^2 + 2\gamma_\ddagger b'(\delta_\ddagger + \alpha_\ddagger\mu_{i\ddagger} + \beta_\ddagger) + (\delta_\ddagger + \beta_\ddagger)^2 + 2\alpha_\ddagger(\delta_\ddagger + \beta_\ddagger)\mu_{i\ddagger} + \alpha_\ddagger^2\mu_{i\ddagger}^2}{r_{B\ddagger}^3} \tag{8}$$

where μ_L, r_L and r_D are the free ligands dipole moment, radius and deoxy heme radius respectively. As above the coefficients of μ_g are taken to be constants for the

compounds in Table 4-1. For ligand association the kinetic expression is:

$$\ln k_L = A'\mu_g^2 + B'\mu_g + C' \qquad (9)$$

The coefficients in Equations 7 and 9 can be evaluated by fitting observed k_{-L} and k_L to a quadratic in μ_g. Using the coefficients so obtained $\ln k_{L\ calc}$ and $\ln k_{-L\ calc}$ can be determined for particular values of μ_g. A plot of calculated vs. observed rate constants, in the absence of other dominating perturbations, should be linear with slope equal to unity.

Materials and Methods

Compounds 1a-g and 2a,b were prepared according to reference 89. Toluene was purified by stirring at 0°C with several changes of conc. H_2SO_4 followed by drying over anhydrous sodium carbonate and distillation from Lithium Aluminum Hydride just prior to solution preparation. Sample solutions for kinetics and CO titrations were prepared by dissolving the ferric compounds in approximately 4 ml of toluene (~10^{-5} M) containing 10^{-4} M of benzophenone. The solutions were degassed in an 80 mL tonometer by freeze-pump-thaw cycles at 10^{-5} torr. The hemin chlorides were reduced by photolysis according to the previously described method.[9] Flash photolysis was carried out with either a xenon photographic flash gun

(Braun 2000) or a flash lamp pumped dye laser (Phase-R DL2100) with rhodamine 6G dye. Decay constants were calculated from transmittence vs. time measurements at 432 nm (five-coordinate heme disappearance) or 410 nm (oxyheme appearance). CO association was monitored at 418 nm and the output of the photomultiplier was recorded on a Bascom-Turner recorder through a log amplifier in absorbance units then directly computed as pseudo-first order rate constants. CO and O_2 concentrations ranged from 5×10^{-5} to 6×10^{-3} M and 5×10^{-4} to 6×10^{-3} M, respectively. CO association rates (l') were calculated from plots of the observed pseudo-first order rate constants vs. CO concentration which typically had correlation coefficients of 0.998 to 1.000 and varied between experiments by less than 5%. O_2 association rates (k's) were calculated from similar plots with correlation coefficients not less than 0.95. Oxygen affinities were determined by CO competition measurements and calculated according to the Gibson equation:[65]

$$R = 1/k + K(O_2)/l'(CO)$$

where l'(CO) was the observed pseudo-first order rate constant determined before the introduction of O_2. Oxygen dissociation was calculated from the observed oxygen association rate and equilibrium constant. Carbon monoxide affinities were determined by direct titration of

the heme with a gas mixture containing 0.072% CO in argon. CO dissociation rates were calculated from $l = l'/L$.

PART C

SPECTRAL SHIFTS UPON REVERSIBLE MODIFICATIONS OF CHO PERIPHERAL SUBSTITUENTS IN PORPHYRIN, CHLORIN AND BACTERIOCHLORIN

CHAPTER 5

A PHENOMENOLOGICAL EXPLANATION FOR THE RED SHIFT OF PROTONATED SCHIFF'S BASE

Introduction

In many naturally occurring porphyrinoid compounds, which contain ketone and/or formyl functional groups, e.g. chlorophylls in photosynthetic apparatii and heme a in cytochrome oxidase, it is often observed that the spectral properties of the *in vivo* and *in vitro* chromophores do not match.[106,107] This is particularly prevalent for the chlorophylls; for example, the visible absorption band of the chlorophyll reaction center P700 is red shifted relative to chlorophyll a (688 nm).[1] Several model studies suggest that P700 is a "special pair" dimer of Chl a.[106,108] However, this dimer model recently has become the topic of considerable dispute and a modified monomeric chlorophyll a has been suggested as a viable model.[109,110]

Similar to the red shift observed for chlorophylls are the protein influences on the linear polyene retinal, which have been linked to the formation and subsequent protonation of a Schiff's base.[111] Bearing this in mind,

it is interesting to speculate whether porphyrinoid carbonyl moieties would react reversibly with nearby amino acid residues in the protein, thereby changing their spectral as well as functional properties. Indeed Wasielewski et al.[109a] have shown that a silyl enol ether, and its analog 9-desoxo-9-10-dehydro chlorophyll a are about 350 mV easier to oxidize than Chl a itself. Pearlstein has found that placing a point charge on the periphery of a Chl a model compound results in a 4 nm red shift in the visible absorption band.[109b] In separate experiments, we[110a] and others[110b,c] have shown that substantial red shifts of the visible absorption bands of Schiff's base porphyrins and chlorins can occur upon protonation.

In order to better understand the nature of the spectra of protonated Schiff's base porphyrin, chlorin, and bacteriochlorin, a systematic study with regard to peripheral substitution and environmental influences is presented here. In the present study, both mono- and di-formyl systems with two different substitution symmetries were examined. This detailed phenomenological approach has yielded essential data necessary for a complete understanding of the spectral changes upon protonation. The theoretical aspect of this work is described in reference 112.

Results and Discussion

As shown by the structures in Figure 5-1, our Schiff's base and related derivatives were synthesized from the parent formyl compounds: nickel 2,6-di-n-pentyl-4-vinyl-8-formyl-1,3,5,7-tetramethylporphine (1b), nickel 1,4-diformyl-6,7-diethyl-2,3,5,8-tetramethylporphine (2b), nickel 2,6-di-n-pentyl-4,8-diformyl-1,3,5,7-tetramethylporphine (3b), copper 2,6-di-n-pentyl-4-vinyl-7-hydroxy-8-acroleinyl-1,3,5,7-tetramethyl chlorin (4b), and copper 2,6-di-n-pentyl-3,7-dihydroxy-4,8-diacroleinyl-1,3,5,7-tetramethyl bacteriochlorin (5b). With the three porphyrins, nickel was inserted because the resultant complexes would be diamagnetic, acid stable, and does not readily bind axial ligands. With the chlorin and bacteriochlorin, nickel insertion was more difficult and required prolonged heating which may be detrimental to the integrity of the macrocycle; therefore copper was chosen. The reason that the "photoproto" type chlorin and bacteriochlorin were used is because of their availability and the fact that the acroleinyl moiety places the CHO group remote enough from the ring to allow facile reaction with a variety of aldehyde-specific reagents; this was not possible for the β-substituted formyl metalloporphyrins owing to steric conjestions about the -CHO.

Figure 5-1. Structures and substitution patterns of formyl porphyrins (1-3), acroleinyl chlorin (4) and bacteriochlorin (5).

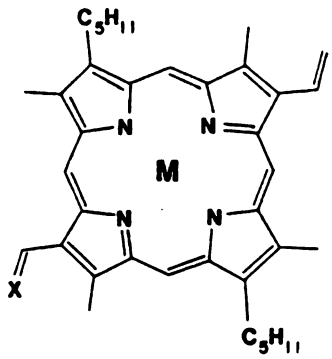

1a X=O M=2H
b X=O M=Ni
c X=NC_4H_9 M=Ni

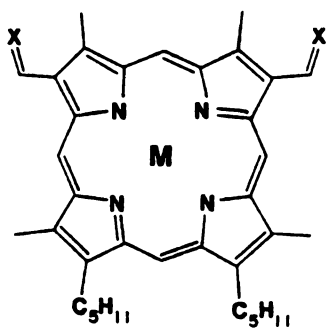

2a X=O M=2H
b X=O M=Ni
c X=NC_4H_9 M=Ni

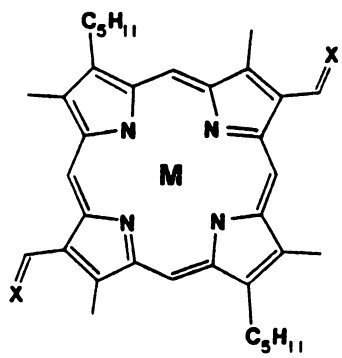

3a X=O M=2H
b X=O M=Ni
c X=NC_4H_9 M=Ni

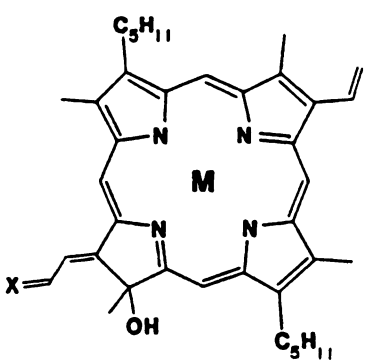

4a X=O M=2H
b X=O M=Cu
c X=NC_4H_9 M=Cu
d X=N⊕ M=Cu
e X=C(CN)$CO_2C_2H_5$ M=Cu
f X=C(CN)$_2$ M=Cu
g X=OH,N M=Cu

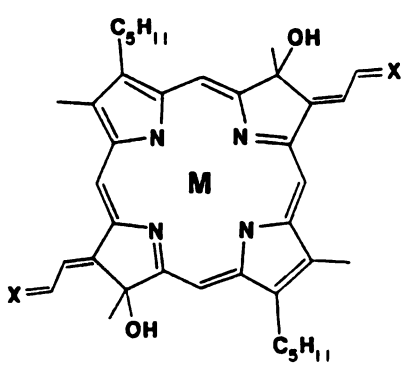

5a X=O M=2H
b X=O M=Cu
c X=NC_4H_9 M=Cu

Figure 5-2 shows the spectral changes associated with protonation and deprotonation of Schiff's base 1c in CH_2Cl_2. The arrows indicate the spectral shifts observed upon addition of 70% perchloric acid-saturated CH_2Cl_2 to 1c. The dashed spectra are those obtained after bubbling triethylamine-saturated air through the solution. Similarly, Figure 5-3 shows the spectral shifts observed upon addition of HF vapor to Schiff's base 4c in CH_2Cl_2. Figure 5-4 contains the spectra of copper bacteriochlorin 5b, 5c, and 5c·CF_3COOH in THF. As shown in Figures 5-2—5-4, for all three macrocycles protonation results in relatively large red shifts in the visible absorption maxima with the Soret region becoming split or broadened. The spectral shifts observed upon Schiff's base protonation are expected to be mimicked by iminium salt formation. Indeed, comparison of the spectrum of 4c·HF (Figure 5-3) with that of the pyrrolidinium perchlorate (Fig. 5-5a) reveals that this is qualitatively true. Attempts to prepare the pyrrolidinium salt of formyl prophyrins (1b, 2b, or 3b) were not successful.

The dramatic spectral changes associated with Schiff's base protonation or iminium salt formation could be due to either delocalization of the positive charge onto the ring or localization of the electropositive hole on the periphery resulting in an electron deficient group conjugating with the ring. In order to differentiate these two possibilities, the electron withdrawing but

Figure 5-2. Spectral shifts associated with protonation and deprotonation of Schiff's Base 1c in CH_2Cl_2. The arrows indicate the direction of change of the absorption spectrum upon dropwise addition of 70% $HClO_4$-saturated CH_2Cl_2. The dashed spectra are those obtained upon addition of Et_3N.

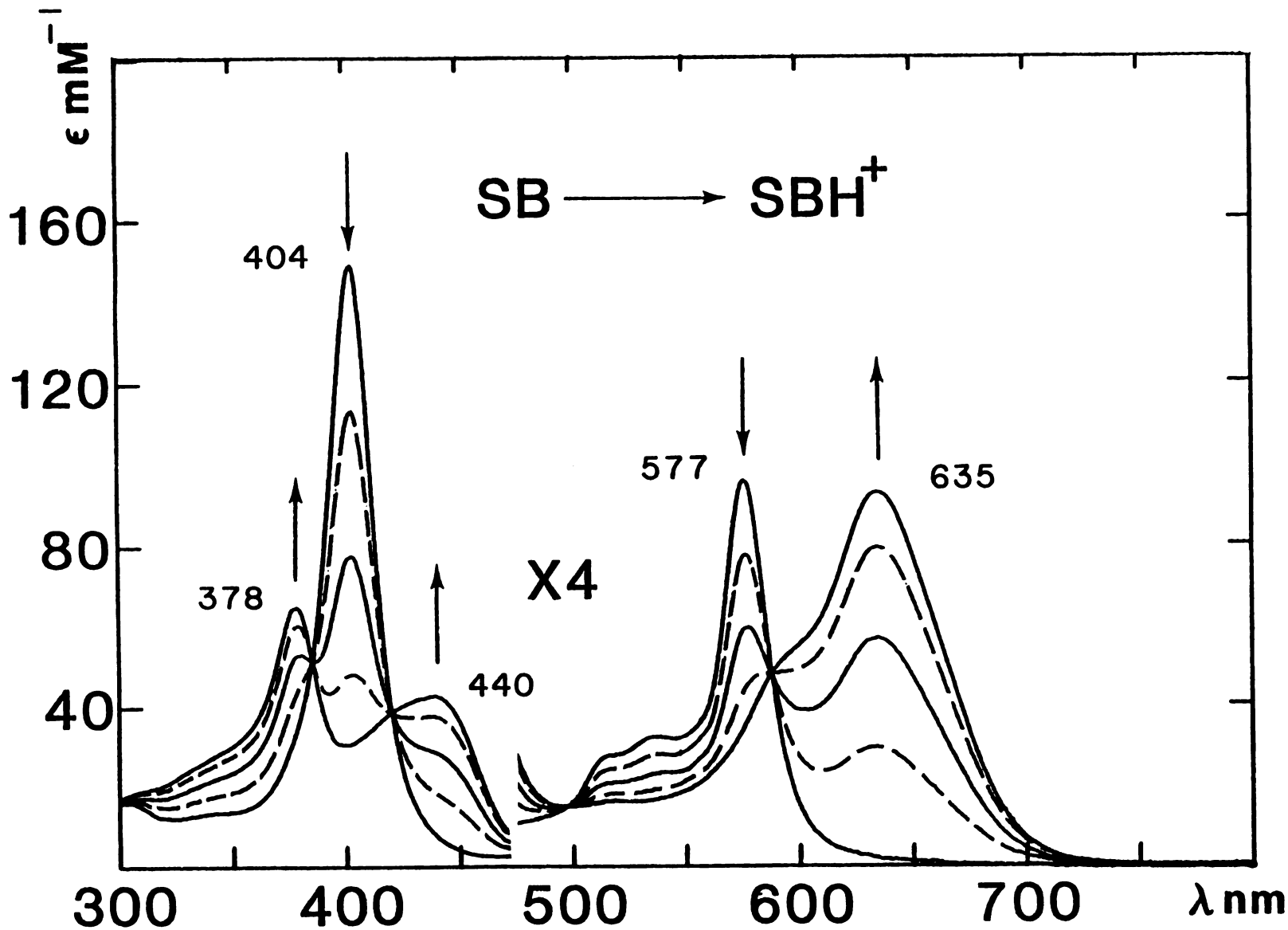
ε mM⁻¹
160
120
80
40
SB → SBH+
404
378
440
X4
577
635
300
400
500
600
700
λ nm

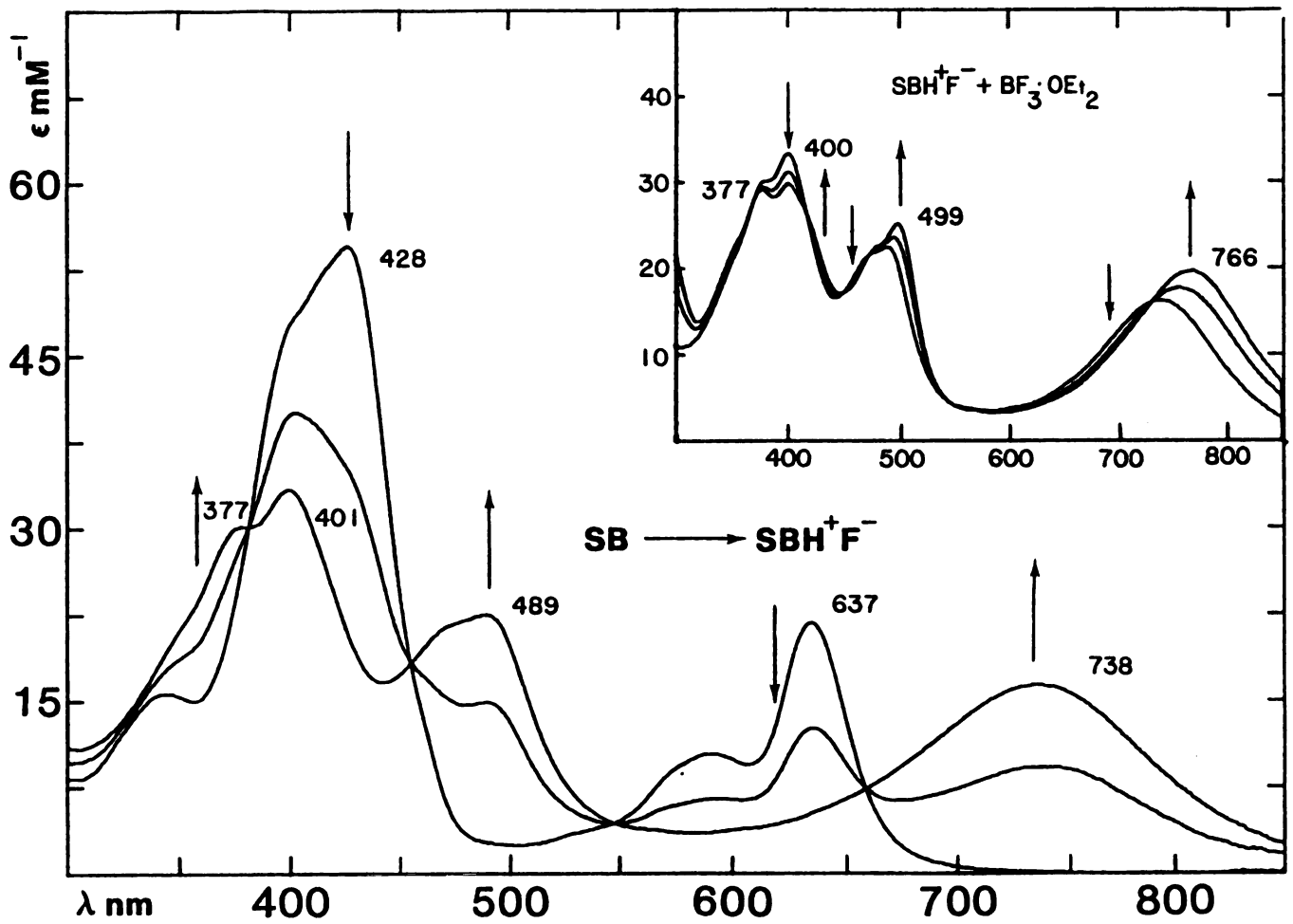

Figure 5-3. Absorption spectra of Schiff's base 4c protonated with HF vapor in CH_2Cl_2, and conversion of 4c·HF to 4c·HBF_4 (inset).

Figure 5-4. Absorption spectra of bacteriochlorin 5b (inset), 5c (——) and $5c \cdot (CF_3CO_2H)_2$ (---) in THF.

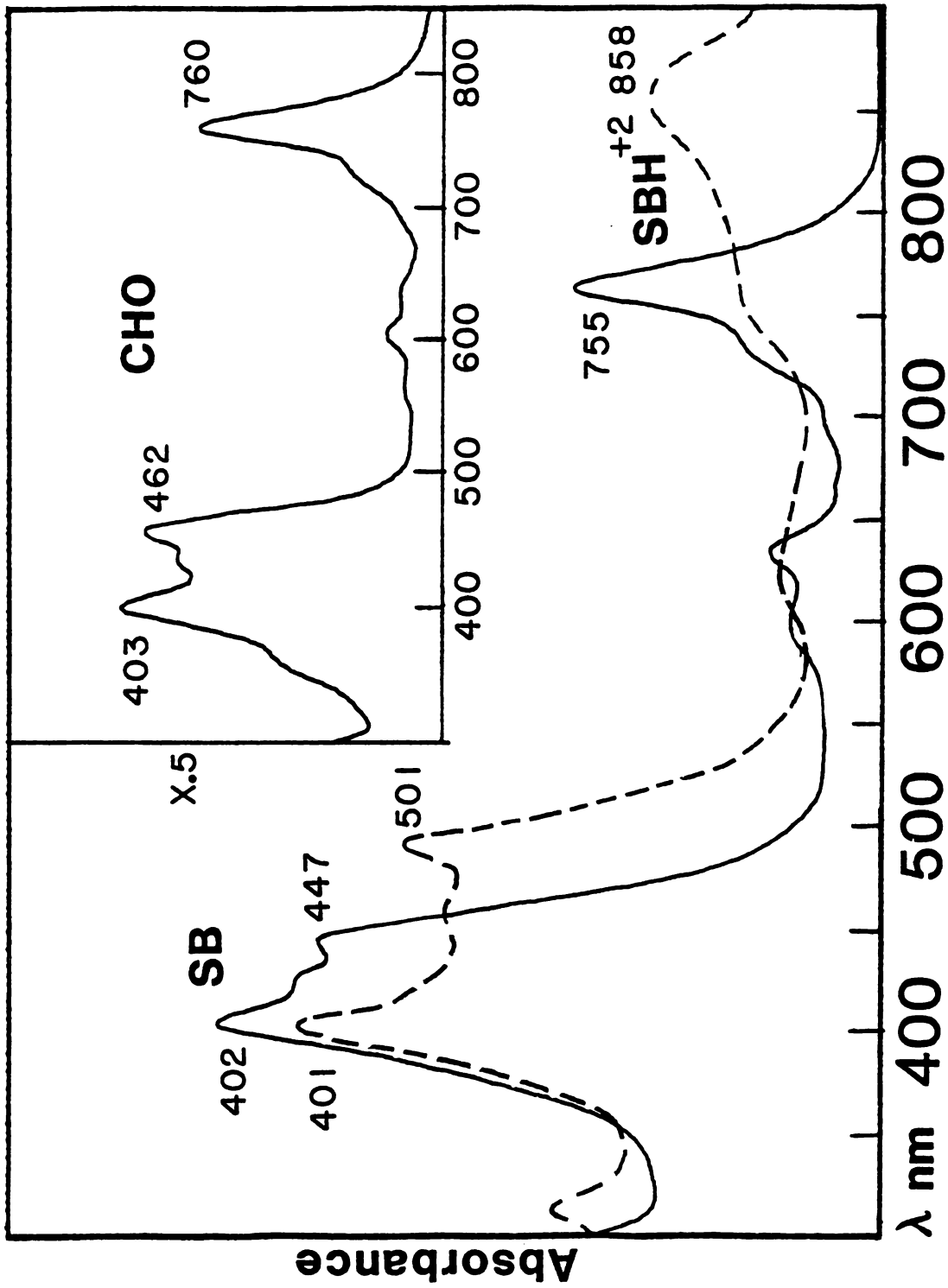
Absorbance
λ nm
400
500
600
700
800
SB
402
401
447
501
X.5
CHO
403
462
760
SBH+2
755
858

coulombically neutral ethyl cyanoacetate and malononitrile adducts, e.g. 4e and 4f, and other carbonyl derivatives were studied. As shown in Figure 5-5, the fact that the spectral characteristics of 4e and 4f are very similar to those for $4c \cdot H^+$ or 4d almost immediately rules out the charge delocalization model. Substitution of an ester for nitrile moiety, as in 4e and 4f, results in a less electron withdrawing substituent, and consequently a smaller degree of red shift (4e: 1520 cm^{-1} vs. 4f: 2056 cm^{-1} shifted from 4b in THF) as well as less splitting in the Soret region ($\Delta\nu_{4e}$: 3630 cm^{-1} vs. $\Delta\nu_{4f}$: 4280 cm^{-1}). Likewise, the substituent effect can also be evidenced by "saturating" the carbonyl group. Figure 5-6 shows the spectral changes associated with addition of pyrrolidine to 4b in CH_2Cl_2. The resultant spectrum is essentially identical to that observed after addition of tetrabutylammonium borohydride to 4b in CH_2Cl_2 (Fig. 5-6, inset). Acidification of the borohydride-treated compound resulted in quantitative conversion to a copper porphyrin.[113,114] Acidification of the pyrrolidine adduct converted it to the pyrrolidinium salt. Based on these observations a hemiaminal[115] structure is proposed as the pyrrolidine adduct 4g. Thus, irreversible reduction or reversible hemiaminal formation produces a blue shift of the visible band by approximately 700 cm^{-1} along with the Soret region coalescing to a single sharp peak. Similarly, as observed for all our

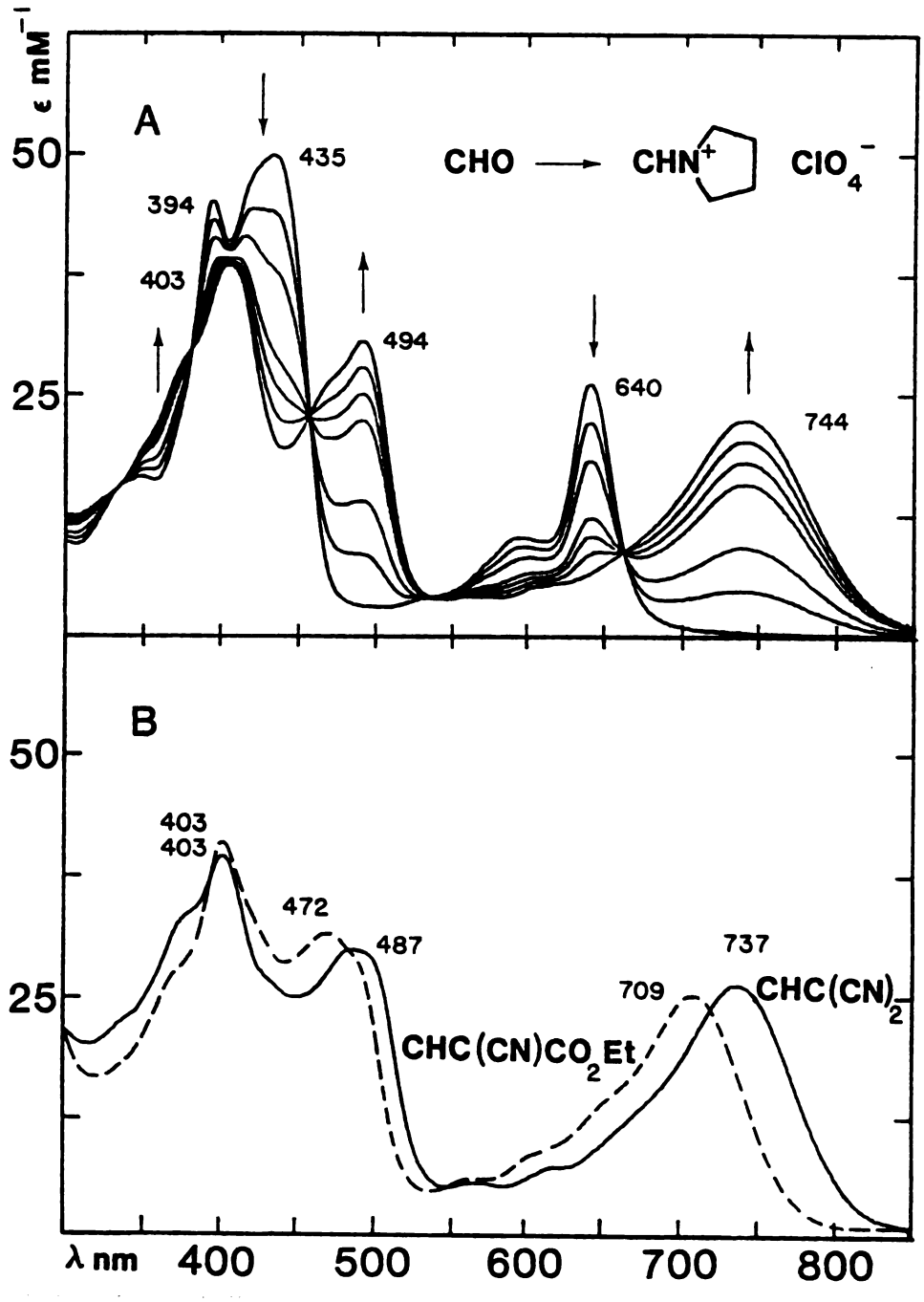

Figure 5-5. A): Absorption spectra monitoring the reaction of 4b with pyrrolidine·$HClO_4$ in THF (total elapsed time ~1 hr). B): Absorption spectra of ethyl cyanoacetate adduct 4e (---) and malononitrile adduct 4f (——) in THF.

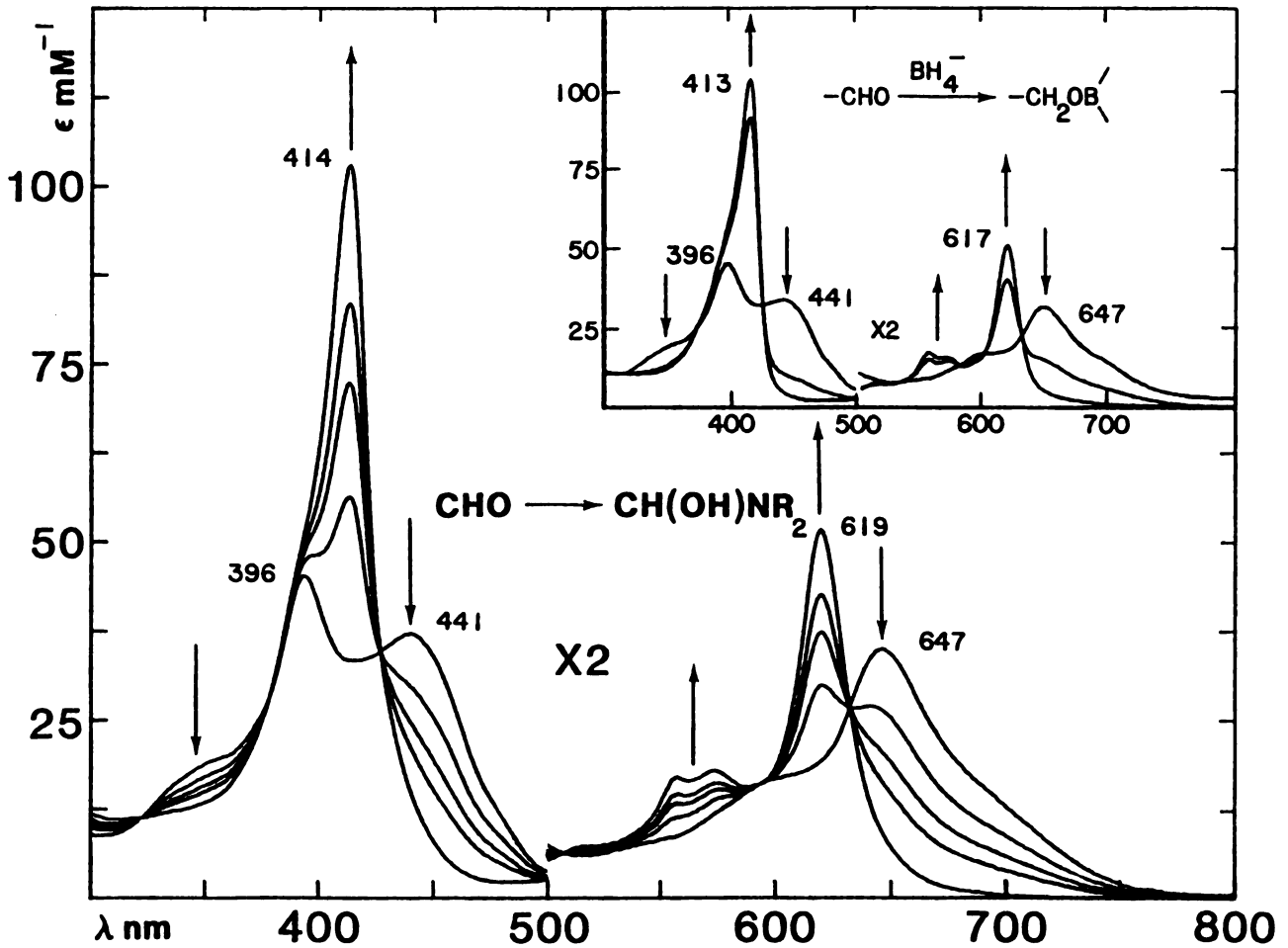

Figure 5-6. Absorption spectra monitoring the reaction of 4b with excess pyrrolidine in CH_2Cl_2 ($R_2 = C_4H_8$). Reduction of 4b with tetrabutylammonium borohydride in CH_2Cl_2 (inset).

Schiff's bases, replacing O with a less electronegative N during Schiff's base formation leads to a blue shift of the visible band relative to their parent formyl or acroleinyl compounds.

From a phenomenological perspective, the above data combined with proton NMR and resonance Raman studies below leave little doubt that the unusual spectral properties of protonated Schiff's base porphyrinoid derivatives is brought about by the presence of a conjugating electron deficient substituent on the ring. The proton NMR spectra during addition of anhydrous HCl to 1c in $CDCl_3$ are reproduced in Figure 5-7. As shown, progressive acidification caused all protons near the C=N group to shift and broaden due to exchange. While the deshielding effect of protonation of the C=N double bond undoubtedly could produce the upfield shift for the -CH=N- proton, the adjacent meso proton, and the adjacent pyrrolic methyl group, the protonation caused the α-imino methylene protons to shift downfield owing to increased electronegativity. That the other peripheral substituents on the porphyrin ring were little perturbed indicates that the positive charge is not substantially delocalized throughout the porphyrin π-system.

The resonance Raman spectra of 1c(SB) and 1c·HCl(SBH^+) in CH_2Cl_2 using 406.7 nm excitation are shown in Figure 5-8. The Raman spectrum of 1c shows strong enhancement of totally symmetric modes at 1598 cm^{-1}

Figure 5-7. 250 MHz NMR spectra of 1c plus hydrogen chloride in $CDCl_3$. Free base, intermediate (0.5 eq. HCl) and complete protonation (1.2 eq. HCl) from bottom to top respectively.

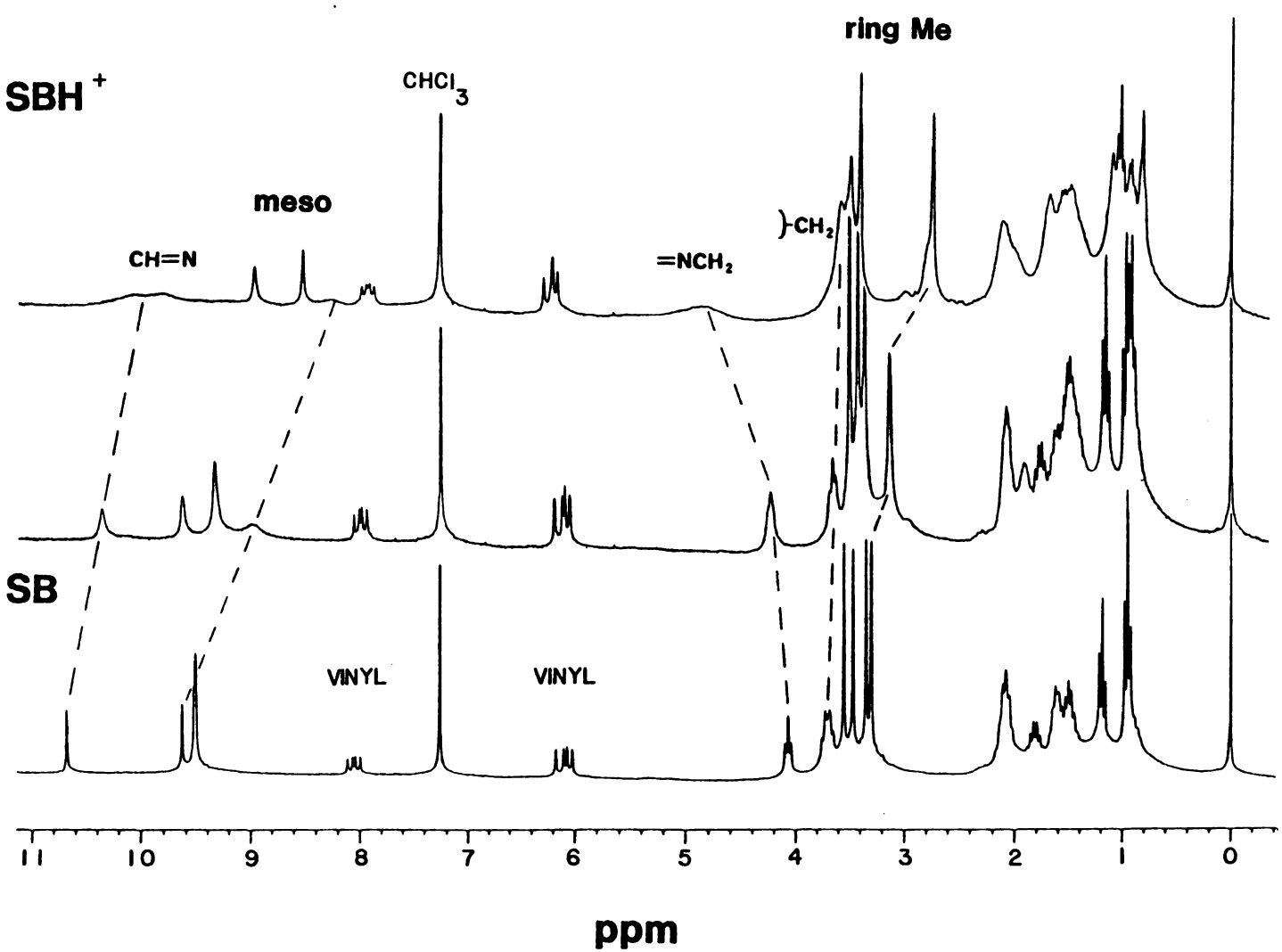
SBH +
SB
CH=N
meso
CHCl3
VINYL
VINYL
=NCH2
}-CH2
ring Me
11
10
9
8
7
6
5
4
3
2
1
0
ppm

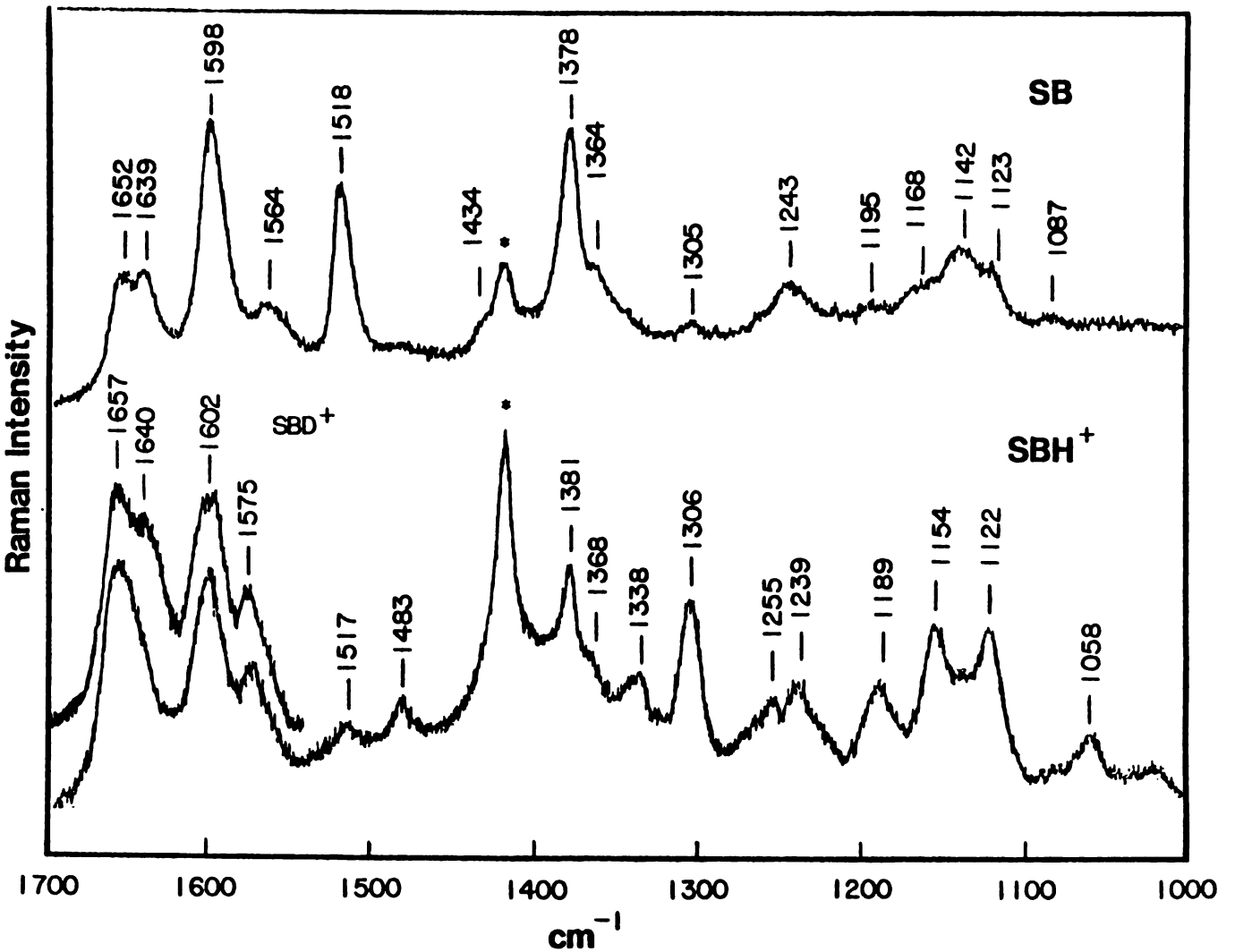

Figure 5-8. Resonance Raman spectra in CH_2Cl_2 with 406.7 nm laser excitation of 1c (top), 1c·HCl (bottom) and 1c·DCl (middle 1550-1700 cm^{-1}).

(ν_2), 1518 cm^{-1} (ν_3) and 1383 cm^{-1} (ν_4), whose assignments are in analogy with those of Abe et al.[116] The line observed at 1652 cm^{-1} corresponds to a B_{1g} mode (ν_{10}) which is most likely enhanced through a Jahn-Teller or intramanifold coupling mechanism;[117] it is commonly observed when studying hemes and heme proteins by Soret excitation Raman.[118] The Schiff's base -C=N-stretching vibration is responsible for the line observed at 1639 cm^{-1}. For the protonated Schiff's base, we note little change in the frequencies of the observed ring vibrations,[119] indicating that protonation effects are localized at the Schiff's base and do not strongly perturb the basic porphyrin bonding pattern. However, the decrease in symmetry, which is apparent in the optical spectrum (Figure 5-2), is reflected in the Raman spectrum of 1c·HCl in that the scattered intensity from non-totally symmetric modes (B_{1g}, A_{2g}, B_{2g}) is much stronger, while that from the totally symmetric modes (A_{1g}) is decreased, relative to the free Schiff's base. Protonation of the Schiff's base shifts the $-\overset{\oplus}{N}=CH-$ stretching frequency into the 1650 cm^{-1} region where it overlaps strongly with ν_{10}. In order to determine its frequency more precisely, we carried out analogous IR experiments which showed $\bar{\nu}$ ($-\overset{\oplus}{N}H=CH-$) = 1650 cm^{-1}; these data form the basis for the assignments of the two vibrational frequencies in Table 5-1. If DCl is used to deuterate the porphyrin Schiff's base, the stretching frequency decreases to

Table 5-1. Vibrations Observed and Normal Coordinate Assignments[a] Ni(II) Porphyrin Schiff's Base Species.

SB	SBH^+	Assignment (#)	SB	SBH^+	Assignment (#)
1652	1657	$B_{1g}(\nu_{10})$	1564	—	$E_u(\nu_{38})$
1639	—	ν_s(-N=CH-)	1517	1518	$A_{1g}(\nu_3)$
—	1650	ν_s(-$\overset{\oplus}{N}$H=CH-)	1378	1381	$A_{1g}(\nu_4)$
—	1640	ν_s(-$\overset{\oplus}{N}$H=CH-)	1305	1306	$A_{2g}(\nu_{21})$
1598	1602	$A_{1g}(\nu_2)$	—	1154	$B_{2g}(\nu_{30})$
—	1575	$B_{1g}(\nu_{11})$	1123	1122	$A_{2g}(\nu_{22})$

[a]Symmetries and mode numbers from Abe *et al.*[12] In the more correct C_{2h} group for **3** and **4**, $\{A_{1g}, B_{1g}, A_{2g}, B_{2g}\}$ become A_g.

1640 cm^{-1} (Figure 5-8, inset). A similar pattern of -C=X- stretching vibtation frequency shifts is observed in retinal Schiff's bases upon protonation and deuteration and the physical mechanism underlying these shifts has been discussed in detail by Aton et al.[120] From this analysis it appears as if the interaction between the C=N stretching vibration and the C=N-H bending mode is somewhat less in the aromatic porphyrin case than in the linear polyene retinal case.

The high frequency (1000-1800 cm^{-1}) resonance Raman spectra of 4d·HCl^- in CH_2Cl_2 and THF as well as 1c·ClO_4 in THF with 406.7 and 488.0 nm excitation are reproduced in Figure 5-9. The low frequency (0-1000 cm^{-1}) region spectra were masked by solvent vibrations and are not shown here. Comparison of the SB and SBH^+ resonance Raman spectra with 406.7 nm laser excitation reveals similar vibrational frequencies for the two except that the peripheral stretching frequency (C=N) for SBH^+ is absent. With 488.0 nm laser excitation of SB 4c·HCl results in a resonance Raman spectrum displaying the typical -C=NHR stretching vibration at 1646 cm^{-1}, in analogy with 1c·HCl. Further comparison of the resonance Raman spectra of 4c·HCl with 406.7 and 488.0 nm excitation reveals large intensity differences between the two spectra. With 488.0 nm excitation, the totally symmetric A_{1g} modes at 1592, 1502, and 1375 cm^{-1} are decreased in intensity relative to the nontotally symmetric

Figure 5-9. Resonance Raman spectra of 4c·HCl (CH_2Cl_2 and THF) and pyrrolidinium perchlorate adduct 4d (THF) with 406.7 and 488.0 nm laser excitation.

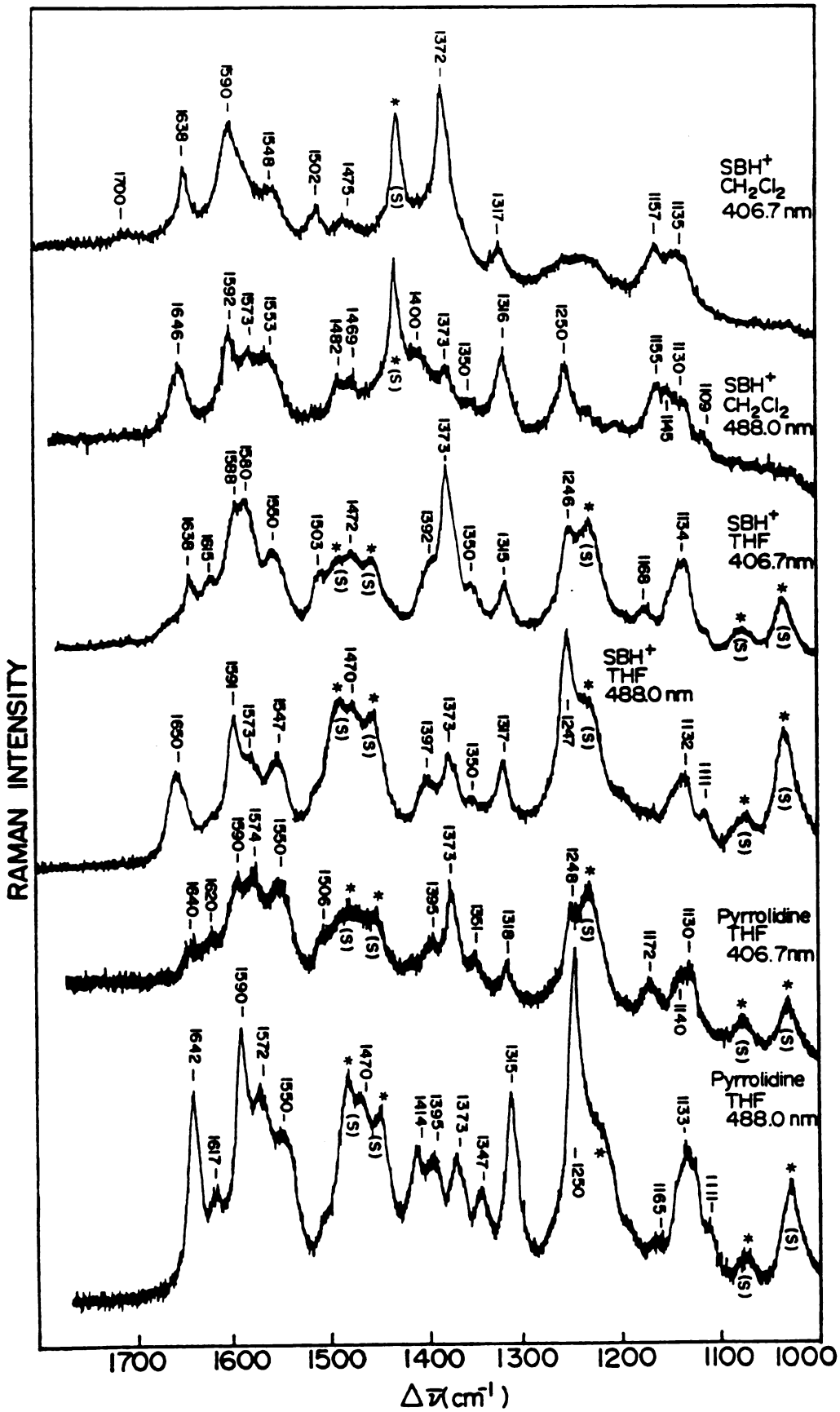
SBH+
CH2Cl2
406.7 nm
SBH+
CH2Cl2
488.0 nm
SBH+
THF
406.7nm
SBH+
THF
488.0 nm
Pyrrolidine
THF
406.7nm
Pyrrolidine
THF
488.0 nm
RAMAN INTENSITY
1700
1600
1500
1400
1300
1200
1100
1000
Δν̄(cm⁻¹)

vibrations. This pattern was also observed for 1c·HCl (as discussed above).

The absent or extremely weak peripheral vibration with excitation at 406.7 nm and its presence with 488.0 nm excitation as well as the less intense totally symmetric vibrations with excitation at 488.0 nm relative to 406.7 nm for SB 4c·HCl and pyrrolidinium perchlorate salt indicates a clear separation of the in-plane polarized transition dipoles, B_x and B_y, along the molecular axis. Where B_x and B_y occur at approximately 400 and 500 nm, respectively. The C=N stretching vibrations occur at 1646 cm^{-1} in CH_2Cl_2, 1650 cm^{-1} in THF for 4c·HCl and for the pyrrolidinium perchlorate in THF at 1642 cm^{-1} which are typical values for SBH^+[5a] and aromatic iminium salts,[121] respectively. Excitation profile arguments predict that resonance enhancement coupled to the polarized Soret maximum fall off rapidly below 440 nm due to the vibrational overtone term in the expression for A-term intensity.[122] This is observed experimentally for $\nu_{C=NHR^+}$ with laser excitation at 488.0, 457.9, 441.6 and 406.7 nm (data not shown). No distinct vibrational patterns such as these have been observed for laser excitation in resonance with the split Soret maxima for either 1c·HCl or aldehyde 4b because the splittings are not great enough (3380 cm^{-1} and 2590 cm^{-1} respectively). In these later examples the 0-0 intensity enhancement term of the y-polarized transition is not sufficiently separated

from the x-polarized transition moment for a distinction to be made by resonance Raman spectroscopy.

From the resonance Raman data for protonated Schiff's bases 1c and 4c and pyrrolidinium salt 4d it would seem reasonable to expect that the spectral shifts upon Schiff's base protonation should also be dependent on the substitution pattern of the macrocycle.

Figure 5-10 shows the spectral shifts observed upon addition of 70% $HClO_4$-saturated CH_2Cl_2 to di-Schiff's bases 2c and 3c in methylene chloride. The two upper sets of spectra are the first protonation step while the lower are the second. The final mono-protonated SB spectra were not obtained directly. They were resolved by incremental substraction of the free Schiff's base spectra from a mixture of the free and mono-protonated SB until the spectrum matched that obtained from incremental subtraction of the diprotonated SB spectrum from a mono- and di-protonated SB mixture. The essential difference between di-Schiff's base 2c and 3c is that the formyl groups lie on either different or the same molecular axes. As shown in Figure 5-10, the second protonation step of 2c results in a 236 cm^{-1} (9 nm) blue shift of the visible band with a red shift of the split Soret. This behavior is exactly reversed with the diametrical (same axis) di-Schiff's base 3c in which the visible band is further red shifted by 561 cm^{-1} (24 nm) and the Soret region blue shifted. Therefore, these results provide

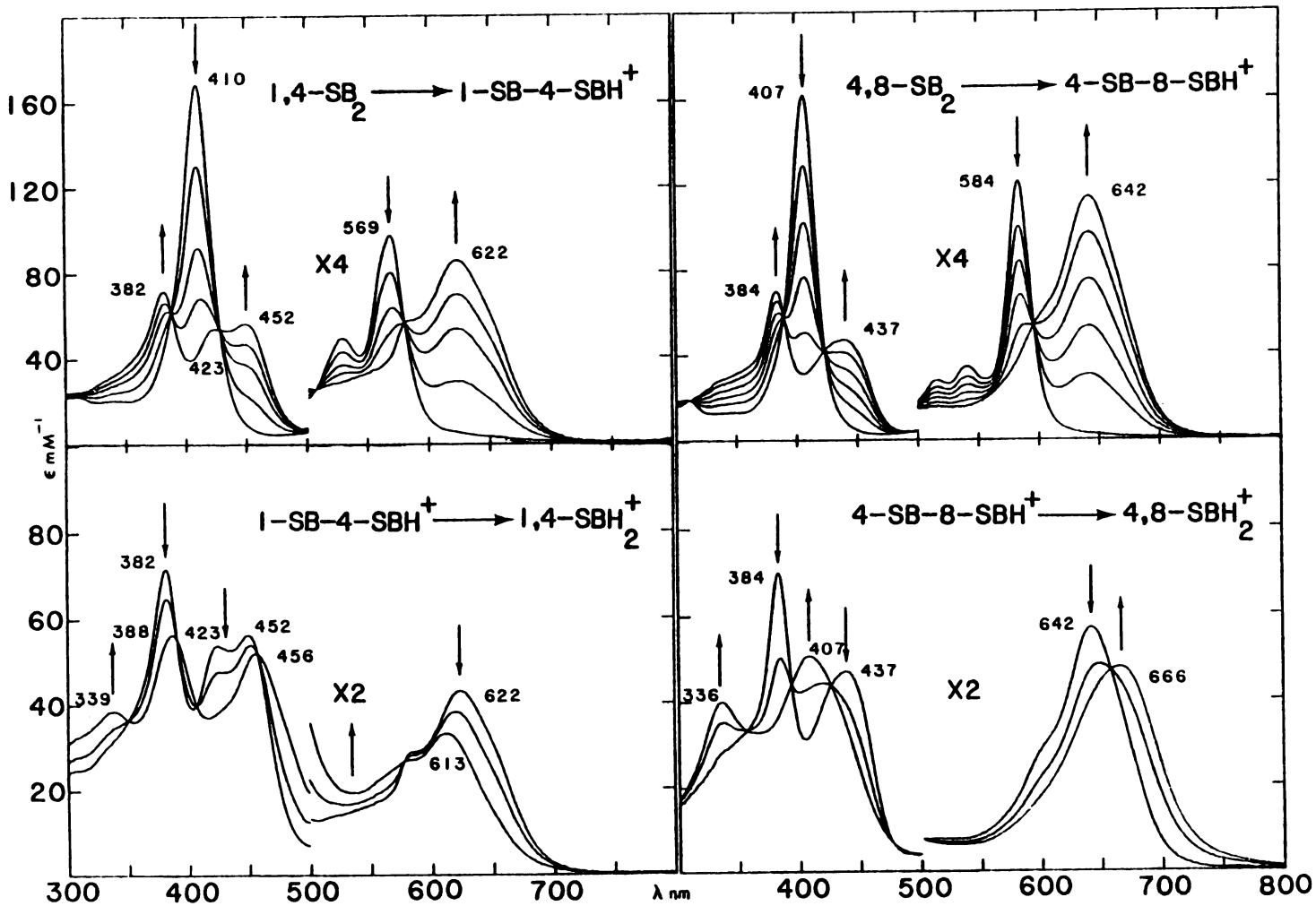

Figure 5-10. Perchloric acid titrations (70% in CH_2Cl_2) of di-Schiff's bases 2c and 3c. Upper left and right are the first protonation step of 2c and 3c respectively. Lower spectra are the second protonation step.

experimental evidence that the red shifts observed for Schiff's base protonation is partially due to perturbation along one porphyrin axis. If single axis perturbation were solely responsible for the observed shifts then it would be expected that the second protonation step of 2c would result in returning the spectrum much more toward the unprotonated Schiff's base. Since di-protonated 2c and di-formyl 2b are both red shifted relative to 2c, it appears that the red shift of the visible band as well as Soret splitting is also partially attributable to the increased electron withdrawing capability of $CH{=}NH^{+}R$ and CHO relative to CH-NR.

Environmental Effects:

If the SBH^{+} formation should leave the position charge localized on the ring peripheral group, the environment of a protonated Schiff's base should also modify its electron withdrawing strength, providing a pathway for spectral tuning. Conceivable mechanisms include: ion pairing, solvation, and hydrogen bonding from SBH^{+} to an acceptor. In discussing solvent and anion effects on the spectra of SBH^{+} and pyrrolidinium salts, we will use the relative difference $\Delta\nu_{CHO}$ where the frequency in wavenumbers of the visible band for 1b in CH_2Cl_2 and 4b in THF are taken as reference points. Quantitative comparison of the spectral maxima for 4c·HX and 4d·X^{-} are avoided here for three reasons: 1) molecular bulk at the imino nitrogen

between the two compounds is different leading to unequal solvation; 2) the proton of SBH^+ may form an H-bond to the 7-hydroxyl group, and 3) H-bonding may occur between the SBH^+ proton and counter anion, resulting in mixed effects.

Figures 5-11 to 5-13, as well as Tables 5-2, 5-3, and 5-4, contain the absorption spectral data for SBH^+ 1c, 4c, and pyrrolidinium salt 4d as a function of counter anion and solvent. For porphyrin 1c in CH_2Cl_2, with the exception of F^-, we observed that the visible absorption maxima vary by 381 cm^{-1} (15 nm) with the larger anions producing larger red shifts. Concomitantly, the lower energy Soret band red shifts and the Soret intensity ratio ($\varepsilon_{380}/\varepsilon_{440}$) increases with increased counter ion size. The position of the 380 nm Soret band remains essentially unaltered. This effect is also present in THF (though less pronounced) but absent in acetonitrile. Titration of 1c with HF in CH_2Cl_2 resulted in a spectrum essentially identical to $SBH^+ClO_4^-$ and was not altered upon addition of BF_3OEt_2, indicating that the pK_a of SB 1c is less than the equilibrium constant for HF_2^- ($K_{eq} = 5\text{-}25$[123a]). Similarly, the visible absorption maxima are varied by 490 and 660 cm^{-1} as a function of counter anion in CH_2Cl_2 for 4c·HX and 4d·X^-, respectively, with the extent of red shift being again dependent on anion size. In THF, the counter anion effect on 4c·HX and 4d·X^- varied $\Delta\nu_{CHO}$ by 600 and 90 cm^{-1}, respectively. In acetonitrile, we

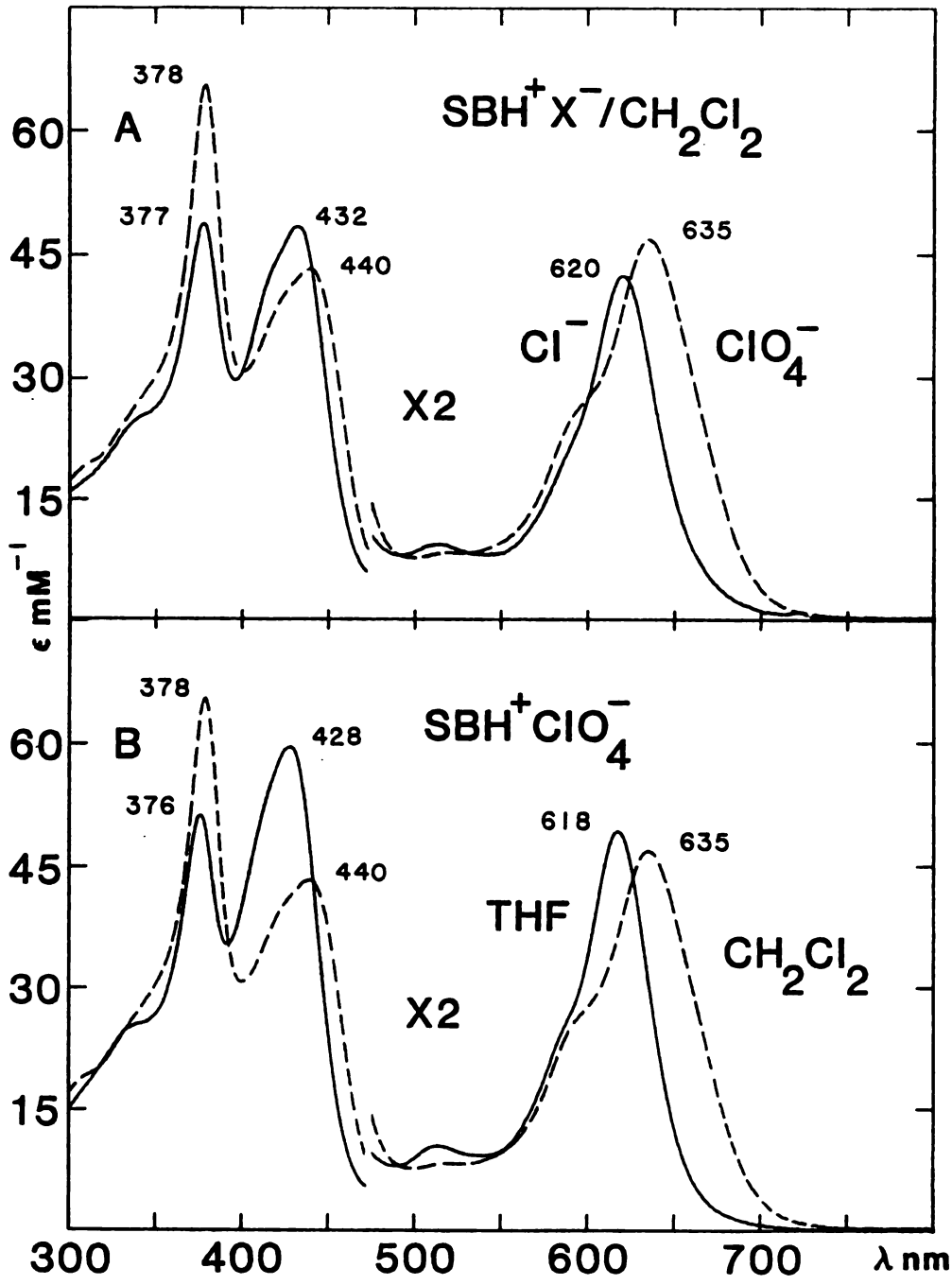

Figure 5-11. Counter anion and solvent dependence of the absorption spectrum of SBH^+1c. A): 1c·HCl (——) and 1c·$HClO_4$ (---); B): 1c·$HClO_4$ in THF (——) and CH_2Cl_2 (---).

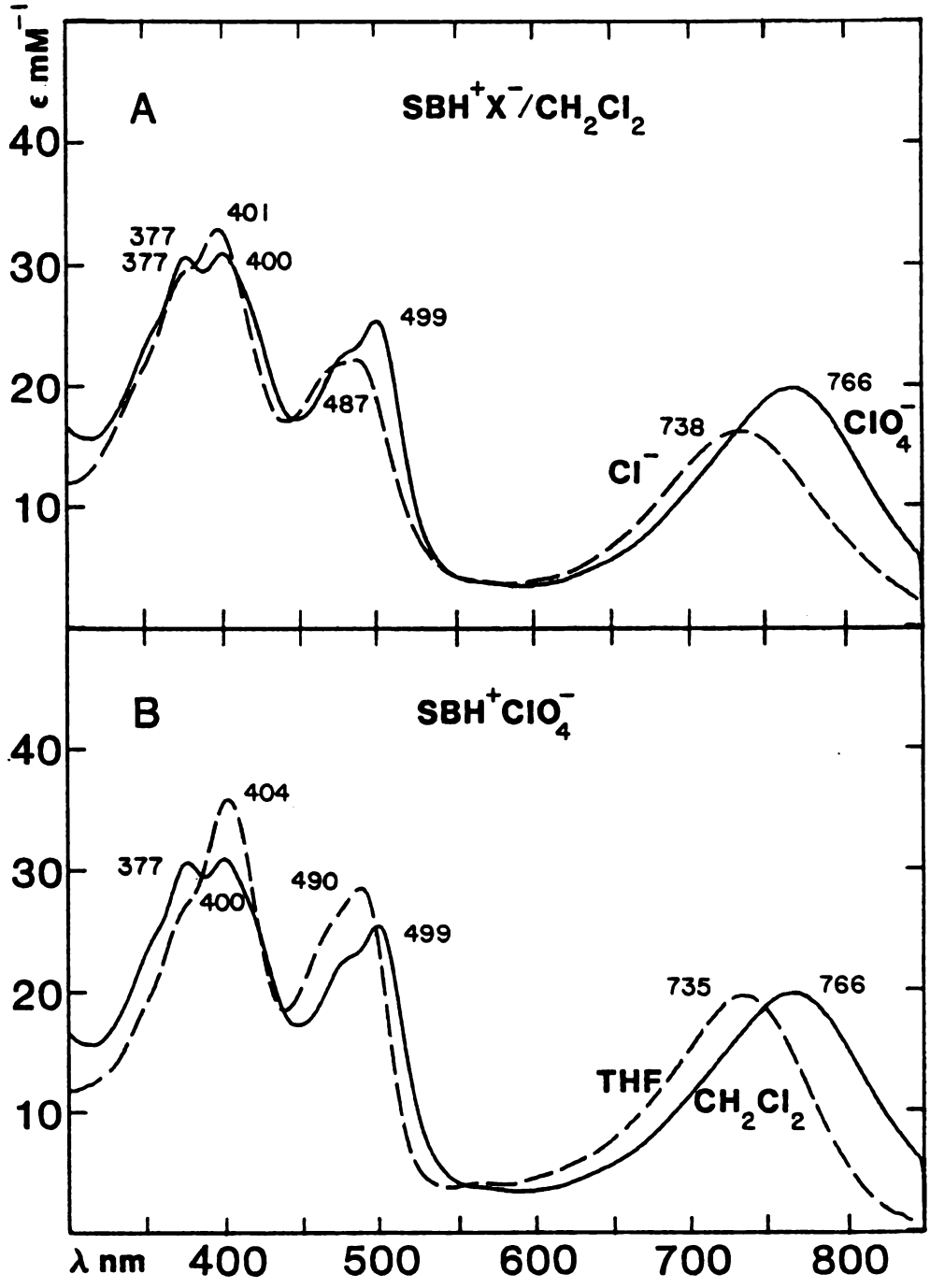

Figure 5-12. Solvent and counterion dependence of the spectrum of SBH^+4c. A): 4c HCl (---) and $4c \cdot HClO_4$ (——) in CH_2Cl_2. B): $4c \cdot HClO_4$ in THF (---) and CH_2Cl_2 (——).

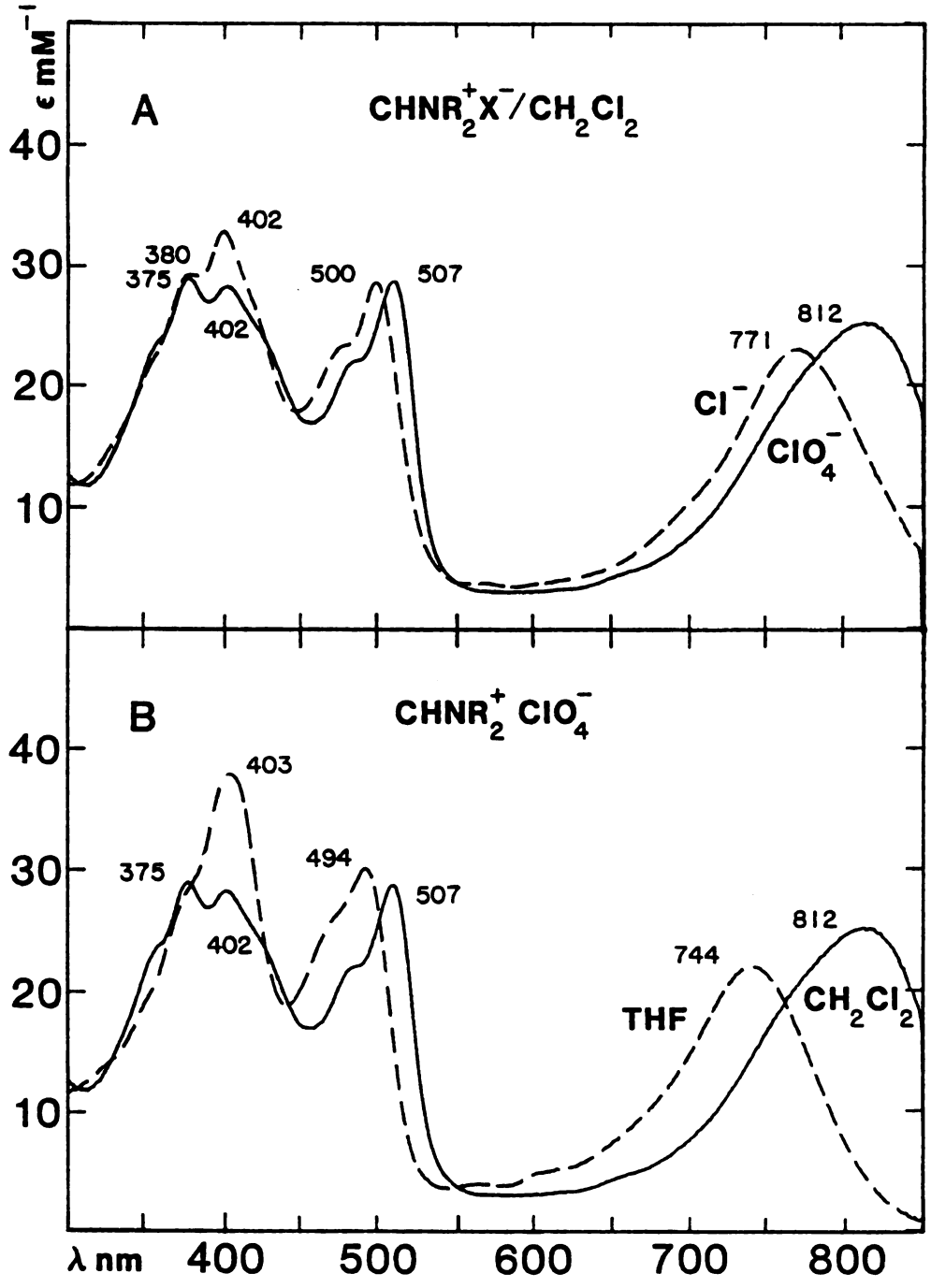

Figure 5-13. Solvent and counterion dependence of the spectrum of $4d \cdot X^-$ ($R_2 = C_4H_8$). A): $4d \cdot Cl^-$ (---) and $4d \cdot ClO_4^-$ (——) in CH_2Cl_2. B): $4d \cdot ClO_4^-$ in THF (---) and CH_2Cl_2 (——).

Table 5-2. UV-Visible Spectral Data for Protonated Schiff's Base 1c as a Function of Counterion and Solvent.

X^-	Solvent	$\Delta\nu_{CHO}$ (cm^{-1})	λ nm (ε mM^{-1} cm^{-1})			$\varepsilon_{380}/\varepsilon_{440}$
$F^-(HF^-_2)$	CH_2Cl_2	1205	634 (22)	438 (42)	379 (64)	1.53
Cl^-	CH_2Cl_2	849	620 (21)	432 (48)	377 (52)	1.10
Br^-	CH_2Cl_2	1003	626 (22)	435 (46)	378 (55)	1.18
I^-	CH_2Cl_2	1230	635 (25)	438 (45)	382 (68)	1.55
ClO^-_4	CH_2Cl_2	1230	635 (23)	440 (42)	378 (65)	1.52
$F^- + BF_3$	CH_2Cl_2	1205	634 (22)	438 (42)	379 (64)	1.53
Cl	THF	611	611 (18)	417 (56)	376 (43)	0.77
ClO_4	THF	797	618 (24)	428 (59)	376 (51)	0.85
Cl	CH_3CN	770	617 (24)	427 (56)	373 (54)	0.96
ClO_4	CH_3CN	770	617 (24)	427 (56)	373 (54)	0.96

Table 5-3. UV-Visible Spectral Data for Protonated Schiff's Base 4c as a Function of Counterion and Solvent.

X	Solvent	$\Delta\nu_{CHO}$ (cm^{-1})	λ nm (ε mM^{-1} cm^{-1})			
F^-	CH_2Cl_2	2080	738 (16)	489 (22)	400 (33)	377[a] (30)
Cl^-	CH_2Cl_2	2080	738 (16)	487 (23)	401 (33)	377[a] (29)
Br^-	CH_2Cl_2	2220	746 (17)	498 (23)	401 (34)	378[a] (30)
I^-	CH_2Cl_2	2570	766 (20)	499 (25)	400 (30)	377 (30)
ClO^-_4	CH_2Cl_2	2570	766 (20)	499 (25)	400 (31)	377 (30)
$F^- + BF_3$	CH_2Cl_2	2570	766 (20)	499 (25)	400 (29)	377 (30)
Cl^-	THF	1420	704 (19)	478 (29)	403 (40)	
ClO_4	THF	2020	735 (20)	490 (30)	404 (37)	
Cl^-	CH_3CN	1960	732 (23)	487 (32)	399 (38)	375[a] (31)
ClO^-_4	CH_3CN	1980	733 (23)	487 (33)	399 (38)	375[a] (30)

[a]Shoulder.

Table 5-4. UV-Visible Spectral Data of 4d as a Function of Counterion and Solvent Composition.

X	Solvent	$\Delta\nu_{CHO}$ (cm^{-1})	λ max (ε mM^{-1} cm^{-1})			
Cl^-	CH_2Cl_2	2650	771 (23)	500 (29)	402 (33)	380 (30)
Br^-	CH_2Cl_2	2770	778 (24)	502 (28)	402 (32)	378 (29)
ClO^-_4	CH_2Cl_2	3310	812 (25)	507 (28)	402 (27)	375 (29)
Cl^-	THF	2090	739 (20)	491 (27)	400 (42)	
Br^-	THF	2130	741 (22)	492 (29)	402 (39)	
ClO^-_4	THF	2180	744 (24)	494 (30)	403 (38)	
Cl^-	CH_3CN	2040	736 (23)	489 (31)	399 (44)	378[a] (33)
Br^-	CH_3CN	2040	736 (24)	489 (31)	398 (42)	378[a] (33)
ClO^-_4	CH_3CN	2040	736 (24)	489 (33)	399 (40)	378[a] (32)

[a]Shoulder.

observed essentially no counter anion effect for either 4c·HX or 4d·X^-. The anion dependence in the Soret region of chlorins 4c·HX and 4d·X^- also paralleled that of porphyrin 1c·HX. There is however, a difference in the protonation of Schiff's base 1c vs. 4c with HF. The spectrum of 4c·HF in CH_2Cl_2 is essentially identical to 4c·HCl (Table 5-2) and 4c·HBF_4 (obtained from addition of $BF_3 \cdot OEt_2$ vapor to 4c·HF[123b]) is identical to 4c·$HClO_4$ (see Figure 5-3 inset and Table 5-2). This could be the result of two effects: the pK_a of 4c is higher than the HF_2^- equilibrium constant or more likely, the presence of the 7-hydroxyl moiety aids in fluoride association with 4c HF, thereby lowering the "free" fluoride concentration.[123c]

The anion dependence on the spectral properties of pyrrolidinium salt 4d is clearly the result of ion pairing, however, the anion dependence of protonated Schiff's bases (1c·HX and 4c·HX) cannot be regarded so simply. Compound 4c·HX and 4d·X^- have very similar anion dependencies in CH_2Cl_2 yet different in THF. Since both solvents have relatively low dielectric constants we expect that the smaller anions are closely associated with the positive charge, producing the observed relative blue shifts with decreasing anion size. For 4d·X^- this accounts for only 90 cm^{-1} in THF while for 4c·HX, there is 600 cm^{-1} difference. This phenomenon may be the result

of Cl^- H-bonded to SBH^+. The diminished anion effect of $4d \cdot X^-$ in THF relative to CH_2Cl_2 is rationalized as arising from positive charge solvation.

Since using perchlorate as the counter ion for protonated 1c and 4c as well as 4d produced the largest red shifts, we assume that in the 3 solvents used, ion pairing with perchlorate is minimal. In THF and acetonitrile, we expect that a positive charge will be much more solvated than in CH_2Cl_2. For pyrrolidinium perchlorate 4d this produces a $\Delta\nu_{CHO}$ of 1130 cm^{-1} (CH_2Cl_2 vs. THF) and 1270 cm^{-1} (CH_2Cl_2 vs. CH_3CN); for $4c \cdot HClO_4$, the solvent dependence is 550 cm^{-1} (CH_2Cl_2 vs. THF) and 590 cm^{-1} (CH_2Cl_2 vs. CH_3CN); and for $1c \cdot HClO_4$, 433 cm^{-1} (CH_2Cl_2 vs. THF) and 459 cm^{-1} (CH_2Cl_2 vs. CH_3CN). However again, we cannot ascribe a single dominating effect to the shifts observed for SBH^+. Intuitively, we would expect that hydrogen bonding from a protonated Schiff's base would result in a blue shift relative to a non-H-bonded SBH^+. Since the pyrrolidinium perchlorate spectral data suggests large contributions from solvation on the extent of visible band red shifting, comparison of $4c \cdot HClO_4$ to $4d \cdot ClO_4^-$ spectral data in H-bond accepting solvents (i.e. THF) vs. non-accepting solvents (i.e. CH_2Cl_2) would lead to no useful conclusions.

The presence of a hydroxyl group in chlorin 4 offers a unique opportunity to study the effect of an

intramolecular H-bonding to CHO or CH=NR. In CH_2Cl_2 we observed that the visible absorption maximum of 4b is red shifted by 169 cm^{-1} with further splitting of the Soret region relative to THF (Figure 5-14). This effect can be titrated away with a variety of hydrogen bond acceptors, i.e. amines and ethers. The inset in Figure 5-14 shows such a titration with pyridine. We observed no solvent dependence on the spectrum of 1b. From the previous discussion the visible absorption band position and Soret splitting are a function of the electron withdrawing strength of the peripheral substituent. Intuitively it is expected that a H-bonded -CHO is more electron withdrawing than a "free" CHO. We believe the spectral difference of 4b in CH_2Cl_2 vs. THF are principally due to intramolecular hydrogen bonding between -CHO and the 7-OH group, where in THF the OH primarily interacts with solvent. Similar red shifting has been observed for copper porphyrin a on addition of H-bond donors in CH_2Cl_2.[2b]

Soret region resonance Raman spectroscopy also offered a deeper insight on the H-bonding effects on 4. The highest frequency vibrations of the aldehyde 4b in CH_2Cl_2 and THF occur at 1656 and 1663 cm^{-1}, respectively. These are assigned to the ν_{CO} stretching frequencies by analogy to formyl substituted metalloporphyrins.[124] The 7 cm^{-1} variation in ν_{CO} between CH_2Cl_2 and THF represents a hydrogen bond strength of approximately 1 kcal/mole,

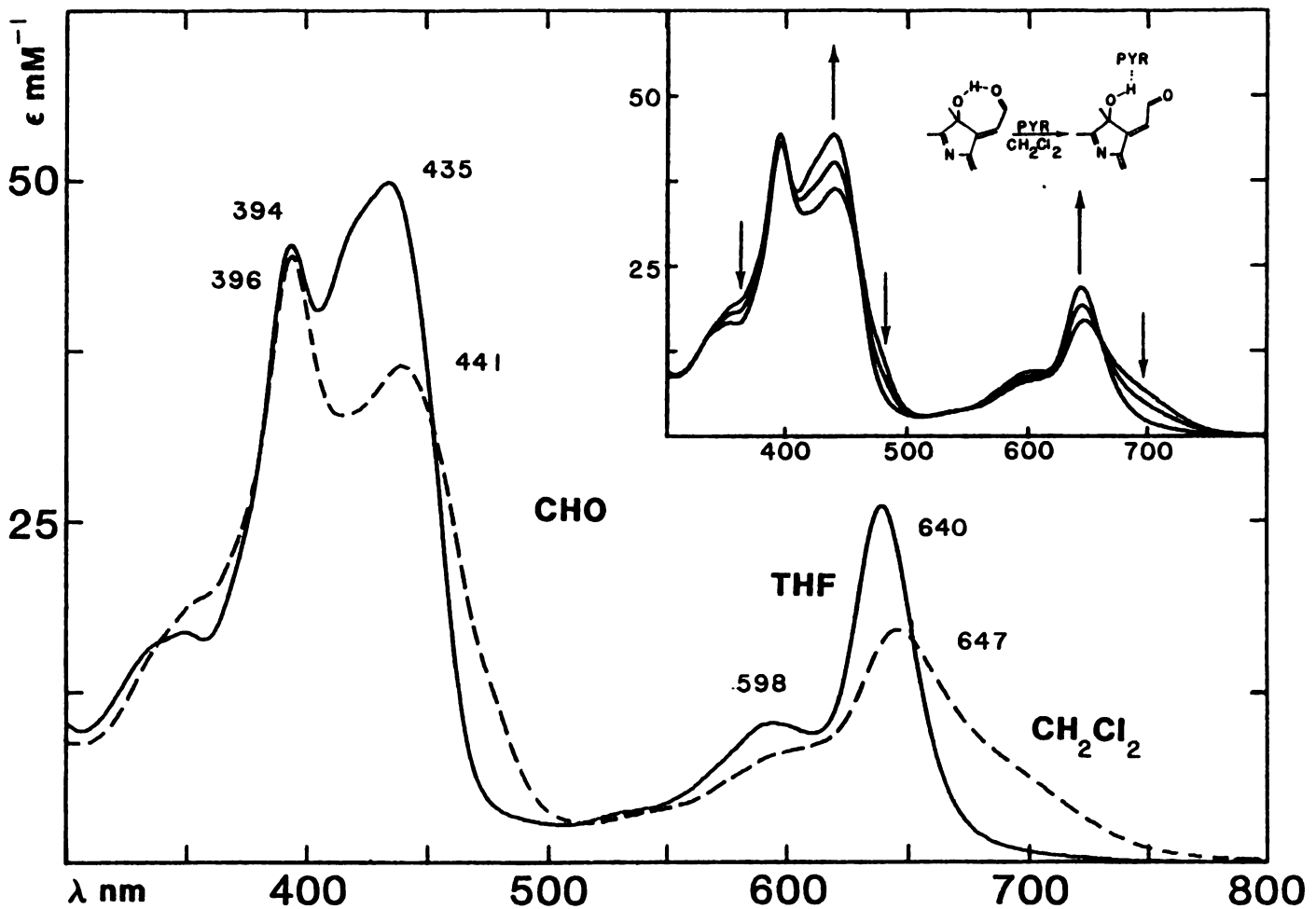

Figure 5-14. Absorption spectra of 4b in THF (——) and CH_2Cl_2 (---). Inset shows the spectra shifts observed upon dropwise addition of pyridine to 4b in CH_2Cl_2.

which predicts an optical red shift of 93 cm^{-1}.[124a] This is in qualitative agreement with out observations.

The resonance Raman spectra of aldehyde 4b in CH_2Cl_2 and THF (Figure 5-15) show that the π electron density sensitivity marker band at 1373 cm^{-1} (ν_4, A_{1g}) and core-size marker bands at 1641 cm^{-1} (ν_{10}, B_{1g}), 1582 cm^{-1} (ν_2, A_{1g}; ν_{13}, A_{2g}) and 1507 cm^{-1} (ν_3, A_{1g}) are not affected by hydrogen bonding at the ring periphery. Vibrations that are affected are: i) 1552 cm^{-1} (CH_2Cl_2) to 1548 cm^{-1} (THF), ii) 1451 cm^{-1} (CH_2Cl_2) to 1469 cm^{-1} (THF), iii) 1352 cm^{-1} (CH_2Cl_2) to 1342 cm^{-1} (THF), and iv) 1150 cm^{-1} (CH_2Cl_2) to 1141 cm^{-1} (THF). These vibrations may involve C_β-C_β, C_β-C_s stretching character or CHO bending,[125] however, further analysis is not possible at the present time. The mode observed at 1622 cm^{-1} is assigned to the C=C stretch of the acroleinyl substituent by analogy to similar group frequencies.[126]

As with aldehyde 4b Schiff's base 4c also forms an intramoleclar hydrogen bond. In the absorption spectrum (Figure 5-16) this is reflected as a 225 cm^{-1} red shift of the visible band and an overlapped splitting of the Soret. Like the aldehyde, the Schiff's base ring vibrations of the Soret region resonance Raman spectrum are not significantly perturbed (Figure 5-15). The major changes upon Schiff's base formation is the disappearance of the C=O frequency at approximately 1660 cm^{-1} and the C=C

Figure 5-15. Soret region resonance Raman spectra of aldehyde 4b and Schiff's base 4c in CH_2Cl_2 and THF with 406.7 nm laser excitation.

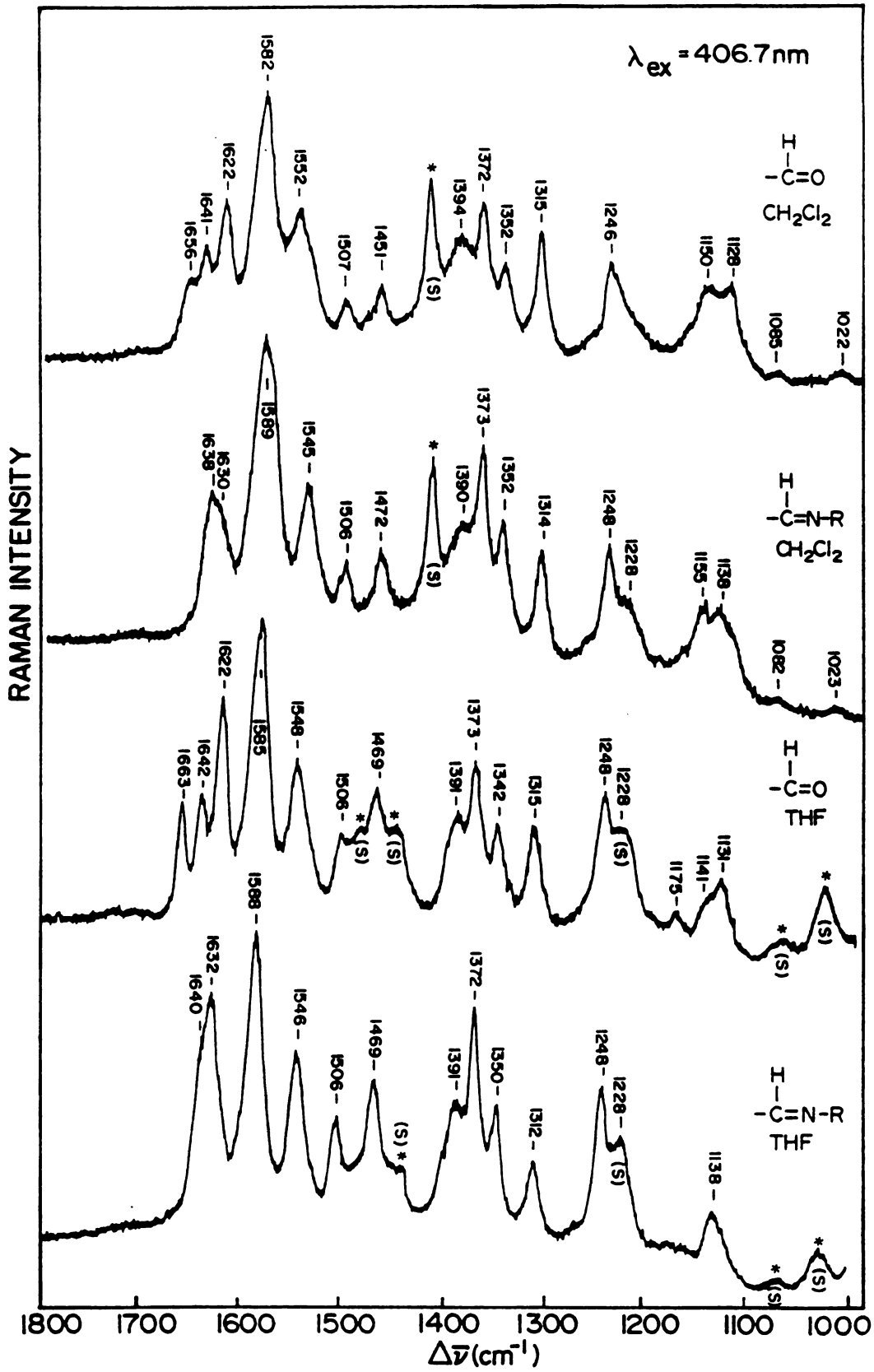
λex = 406.7nm
H
-C=O
CH2Cl2
1656
1641
1622
1582
1552
1507
1451
1394
1372
1352
1315
1246
1150
1128
1085
1022
H
-C=N-R
CH2Cl2
1639
1630
1589
1545
1506
1472
1390
1373
1352
1314
1248
1228
1155
1138
1082
1023
H
-C=O
THF
1663
1642
1622
1585
1548
1506
1469
1391
1373
1342
1315
1248
1228
1175
1141
1131
H
-C=N-R
THF
1640
1632
1588
1546
1506
1469
1391
1372
1350
1312
1248
1228
1138
RAMAN INTENSITY
1800
1700
1600
1500
1400
1300
1200
1100
1000
Δν̄(cm⁻¹)

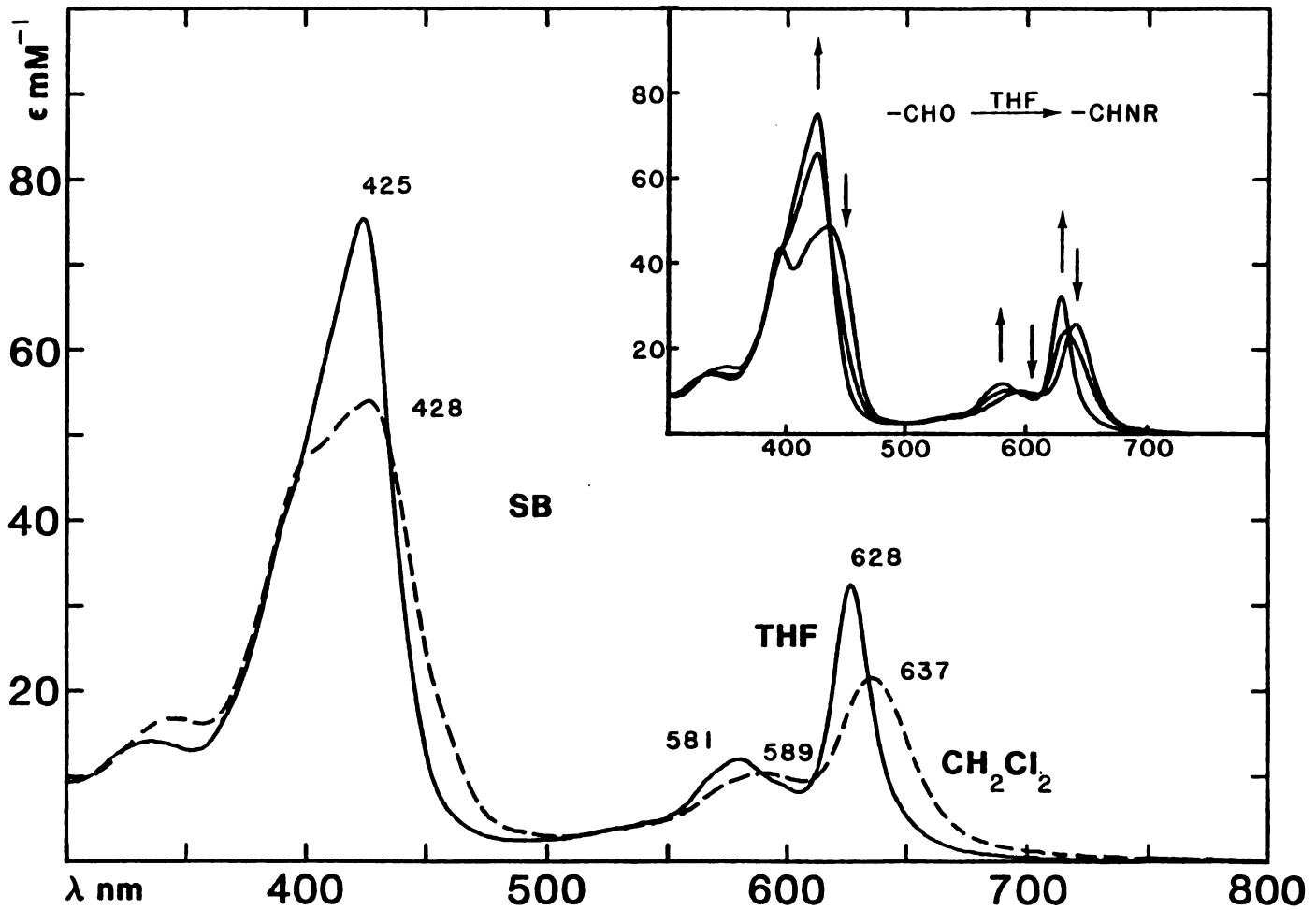

Figure 5-16. Absorption spectra of n-butyl Schiff's base 4c in THF (——) and CH_2Cl_2 (---). Conversion of 4b to 4c in THF with excess n-butylamine and catalytic amounts of HCl (inset).

vibration at 1622 cm^{-1} with the appearance of a band at approximately 1630 cm^{-1}.[128] This new vibration is assigned to the C=NR vibration in analogy to previously reported assignments.[110a] Due to overlap with a band at approximately 1640 cm^{-1} the exact position of the C=NR vibration was not possible to determine. Comparison of the 1640-1630 cm^{-1} region of SB·4c in CH_2Cl_2 and THF reveals that in THF the overlapping bands are more intense and narrower than in CH_2Cl_2. We interpret this as an increase of $\nu_{C=N}$ due to an intramolecular hydrogen bond to the 7-OH group in CH_2Cl_2. Other evidence is obtained in the 1150-1130 cm^{-1} region. For CHO and CHNR there are two bands in CH_2Cl_2 (CHO: 1150, 1128 cm^{-1}, $CHNR^+$: 1155, 1138 cm^{-1}), while in THF these bands apparently collapse (CHO: 1141, 1131 cm^{-1}, CHNR: 1138 cm^{-1}). The other solvent sensitive bands of CHO are not very much perturbed for CHNR.

Besides solvent and anion effects demonstrating the variability of the spectral shifts associated with Schiff's base protonation, further evidence for separation of the in-plane polarized transition dipoles is also provided. The effect of solvent and anion on the Soret region in general is that the position of the higher energy Soret component remains essentially invariant while the lower energy component parallels the shifts observed by the visible region absorbance maximum (see Figures 5-11, 5-12, 5-13 and Tables 5-2, 5-3, 5-4). Since the lower

energy Soret component is sensitive to ion pairing, solvation and hydrogen bonding, it seems logical to conclude that the lower energy Soret band is predominantly the in-plane polarized transition dipole along the protonated Schiff's base axis, while the invariability of the higher energy Soret band suggests it is the other polarization transition dipole. These assignments were confirmed by resonance Raman spectroscopy (above) for 4c·HCl and $4d \cdot ClO_4^-$.

Redox Potentials:

Electrochemical redox potentials of porphyrinoid compounds often give useful information concerning the orbital energies of the system since, to a first approximation, the redox span of the monocation to mono-anion radical formation corresponds to the HOMO-LUMO energy gap.[129] Unfortunately, cyclic voltammograms for 4c, 4c·HX or 4d gave only ill-defined redox waves. Therefore, the aldehyde 4b, ethyl cyanoacetate 4e, and malononitrile 4d adducts were investigated as models. The CV of these compounds in THF are reproduced in Figures 5-17 to 5-19. The reversible formation of cation and anion radical species can be readily observed. The apparently coupled irreversible waves at -1160 and 40 mV for 4e and at -1150 and 130 mV for 4f, which were absent in 4b, are probably due to redox reactions occurring at the ring periphery.

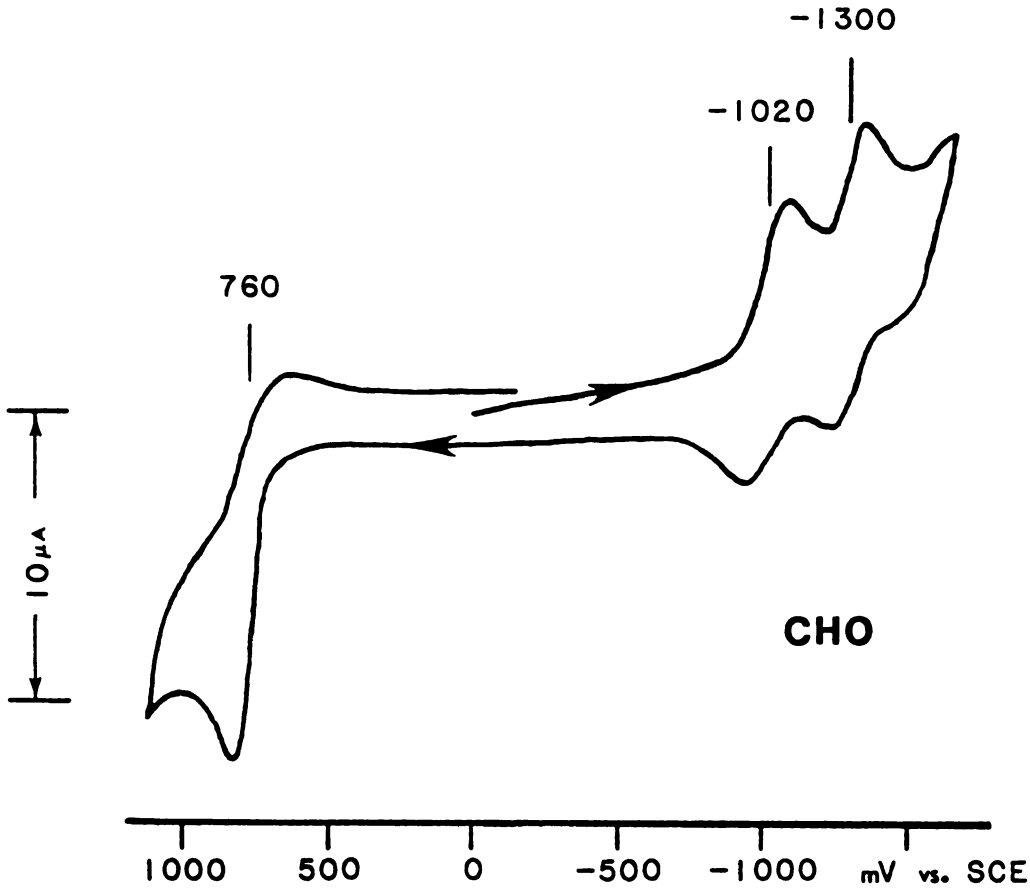

Figure 5-17. Cyclic voltammogram of 4b in THF containing 0.1 M tetrabutylammonium perchlorate (TBAP). Scan rate was 100 mV/sec.

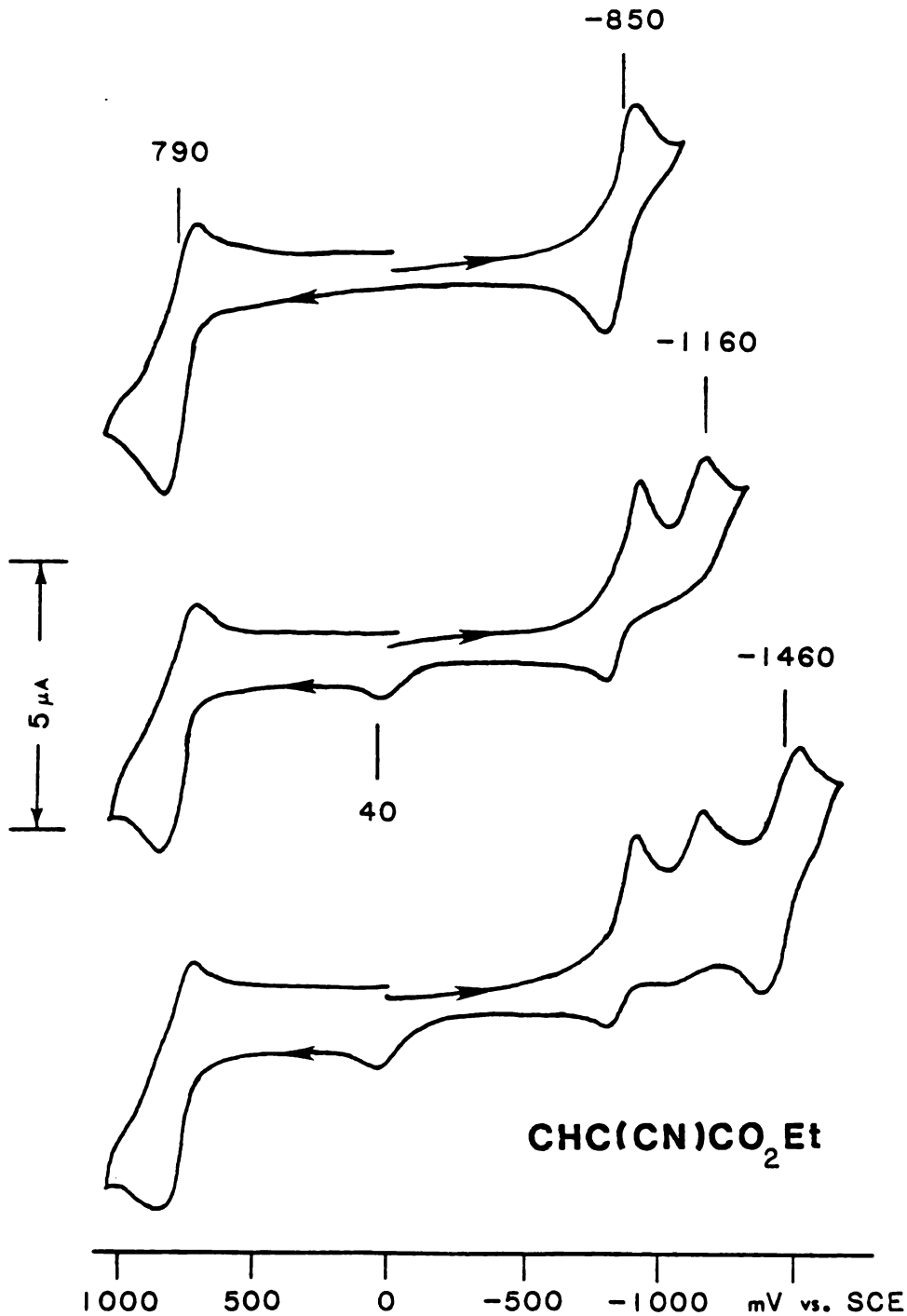

Figure 5-18. Cyclic voltammograms of ethyl cyanoacetate adduct 4e in THF containing 0.1 M TBAP at a scan rate of 100 mV/sec. Scan direction was reversed after first, second and third reduction wave (top to bottom respectively).

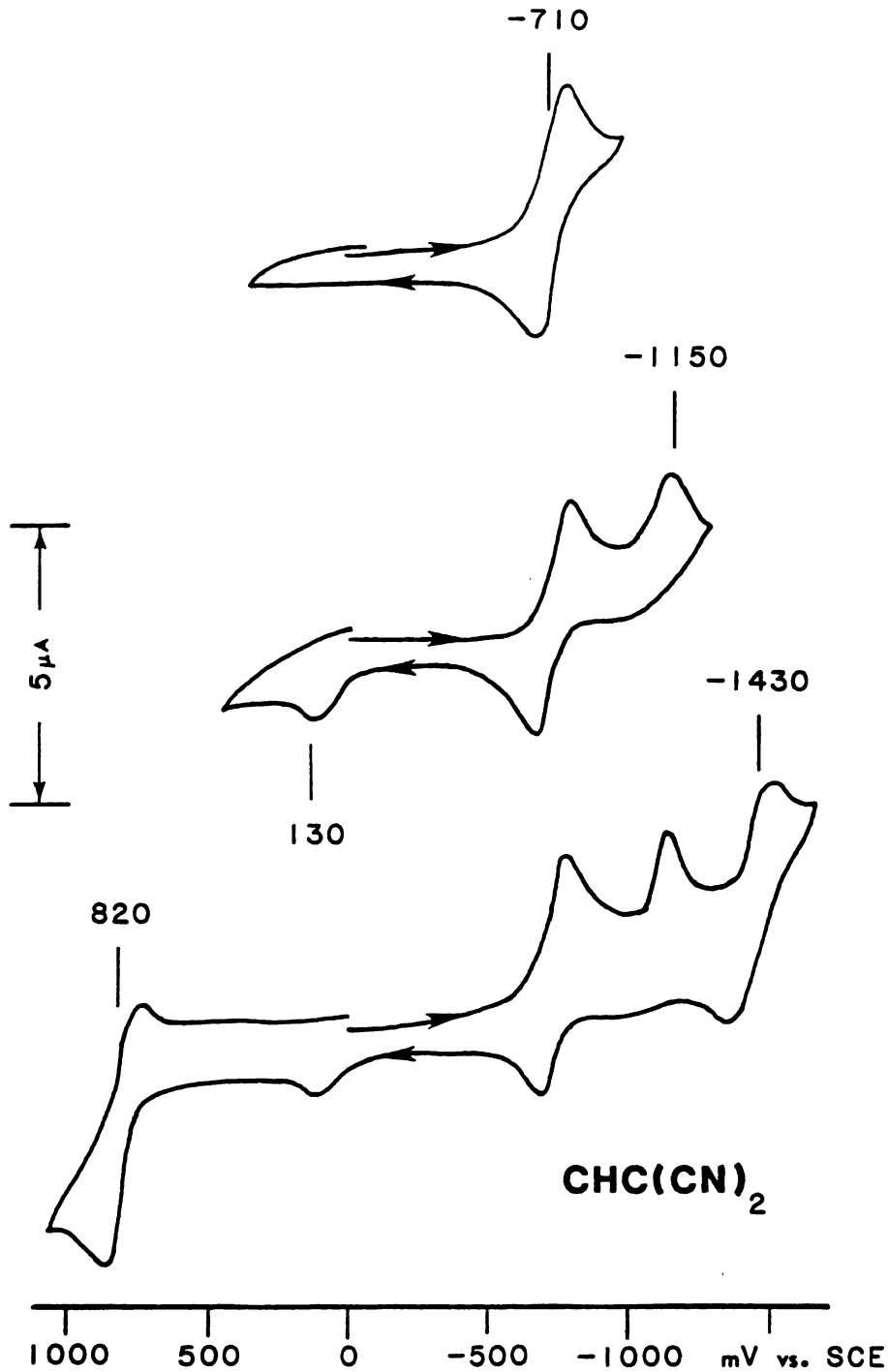

Figure 5-19. Cyclic voltammograms of malononitrile adduct 4f in THF containing 0.1 M TBAP (100 mV/sec). Scan direction was reversed after first (top), second (middle) and third (bottom) reduction wave.

While it may be difficult to ascertain to what extent coulombic forces will perturb the redox potentials of SBH^+, the model studies indicate it seems certain that SBH^+ will be easier to reduce but somewhat harder to oxidize than the parent aldehyde (Fig. 5-20). As is the case with mono-formyl vs. di-formyl porphyrins,[114a] the effect of increasing the electron withdrawing power of the substituents serves to decrease the HOMO-LUMO gap, indicating the presence of a strong resonance effect. Also similar to formyl porphyrins, the electron withdrawing substituents seem to mostly affect the energy of the LUMO. This has been interpreted as an evidence that the substituent lowest vacant π^* orbital lies very close to the macrocycle lowest π^* orbital to allow mixing.[114a] Therefore, protonation of Schiff's bases further splits the excited states degeneracy and lowers the π^* orbital energies, but leaving the π orbitals essentially unaltered. Indeed, resonance Raman and NMR spectra of 1c·HCl (above and reference 110a) showed that the ground state is not very much perturbed. Detailed theoretical discussions of orbital structures are given in reference 112.

Summary

By measuring the optical spectra of derivatives produced by reversible modifications at the -CHO group on porphyrinoid macrocycles in conjunction with proton NMR and resonance Raman spectroscopies, we have shown that

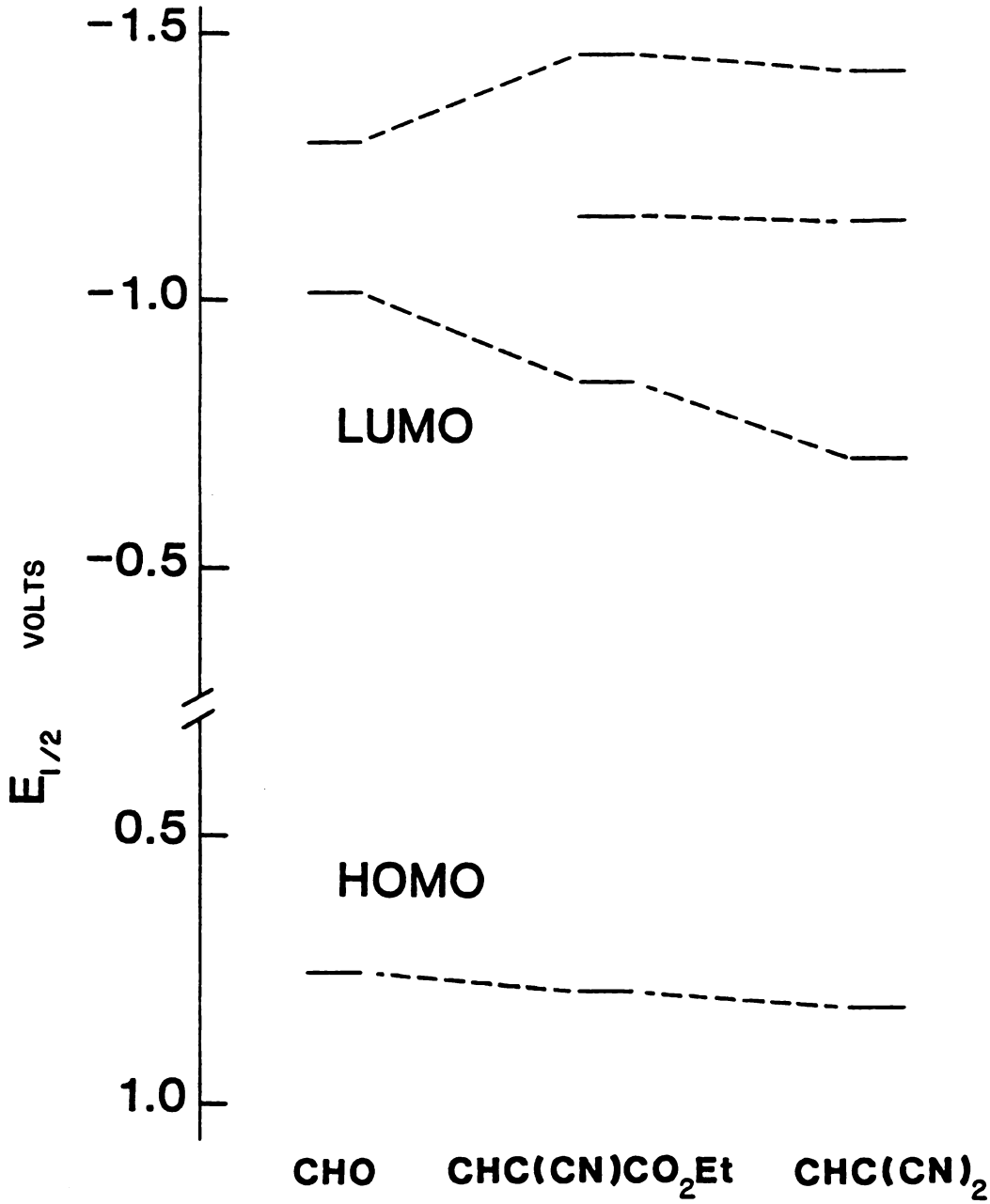

Figure 5-20. Half-wave redox potentials of aldehyde 4b, ethyl cyanoacetate adduct 4e and malononitrile adduct 4f (measured in THF vs. SCE).

the unusual red shift of absorption maxima in the visible region and the Soret band splitting observed for Schiff's base porphyrins and chlorins upon protonation is due to the resonance effect of a strong electron withdrawing group on the ring periphery, not because of a delocalization of the positive charge onto the ring. We have further demonstrated that the conversion of a carbonyl to a Schiff's base peripheral group would subject the spectral properties of chlorin and porphyrin to a greater degree of environmental control than otherwise possible. In view of the large variations in the visible absorption maxima of photosynthetic chlorophylls, our result would certainly make a Schiff's base chlorophyll an interesting model for reaction centers. Even more intriguing is the fact that there are large differences in oxidation potentials of P700 and P680. Titrations of P700 yield a midpoint potential ranging between +0.4 and +0.5 V versus the normal hydrogen electrode (NHE) whereas the minimum potential needed to oxidize water to oxygen at physiological pH sets a lower limit of +0.8 V for P680, which makes an electron withdrawing system such as 4c very attractive. Further investigations, particularly EPR and electrochemical studies of Schiff's base chlorophylls are needed to verify the validity of these proposals.

Materials and Methods

Visible spectra were recorded on a Cary 219 spectrophotometer interfaced to a Bascom-Turner recorder. Spectra shown here were recalled directly from floppy diskettes. NMR spectra were obtained using a Bruker WM-250 instrument. Elemental analyses were performed by Spang; C, H, N analyses were within 0.5%. Cyclic voltammetry was performed using a Bioanalytical Systems CV-1A unit or a Pine Instrument RDE-3 potentiostat in a specially constructed glass cell which contains two platinum spherical electrodes sealed through the cell wall. All measurements were carried out in THF containing 0.1 M tetrabutylammonium perchlorate at a scan rate of 100 mV/sec. Resonance Raman spectra were recorded using a Spex 1401 double monochromator and the associated Ramalog electronics. Laser excitations at 406.7 and 488.0 nm were obtained with a Spectra Physics 164-11 krypton ion laser equipped with a high-field magnet. Incident powers were 20-40 mW. All spectra were collected at 90° scattering geometry at room temperature. To ensure no sample decomposition, optical spectra were recorded before and after each RR experiment.

Materials:

CH_2Cl_2, CH_3CN and triethylamine were freshly distilled from CaH, tetrahydrofuran from lithium aluminum hydride before use. Pyrrolidine hydroperchlorate and hydrobromide were prepared by addition of the concentrated acid to

pyrrolidine in THF until the solution was just acidic enough to wet pH paper. Water was azeotroped out with benzene on a rotary evaporator followed by three crystallizations from THF/ethyl acetate. Pyrrolidine hydrochloride was prepared by bubbling an etheral solution of pyrrolidine with anhydrous HCl followed by crystallizations (3X) from THF/ethyl acetate. All other commercially obtained chemicals were used without further purification.

Nickel 2,6-di-n-pentyl-4-vinyl-8-formyl-1,3,5,7-tetramethyl-porphine (1b):

Chlorin 4a (vide infra, 100 mg) in CH_2Cl_2 (100 ml) was reduced by addition of sodium borohydride (50 mg) in methanol (2 mL) followed by quenching with dilute acetic acid after 5 min. The resultant diol porphyrin was dissolved in pyridine (100 mL) followed by addition of aqueous sodium periodate (5%, 30 mL), heated on a steam bath for 30 min, cooled, diluted with CH_2Cl_2 and extracted with 15% aqueous HCl. The crude product was purified by column chromatography using silica gel, crystallized from CH_2Cl_2-MeOH and characterized by NMR and UV-vis spectroscopies. Yield of 1a: 60 mg. Nickel insertion was accomplished by refluxing 1a (60 mg) in CH_2Cl_2/MeOH with excess $Ni(OAC)_2$ for approximately 2 hours followed by crystallization from CH_2Cl_2/MeOH. Yield 1b: 55 mg. NMR δ ($CDCl_3$) pentyl: 0.89 (6 H, m), 1.95 (4 H, m), 3.53 (4 H, m); ring Me: 3.16 (3 H, s), 3.20 (3 H, s),

3.37 (3 H, s), 3.42 (3 H, s); vinyl: 6.09 (2 H, m), 7.94 (1 H, m); meso: 8.97 (1 H, s), 9.13 (1 H, s), 9.29 (1 H, s), 9.96 (1 H, s); CHO: 11.06 (1 H, s). λ_{max} (ε_{mM}) in CH_2Cl_2: 409 nm (114), 516(5.9), 542(6.9), 589(21).

Nickel 6,7-di-n-pentyl-1,4-diformyl-2,3,5,8-tetramethylporphine (2b) and Nickel 2,6-di-n-pentyl-4,8-diformyl-1,3,5,7-tetramethylporphine (3b):

The appropriate divinyl porphyrin[114] (100 mg) dissolved in pyridine (100 mL) was added to a solution of osmium tetroxide (100 mg) in pyridine (10 mL) and stirred at room temperature for 1 hr. To this was added an aqueous sodium sulfite solution (15%, 30 mL) and heated on a steam bath for 30 min. followed by partition between CH_2Cl_2/H_2O. The porphyrin glycols were then oxidized with sodium periodate and purified as with 1a. The yield for either porphyrin: ~80%. Nickel insertion was accomplished as with 1a except that overnight reflux was necessary for completion. NMR 2b $\delta(CDCl_3)$pentyl: 1.01 (6 H, t), 1.58 (8 H, m), 2.00 (4 H, m), 3.52 (4 H,t); ring Me: 2.52 (6 H, s) 3.52 (6 H, s); meso: 8.82 (1 H, s), 9.39 (2 H, s), 10.54 (1 H, s); CHO: 10.53 (2 H, s).

λmax (ε_{mM}): 423 nm (125), 535(11.5), 578(21). NMR 3b $\delta(CDCl_3)$pentyl: 0.92 (6 H, t), 1.55 (8 H, m), 1.90 (4 H, m), 3.5 (4 H, m); ring Me: 3.10 (6 H, s), 3.42

(6 H, s); meso: 8.83 (2 H, s), 9.76 (2 H, s); CHO: 11.1 (2 H, s). λ_{max} (ε_{mM}): 412 nm (119), 509(5.5, 607(35).

2,6-di-n-pentyl-4-vinyl-7-hydroxyl-8-acroleinyl-1,3,5,7-tetramethylchlorin (4a) and 2,6-di-n-pentyl-3,7-dihydroxy-4,8-diacroleinyl-1,3,5,7-tetramethylbacteriochlorin (5a):

2,6-Di-n-pentyl-4,8-divinyl-1,3,5,7-tetramethylporphine[9] (200 mg) in CH_2Cl_2 was photolyzed with aeration for 30 min in a water cooled photolysis apparatus with a 250 W tunsten halogen lamp. The reaction mixture was then concentrated and chromatographed on silica gel. CH_2Cl_2 elution afforded unreacted divinyl porphyrin, followed by the monooxygen adduct then the trans-di-adduct. The cis-di-adduct was obtained by elution with 5% MeOH-CH_2Cl_2. Pure epimeric mono-adduct and cis-di-adduct were crystallized from MeOH-CH_2Cl_2. NMR of the chlorin is obtained (90 mg) in $CDCl_3$: δ pentyl: 0.89 (3 H, t), 9.06 (3 H, t), 1.5 (4 H, m), 1.98 (2 H, q), 2.12 (2 H, q), 3.7 (4 H, m); ring Me: 1.60 (3 H, s), 3.22 (3 H, s), 3.45 (3 H, s), 3.51 (3 H, s); OH: 2.9 (1 H, b); vinyl: 6.18 (2 H, m), 8.1 (1 H, m); =CHCHO: 6.8 (1 H, d), 10.2 (1 H, d); meso-H: 8.17 (1 H, s), 8.56 (1 H, s), 9.60 (1 H, s), 9.72 (1 H, s); NH: -3.43 (1 H, s), -3.61 (1 H, s), λ_{max} (ε_{mM} in THF): 336 nm (24), 391(80), 411(91), 423(89), 504(6.1) 568(18), 601(7.9), 660(46). The cis-bacteriochlorin 2a δ($CDCl_3$)pentyl: 0.88 (6 H, t), 1.5 (16 H, m), 1.93 (4 H, q), 3.76 (4 H, m);

ring Me: 1.63 (6 H, s), 3.14 (6 H, s); OH: 5.84 (2 H,s); =CHCHO: 7.14 (2 H, d), 10.58 (2 H, d); meso-H: 8.30 (2 H, s), 8.55 (2 H, s); NH: -4.41 (2 H, s); λ_{max} (ε_{mM} in THF): 350(23), 419(55), 443(75), 581(12), 659(6.1), 692(5.6), 729(70). The trans isomer had identical spectral properties. Copper was inserted by standard procedures.[27b]

Schiff's Base Formation:

i) Schiff's bases ic, 2c, and 3c: Nickel formyl porphyrins 1b, 2b and 3b were refluxed in benzene containing excess n-butylamine for 3 hr. Water produced was removed by allowing the condensate to filter through a silica gel pad prior to returning to the flask. Lypholyzation afforded pure 1c, 2c and 3c. The Schiff's bases were each characterized by NMR and visible spectroscopies. NMR 1c $\delta(CDCl_3)$pentyl: 0.94 (6 H, t); 1.50 (8 H, m); 2.09 (4 H, m), 3.71 (4 H, m); butyl: 1.18 (3 H, t), 1.63 (2 H, m), 1.82 (2 H, m), 4.07 (2 H, t); ring Me: 3.29 (3 H, s), 3.34 (3 H, s), 3.47 (3 H, s), 3.54 (3 H, s); vinyl: 6.08 (2 H, m), 8.06 (1 H, m); Meso: 9.50 (3 H, m), 9.65 (1 H, s); CHN: 10.64 (1 H, s), λ_{max} (ε_{mM}): 404 nm (149), 515(4.6), 538(5.5), 577(16). NMR 2c $\delta(CDCl_3)$ pentyl: 0.96 (6 H, t), 1.52 (8 H, m), 2.09 (4 H, m), 3.72 (4 H, t); butyl: 1.20 (6 H, t), 1.65 (4 H, m), 1.83 (4 H, m), 4.07 (4 H, t); ring Me: 3.34 (6 H, s), 3.42 (6 H, s); meso and CHN; 9.38 (1 H, s), 9.42 (3 H,s), 10.58 (2 H, s). NMR 3c $\delta(CDCl_3)$ pentyl: 0.96 (6 H, t),

1.50 (8 H, m), 2.08 (4 H, m), 3.73 (4 H, t); butyl: 1.18 (3 H, t), 1.64 (2 H, m), 1.83 (2 H, m), 4.06 (2 H, t); ring Me: 3.25 (6 H, s), 3.56 (6 H, s); meso: 9.51 (2 H,s), 9.54 (2 H, s); CHN: 10.68 (2 H, s), λ_{max} (ε_{mM}): 407 nm (162), 515(7.2), 541(8.7), 584(29).

ii) Schiff's base 4c: To 4b (2 mg) in CH_2Cl_2 (3 ml) was added 5 drops n-butylamine and allowed to stand 15 minutes followed by evaporation under a stream of dry argon. The absorption spectrum was identical to that from (iii) in CH_2Cl_2 or THF.

iii) Schiff's base by spectrophotometric method: To an ~10^{-5} M solution of 1b, 2b, 3b (CH_2Cl_2) 4b or 5b (THF) was added 1 drop of n-butylamine and then 1 mL of air equilibrated over conc. HCl was bubbled through the solution. Reactions were complete within 10 min. Isosbestic points: 1b to 1c (nm); 375, 409, 500, 582; 2b to 2c: none; 3b to 3c: none; 4b to 4c (nm): 395, 436, 500, 591, 612, 635; 5b to 5c: none. To 4b (~10^{-5} M) in CH_2Cl_2 was added 2 drops of a solution containing 3 drops of n-butylamine in 5 mL CH_2Cl_2 and a catalytic amount of HCl. Reaction required about 2 hr for completion. Isosbestic points: 396, 445, 517, 647 nm.

Pyrrolidinium Salt (4d):

To 5 mg 4b in CH_2Cl_2 (5 mL) was added 1 equivalent of pyrrolidine hydroperchlorate and 1 drop of trimethyl orthoformate, allowed to stand 48 hours at room

temperature, diluted with benzene and lypholyzed. The UV-vis spectrum was identical to that obtained below.

To ~10^{-5} M 4b in CH_2Cl_2 or THF was added a couple of crystals of pyrrolidine HX and the spectrum monitored. Isosbestic points (THF): 4b to 4d·ClO_4: 383, 459, 538, 662 nm.

Malononitrile adduct (4f):

i) To ~10^{-5} M 4b in THF was added 1 drop of malononitrile and 1 drop of triethylamine. Reaction was complete within 10 min. Isosbestic points: 385, 457, 564, 659 nm.

ii) 7 mg 4a was dissolved in 30 mL THF. To this solution 4 drops of malononitrile and 3 drops of triethylamine were added. This was refluxed 2 hr followed by dilution with ether. The ether phase was extracted with 20% acetic acid (4X), washed with H_2O (2X), brine (2X), dried over anhydrous Na_2So_4, and evaporated in vacuo; yield: quantitative. NMR $\delta(CDCl_3)$pentyl: 0.89 (3 H, t), 1.07 (3 H, t), 1.3 (4 H, m), 1.6 (6 H, m), 2.3 (2 H, m), 3.7 (2 H, m), 4.0 (2 H, m); ring Me: 1.27 (3 H, s), 3.44 (3 H, s), 3.58 (3 H, s), 3.68 (3 H, s); OH: 6.7 (1 H, s); vinyl: 6.26 (2 H, m), 6.18 (1 H, m); =CHCH=$C(CN)_2$: 2.84 (1 H, d), 7.67 (1 H, s); meso H: 8.26 (1 H, s), 9.86 (2 H, s), 9.89 (1 H, s); NH: -3.6 (1 H, s), -4.1 (1 H, s).

Ethyl Cyanoacetate Adduct (4e):

This was prepared as in (i) for malononitrile. Reaction required about 10 hours for completion. Isosbestic points: 380, 455, 535, 655 nm.

Pyrrolidine Hemiaminal:

To ~10^{-5} M 1b in THF or CH_2Cl_2 was added 1 drop of pyrrolidine. Reaction was completed within 30 minutes. Isosbestic points (THF): 321, ~370, 423, 496, 578, 602, 628 nm.

Schiff's Base Protonation/Deprotonation:

i) HF, HCl, HBr in CH_2Cl_2: To ~10^{-5} M 1c or 4c in CH_2Cl_2 was bubbled air which had been equilibrated over the respective concentrated acid. (This was easily accomplished by withdrawing the air inside a bottle of acid with a small syringe and then passing the air into the cuvette.) The resultant SB·HCl spectra were identical as in (ii). BF_3OEt_2 was introduced to SB·HF by bubbling BF_3OEt_2-saturated air through the solution.

ii) To ~10^{-5} M Schiff's base in CH_2Cl_2, THF or CH_3CN was added dropwise an anhydrous HCl-saturated CH_2Cl_2 solution.

iii) HI: To ~10^{-5} M 1c or 4c in CH_2Cl_2 was injected a small amount of HI vapor prepared by adding conc. sulfuric acid to KI.

iv) $HClO_4$: To ~10^{-5} M Schiff's base in CH_2Cl_2, THF, or CH_3CN was added dropwise a 70% $HClO_4$-saturated methylene chloride solution.

v) SBH^+ were returned to the original SB by bubbling triethylamine-saturated air through the acidified solution.

Borohydride Reduction:

To ~10^{-5} M 4b in CH_2Cl_2 was added a couple of crystals of tetrabutylammonium borohydride and the UV-vis spectrum monitored. Isosbestic points: 321, 370, 423, 496, 578, 602, 628 nm. Addition of 2 drops of 1:1:1 CH_3OH:TFA:H_2O solution yielded a typical copper porphyrin spectrum. Isosbestic points: 313, 345, 369, 409, 544, 557, 528 nm. λ_{max} (Cu porphyrin): 400, 528, 570 nm.

REFERENCES AND NOTES

REFERENCES AND NOTES

1. Wilkstrom, M; Krab, K.; Saraste, M. "Cytochrome Oxidase", Academic Press:New York, 1981.

2. a. Murphy, M.J.; Siegel, L.M.; Tove, S.R.; Kamin, H. (1974) Proc. Nat'l. Acad. Sci USA 71, 612; b. Vega, J.M.; Garrett, R.H.; Siegle, L.M. (1975) J. Biol. Chem. 250, 7980; c. Vega, J.M.; Kamin, H. (1977) J. Biol. Chem. 252, 896.

3. a. Barrett, J. (1956) Biochem. J. 64, 626; b. Yamanaka, T.; Kihimoto, S.; Okunuki, K. (1963) J. Biochem. 53, 416; c. Yamanaka, T.; Ota, A.; Okunuki, K. (1960) Biochem. Biophys. Acta 44, 397; d. Kuronen, T.; Ellfolk, N. (1972) Biochem. Biophys. Acta 275, 308.

4. a. Siegle, L.M.; Murphy, M.J.; Kamin, H. (1973) J. Biol. Chem. 248, 251; b. Murphy, M.J.; Siegle, L.M.; Kamin, H. (1973) J. Biol. Chem. 248, 2801; c. Murphy, M.J.; Siegle, L.M. (1973) J. Biol. Chem. 248, 6911; d. Siegle, L.M.; Davis, P.S.; Kamin, H. (1974) J. Biol. Chem. 249, 1572; e. Murphy, M.J.; Siegle, L.M.; Kamin, H. (1974) J. Biol. Chem. 249, 1610.

5. Chang, C.K. (1980) Biochem. 1971.

6. Young, R.; Chang, C.K.; Ward, B., manuscript in preparation.

7. See also: Stolzenberg, A.M.; Strass, S.H.; Holm, R.H. (1981) J. Am. Chem. Soc. 103, 4763.

8. Jacob, G.S.; Orme-Johnson, W.H. (1979) Biochem. 2967.

9. Ward, B.; Chang, C.K. (1982) Photochem. Photobiol. 35, 757.

10. Chang, C.K. in "The Biological Chemistry of Iron" Dunford, H.B. et al. (eds.) D. Reidel:Boston 1982, pp. 313-334 and references therein.

11. Brault, D.; Rougee, M. (1973) Nature (New Biol.) 241, 19.

12. a. White, D.K.; Cannon, J.B.; Traylor, T.G. (1979) J. Am. Chem. Soc. 101, 2443; b. Rougee, M.; Brault, D. (1975) Biochem. 14, 4100.

13. a. Smith, M.H. (1959) Biochem. J. 73, 90; b. Sono, M.; McCray, J.A.; Asakura, T. (1977) J. Biol. Chem. 252, 7475.

14. Wayland, B.B.; Mehne, L.F.; Swartz, J. (1978) J. Am. Chem. Soc. 100, 2379.

15. a. Caughey, W.S.; Alben, J.O.; McCoy, S.; Boyer, S.H.; Charache, S.; Hathaway, P. (1969) Biochem. 8, 59; b. Chang, C.K.; Dolphin, D. (1976) Proc. Nat'l. Acad. Sci. USA 73, 3338; c. Traylor, T.G.; Campbell, D.; Sharma, V.; Geibel, J. (1979) J. Am. Chem. Soc. 101, 5376; d. Ward, B.: Wang, C.B.; Chang, C.K. (1981) J. Am. Chem. Soc. 101, 5236.

16. Gansow, O.A.; Vernon, W.D. in "Topics in Carbon-13 NMR Spectroscopy", Levy, G.C. (ed.) Vol. 2, John Wiley:New York, 1976, pp. 270-325 and references therein.

17. Karplus, M.; Pople, J.A. (1963) J. Chem. Phys. 38, 2803.

18. Phillips, J.N. (1960) Rev. Pure & Appl. Chem. 10, 35.

19. Parmely, R.C.; Goff, H.M. (1980) J. Inorg. Chem. 102, 841.

20. Buchler, J.W.; Kokisch, W.; Smith, P.D. (19) Structure and Bonding 34, 79.

21. Geible, J.; Chang, C.K.; Traylor, T.G. (1975) J. Am. Chem. Soc. 97, 5924.

22. Brinigar, W.S.; Chang, C.K. (1974) J. Am. Chem. Soc. 96, 5595.

23. Chang, C.K. (1979) in "Biochemical and Clinical Aspects of Oxygen", Academic Press:New York, pp. 449-451.

24. Nakamoto, K. (1970) "Infrared Spectra of Inorganic and Coordination Complexes", Wiley-Interscience: New York.

25. Olson, L.W.; Schaeper, D.; Lancon, D.; Kadish, K.M. (1982) J. Am. Chem. Soc. 104, 2042.

26. a. Lancaster, J.R.; Vega, J.M.; Kamin, H.; Orme-Johnson, N.R.; Orme-Johnson, W.H.; Kreuger, R.J.; Siegel, L.M. (1979) J. Biol. Chem. 254, 1268; b. Johnson, M.K.; Thompson, A.J.; Walsh, T.A.; Barber, D.; Greenwood, C. (1980) Biochem. J. 189, 1393.

27. a. Adler, A.D.; Longo, F.R.; Finarelli, J.D.; Goldmacher, J.; Assour, J.; Korsakoff, L. (1967) J. Org. Chem. 32, 476; b. Fuhrrop, J.H.; Smith, K.M. (1975) in "Porphyrins and Metalloporphyrins" Smith, K.M. (ed.) Elsevier:New York, p. 803.

28. a. Chang, C.K.; Traylor, T.G. (1975) Proc. Nat'l. Acad. Sci. USA 72, 1166; b. Traylor, T.G.; Chang, C.K.; Geibel, J.: Berzinis, A.; Mincey, T.; Cannon, J. (1979) J. Am. Chem. Soc. 101, 6716.

29. a. Brault, D.; Morliere, P.; Rougee, M.; Land, E.J.; Santus, R.; Swallow, A.J. (1980) J. Amer. Chem. Soc. 102, 1015; b. Shafferman, A.S.; Stein, G. (1974) Science 183, 428; c. van Leeuwen, J.W.; Tromp, J.; Nauta, H. (1979) Biochem. Biophys. Acta 577, 394; d. Goff, H.; Simic, M.G. (1975) Biochem. Biophys. Acta 392, 201; e. Simic, M.G.; Taub, I.A.; Tocci, J.; Hurwitz, P.A. (1975) Biochem. Biophys. Res. Comm. 62, 161; f. Simic, M.G.; Taub, I.A. (1978) Biophys. J. 24, 285.

30. Neckers, D.C. (1967) "Mechanistic Organic Photochemistry", Chapter 7, Reinhold Publishing Corp.:New York.

31. a. Dolphin, D.; Sams, J.R.; Tsin, T.B.; Wong, K.L. (1976) J. Amer. Chem. Soc. 98, 6970; b. Reed, C.A.; Mashiko, T.; Scheidt, W.R.; Spartalian, K.; Lang, G. (1980) J. Amer. Chem. Soc. 102, 2302.

32. a. Castro, C.E.; Robertson, C.; Davis, H. (1974) Bioorg. Chem. 3, 343; b. Simic, M.G.; Taub, I.A. (1977) Faraday Discuss. Chem. Soc. 63, 270.

33. a. Rao, P.S.; Hayon, E. (1974) J. Amer. Chem. Soc. 96, 1287; b. Bansal, K.M.; Henglein, A. (1974) J. Phys. Chem. 78, 160; c. Bansal, K.M.; Henglein, A.; Sellers, R.M. (1974) Ber. Bunsenges Phys. Chem. 78, 569.

34. a. Kitagawa, T.; Orii, Y. (1978) J. Biochem. 84, 1245; b. Adar, F.; Yonetani, T. (1978) Biochem. Biophys. Acta 502, 80; c. Salmeen, I.; Rimai, L.; Babcock, G.T. (1978) Biochem. 17, 800.

35. Vorkink, W.P.; Cusanovich, M.A. (1974) Photochem. Photobiol. 19, 205.

36. Poff, K.L.; Butler, W.L. (1975) Plant Physiol. 55, 427.

37. Kitagawa, T.; Nagai, K. (1979) Nature 281, 503.

38. Kitagawa, T.; Fukumori, Y.; Yamanaka, T. (1980) Biochem. 19, 5721.

39. a. Lipscomb, J.D.; Sligar, S.G.; Namtvedt, M.J.; Gunsalas, I.C. (1976) J. Biol. Chem. 251, 1116; b. Schmidt, W.; Butler, W.L. (1976) Photochem. Photobiol. 24, 71.

40. Manabe, K.; Poff, K.L. (1978) Plant Physiol. 61, 961.

41. Bocian, D.F.; Lemeley, A.T.; Peterson, N.O.; Brudvig, G.W.; Chan, S.I. (1979) Biochem. 18, 4396.

42. Huber, R.; Epp, O.; Formanek, H. (1970) J. Mol. Biol. 52, 349.

43. Heidner, E.J.; Ladner, R.C.; Perutz, M.F. (1976) J. Mol. Biol. 104, 707.

44. Norvell, J.C.; Nunes, A.C.; Schoenborn, B.P. (1975) Science 190, 568.

45. Steigemann, W.; Weber, E.; (1979) J. Mol. Biol. 127, 309.

46. Padlan, E.A.; Love, W.E. (1975) J. Biol. Chem. 249, 4067.

47. Peng, S.M.; Ibers, J.A. (1976) J. Am. Chem. Soc. 98, 8032.

48. Hoard, J.L. (1975) in "Porphyrins and Metalloporphyrins", Smith, K.M. (ed.) Elsevier:New York, p. 351.

49. Moffatt, K.; Deatherage, J.F.; Seybert, D.W. (1979) Science 206, 1035.

50. Perutz, M.F. (1979) Ann. Rev. Biochem. 48, 327.

51. Caughey, W.S. (1970) Ann. N.Y. Acad. Sci. 174, 148.

52. Perutz, M.F. (1976) Br. Med. Bull. 32, 195.

53. Collman, J.P.; Brauman, J.I.; Halbert, T.R.; Suslick, K.S. (1976) Proc. Nat'l. Acad. Sci. USA 73, 333.

54. Collman, J.P.; Brauman, J.I.; Doxsee, K.M. (1979) Proc. Nat'l. Acad. Sci. USA 76, 6035.

55. Traylor, T.G.; Berzinis, A.P. (1980) Proc. Nat'l. Acad. Sci. USA 77, 3171.

56. Geibel, J.; Cannon, J.; Campbell, D.; Traylor, T.G. (1978) J. Am. Chem. Soc. 100, 3575.

57. Traylor, T.G.; Campbell, D.; Tsuchiya, S. (1979) J. Am. Chem. Soc. 101, 4748.

58. Battersby, A.R.; Hamilton, A.D. (1980) J. Chem. Soc., Chem. Commun., 117.

59. Collman, J.P.; Brauman, J.I.; Collins, T.J.; Iverson, B.; Sessler, J.L. (1981) J. Am. Chem. Soc. 102, 2450.

60. a. Traylor, T.G.; Michell, M.J.; Tsuchiya, S.; Campbell, D.H.; Stynes, D.V.; Koga, N. (1981) J. Am. Chem. Soc. 103, 5234; b. Collman, J.P.; Brauman, J.I.; Iverson, B.L.; Sessler, J.L.; Morris, R.M.; Gibson, Q.H. (1983) J. Am. Chem. Soc. 105, 3052.

61. Busch, D.H.; Zimmer, L.L.; Gryzbowski, J.J.; Olszanski, D.; Jackels, S.; Callahan, R.; Christoph, G.G. (1981) Proc. Nat'l. Acad. Sci. USA 78,

62. Copper(II) porphyrins do not coordinate any ligand and cannot be reduced to Cu(I) state; instead they reduce to Cu(II) porphyrin anion radicals below -1.4 V (SCE).

63. a. 5,6,7,8-Tetrahydroimidazo[1,5-a]pyridine was synthesized by hydrogenation of 2,3a-diazaindene (Bower, J.D.; Ramage, G.R. (1955) J. Chem. Soc., 2384); b. 1,5-Dicyclohexylimidazole was a generous gift from Professor T.G. Traylor.

64. However, we did observe a positive shift in 1' as a function of N-methylimidazole concentration for FeSP-13 and FeSP-14. At N-MeIm concentration ranging from 0.1-3.0 M, FeSP-13 had an 1' increase of about 200%. On the other hand, CuFe-4 had a corresponding shift of less than 20% (0.1-1.0 M). This indicates that with 1' less than about 10^4, equilibria on the proximal side (base-off[37]) present a somewhat serious problem. For this reason, any O_2 vs. CO comparisons for FeSP-13 and FeSP-14 are probably not reliable and therefore, are not discussed. With 1' greater than 2×10^4, proximal base equilibria should present little difficulty. Indeed, 1' of FeCu-5 or FeSP-15 is unaffected by base concentration.

65. Antonini, E.; Brunori, M. (1971) in "Hemoglobin and Myoglobin in Their Reactions with Ligands", North-Holland:Amsterdam, p. 219.

66. Traylor, T.G.; Stynes, D.V. (1980) J. Am. Chem. Soc. 102, 5938.

67. Seybert, D.W.: Moffat, K.: Gibson, Q.H.; Chang, C.K. (1977) J. Biol. Chem. 252 4225.

68. Traylor, T.G.; White, D.K.; Campbell, D.H.; Berzinis, A.P., J. Am. Chem. Soc., in press.

69. Hatada, M.H.; Tulinsky, A.; Chang, C.K. (1980) J. Am. Chem. Soc. 102, 7115.

70. Szabo, A., (1978) Proc. Nat'l. Acad. Sci. 75, 2108.

71. Ortho-substituted TPP's cannot be compared directly since kinetically they behave differently from nomal hemes or even unsubstituted TPP (Traylor, T.G. and Hambright, P.; private communication).

72. Traylor, T.G. (1981) Acc. Chem. Res. 14, 102.

73. a. Sono, M; Asakura, T. (1975) J. Biol. Chem. 250, 5227; b. Asakura, T.; Sono, M. (1974) J. Biol. Chem. 249, 7087; c. Mamoru, T,; Woodrow III, G.V.; Yonetani, T. (1973) Biochem. Biophys. Acta 317, 34; d. Antonini, T.; Brunori, M.; Caputo, A.; Chiancone, E.; Fanelli, A.R.; Wyman, J. (1964) Biochem. Biophys. Acta 79, 284; e. Seybert, D.W.; Moffat, K.; Gibson, Q.H. (1975) Biochem. Biophys. Res. Comm. 63, 43; f. Antonini, E; Gibson, Q.H. (1960) Biochem. J. 76, 534; g. Sono, M.; Smith, P.D.; McCray, J.A.; Asakura, T. (1976) J. Biol. Chem. 251, 1418.

74. Seybert, D.W.; Moffat, K.; Gibson, Q.H. (1976) J. Biol. Chem. 251, 45.

75. Iizuka, T.; Watanabe, K.; Makino, R.; Sakaguchi, K.; Mitani, F.; Isimura, Y.; Kawabe, K.; Yoshida, Z.; Ogoshi, H. (1982) "Oxygenases and Oxygen Metabolism", Academic Press:New York, pp. 445-450.

76. Jue, T.; Krishnamoorthi, R.; Lamar, G.N. (1983) J. Am. Chem. Soc. 105, 5701.

77. Wallace, W.J.; Houtchens, R.A.; Maxwell, J.C.; Caughey, W.S. (1982) J. Biol. Chem. 257, 4966 and references therein.

78. a. Yonetani, T.; Asakura, T. (1969) J. Biol. Chem. 244, 4580; b. Teale, F.W.J. (1959) Biochem. Biophys. Acta 35, 543.

79. a. Dinello, R.K.; Chang, C.K. (1978) "The Porphyrins" Dolphin, D. (ed.) Vol. 1, Academic Press:New York, p. 305; b. Chang, C.K. (1981) J. Org. Chem. 46, 4610.

80. Falk, J.E. (1964) "Porphyrins and Metalloporphyrins", Elsevier:New York, p. 28.

81. Perutz, M.F. (1980) Proc. R. Soc. London, Ser. B 208, 135.

82. Autsin, R.H.; Beeso, K.W.; Eisenstein, L.; Fraunfelder, H.; Gunsalus, I.E. (1975) Biochem. 14 5355.

83. Alberding, N.; Chan, S.S.; Eisenstein, L.; Fraunfelder, H.; Good, D.; Gunsalis, I.C.; Nordlund, T.M.; Perutz, M.F.; Reynolds, A.H.; Sorenson, L.R. (1978) Biochem. 17, 43.

84. Baldwin, J.M.; Chothia, C.J. (1979) J. Mol. Biol. 129, 175.

85. Doster, W.; Beece, D.; Bowne, S.F.; Dilorio, E.E.; Eisenstein, L.; Fraunfelder, H.; Reinisch, L.; Shyamsunder, E.; Winterhalter, K.H.; Yue, K.T. (1982) Biochem. 20, 4831.

86. Traylor, T.G.; Campbell, D.; Sharma, V.; Geibel, J. (1979) J. Am. Chem. Soc. 101, 5376.

87. Shaanan, B. (1982) Nature 296, 683.

88. Phillips, S.E.V.; Schoenborn, B.P. (1981) Nature 292, 81.

89. Young, R.; Chang, C.K., manuscript in preparation.

90. McClellan, A.L. "Tables of Experimental Dipole Moments", Rahara Enterprises:El Cerito, 1974.

t-Butyl	t-Butyl Benzene	0.51
3,5-CH_2OM3	MeOMe	1.35
	EtOEt	1.27
	$PhCH_2OCH_2Ph$	
3,5-CH_2OH	$PhCH_2OH$	1.67-1.73
3,5-CO_2Bu	$PhCO_2Et$	1.85-1.93
3,5-CONHBu	PhCONHEt	3.6
3,5-$CONEt_2$	$PhCONMe_2$	3.8-3.9
3,5-$CONiPr_2$	$PhCONMe_2$	

91. Dippy, J.F.J. (1939) Chem. Rev. 25, 151.

92. Glasstone, S.; Laidler, K.J.; Eyring, H. (1941) McGraw Hill:New York.

93. Hushimoto, T.; Basolo, F. (1981) Comments Inorg. Chem. 1, 199 and references therein.

94. a. Collman, J.P.; Gagne, R.R.; Reed, C.A.; Robinson, W.T.; Rooley, G.A. (1974) Proc. Nat'l. Acad. Sci. USA 71, 1326; b. Jamesson, G.B.: Rodley, G.A.; Robinson, W.T.; Gagne, R.R.; Reed, C.A.; Collman, J.P. (1978) Inorg. Chem. 17, 850.

95. Momenteau, M.; Lavalette, D.J. (1982) J. Chem. Soc., Chem. Commun., 341.

96. a. Collman, J.R.; Brauman, J.I.; Halbert, T.R.; Suslick, K.S. (1976) Proc. Nat'l. Acad. Sci. USA 73, 3333; b. Barlow, C.H.; Maxwell, J.C.; Wallace, W.J.; Caughey, W.S. (1973) Biochem. Biophys. Res. Commun. 55, 91; c. Maxwell, J.C.; Volpe, J.A.; Barlow, C.H.; Caughey, W.S. (1974) Biochem. Biophys. Res. Commun. (1974) 58, 166; d. Maxwell, J.C.; Caughey, W.S. (1974) Biochem.Biophys. Res. Commun. 60, 1309.

97. Pin, S.; Alpert, B.; Michalowicz, A. (1982) FEBS Lett. 147, 106.

98. Case, D.A.; Huynh, B.H.; Karplus, M.J. (1979) J. Am. Chem. Soc. 101, 4433.

99. Perutz, M.F. (1965) J. Mol. Biol. 13, 646.

100. Phillips, S.E.V. (1978) Nature 273, 247.

101. Moody, G.J.; Thomas, J.D.R. (1971) "Dipole Moments in Inorganic Chemistry", Edward Arnold:London.

102. Hayashi, Y.; Yamada, H.; Yamazaki, I. (1976) Biochem. Biophys. Acta 427, 608.

103. a. Collman, J.P.; Brauman, J.I.; Doxee, K.M. (1979) Proc. Nat'l. Acad. Sci. USA 76, 6035; b. Tucker, P.W.; Phillips, S.E.V.; Perutz, M.F.; Houtchens, R.; Caughey, W.S. (1978) Proc. Nat'l. Acad. Sci. USA 75, 1076; c. Wallace, W.J.; Volpe, J.A.; Maxwell, J.C.; Caughey, W.S.; Charache, S. (1976) Biochem. Biophys. Res. Commun. 68, 1739; d. Caughey, W.S. (1970) Ann. N.Y. Acad. Sci. 174, 148.

104. Ward, B.; Chang, C.K.; Hunt, K., manuscript in preparation.

105. Minkin, V.I.; Osipov, O.A.; Zhdanov, Y.A. (1970) "Dipole Moments in Organic Chemistry", translated by Hazzard, B.J., Plenum Press:New York, p. 119.

105. a. Katz, J.J.; Norris, J.R.; Shipman, L.L.; Thurnauer, M.C.; Wasielewski, M.R. (1978) Ann. Rev. Biophys. Bioengineer. 7, 393; b. Maggiora, G.M. (1979) Int. J. Quantum Chem. 16, 331; c. Sauer, K. (1979) Ann Rev. Phys. Chem. 30, 155.

107. a. Callahan, P.M.; Babcock, G.T. (1983) Biochem. 22, 452; b. Babcock, G.T.; Callahan, P.M. (1983) Biochem. 22, 2314.

108. a. Fajer, F.J.; Chang, C.K.; Wang, C.B.; Bergkamp, M.A.; Netzel, T.L. (1982) J. Phys. Chem. 86, 3754; b. Netzel, T.L.; Bergkamp, M.A.; Chang, C.K. (1982) J. Am. Chem. Soc. 104, 1952.

109. a. Wasielewski, M.R.; Norris, J.R.; Shipman, L.; Lin, C.-P.; Svec, W.A. (1981) Proc. Nat'l. Acad. Sci. USA 78, 2957; b. Davis, R.C.; Ditson, S.L.; Fentiman, A.F.; Pearlstein, R.M. (1981) J. Am. Chem. Soc. 103, 6823.

110. a. Ward, B.; Callahan, P.M.; Young, R.; Babcock, G.T.; Chang, C.K. (1983) J. Am. Chem. Soc. 105, 634; b. Pearlstein, R.M.; Ditson, S.L.; Davis, R.C.;

Tentiman, A.F. (1982) Biophys. J. 37, 112a; c. Maggiora, L.L.; Maggiora, G.M., J. Am. Chem. Soc., manuscript submitted.

111. a. Lewis, A.; Marcus, M.A.; Ehenberg, E.; Crespi, H. (1978) Proc. Nat'l. Acad. Sci. 75, 4642; b. Motto, M.G.; Sheves, M.; Tsujimoto, K.; Balogh-Nair, V.; Nakanishi, K. (1980) J. Am. Chem. Soc. 102, 7947.

112. Hanson, L.K.; Chang, C.K.; Ward, B.; Callahan, P.M.; Babcock, G.T.; Head, J.D., J. Am. Chem. Soc., manuscript submitted.

113. DiNello, R.K.; Chang, C.K. (1978) in "The Porphyrins" Dolphin, D. (ed.) Academic Press:New York, p. 305.

114. a. Chang, C.K.; Hatada, M.H.; Tulinsky, A. (1983) J. Chem. Soc. Perkin. Trans. II, 371; b. Chang, C.K., unpublished work.

115. March, J. (1968) in "Advanced Organic Chemistry: Reactions, Mechanisms and Structure", McGraw-Hill:New York, p. 667.

116. Abe, M.; Kitagawa, T.; Kyogoku, Y. (1978) J. Chem. Phys. 69, 4526.

117. Shelnutt, J.A. (1981) J. Chem. Phys. 74, 6644.

118. Callahan, P.M.; Babcock, G.T. (1981) Biochem. 20, 452.

119. The 3-4 cm^{-1} increases which are apparent in ν_2 and in ν_{10} upon formation of the protonated Schiff's base most likely arise from a slight porphyrin core contraction accompanying the protonation reaction.[14]

120. Aton, B.; Doukas, A.G.; Narva, D.; Callender, R.H.; Dinur, U.; Honig, B. (1980) Biophys. J. 29, 79.

121. Leonard, N.J.; Paukstelis, J.V. (1963) J. Chem. Soc. 28, 3021.

122. Felton, R.H.; Yu, N.-T. (1978) in "The Porphyrins", Dolphin, D. (ed.) Vol. 3, Part A, Academic Press:New York, p. 347.

123. a. O'Donnell, T.A. (1973) in "Comprehensive Inorganic Chemistry", Vol. 2, Trotman-Dickenson, A.F. (ed.), Pergamon Press:New York, p. 1042; b. Emeleus, H.F. (1969) in "The Chemistry of Fluorine and It's Compounds" Academic Press: New York, p. 33; c. The formation of $SBH^+HF_2^-$ is described by the two equilibria:

$$SB + HF \overset{K_1}{\rightleftharpoons} SBH^+ + F^-$$

$$HF + F^- \overset{K_2}{\rightleftharpoons} HF_2^-$$

In order that protonation yields SBH^+HF^- $K_2 > K_1$, resulting in an upper limit for SBH^+ pK_a of ca. 15, (assuming aqueous solution values). For SB4c a third equilibrium is introduced due to the presence of the 77-OH moiety, namely:

$$7\text{-}OH + F^- \overset{K_3}{\rightleftharpoons} 7\text{-}OHF^-$$

Due to coloumbic attraction between SBH^+ and F^- it does not seem unreasonable to expect that $K_3 > K_2$.

124. a. Babcock, G.T.; Callahan, P.M. (1983) Biochem. 22, 2314; b. Van Steelandt-Frentrup, J.; Salmeen, I.; Babcock, G.T. (1981) J. Am. Chem. Soc. 103, 5981; c. $\nu_{C=O}$ for α_s methyl cinnamaldehyde occurs at 1658 cm^{-1} ($CHCl_2$) (Ref.

125. a. Choi, S.; Lee, J.J.; Wei, J.H.; Spiro, T.G. (1983) J. Am. Chem. Soc. 105, 3692; b. Green, J.H.S.; Harrison, D.J. (1976) Spectro. Chemica Acta 32A, 1265.

126. $\nu_{C=C}$ of α,β unsaturated aldehydes ranges from from 1618-1695 cm^{-1} (ref. 127a).

127. a. Dolphin, D.; Wick, A. (1977) "Tabulation of Infrared Spectral Data", Wiley Interscience: New York, p. 37; b. ibid. p. 170.

128. By analogy with cinnamaldehyde where $\nu_{C=O}$ and $\nu_{C=C}$ occur at 1674 and 1622 cm^{-1} respectively. Monitoring n-butyl Schiff's base formation of cinnamaldehyde by IR absorption in CH_2Cl_2 (Fig. R-1) resulted in disappearance of ν_{CHO}

and $\nu_{C=C}$ with the concomitant appearance of a band at 1632 cm^{-1} (C=N) and a very weak band at 1614 cm^{-1} (C=C).

129. Felton, R.H. (1978) in "The Porphyrins", Dolphin, D. (ed.) Academic Press:New York, Vol. 1, p. 53.

130. a. Govindjee (ed.) (1978) "Bioenergetics of Photosynthesis", Academic Press:New York; b. Bearden, A.J.; Malkin, R. (1975) Quart. Rev. Biophysics 7, 131; c. Evans, M.C.; Shira, C.H.; Slibus, A.R. (1977) Biochem. J. 162, 75.

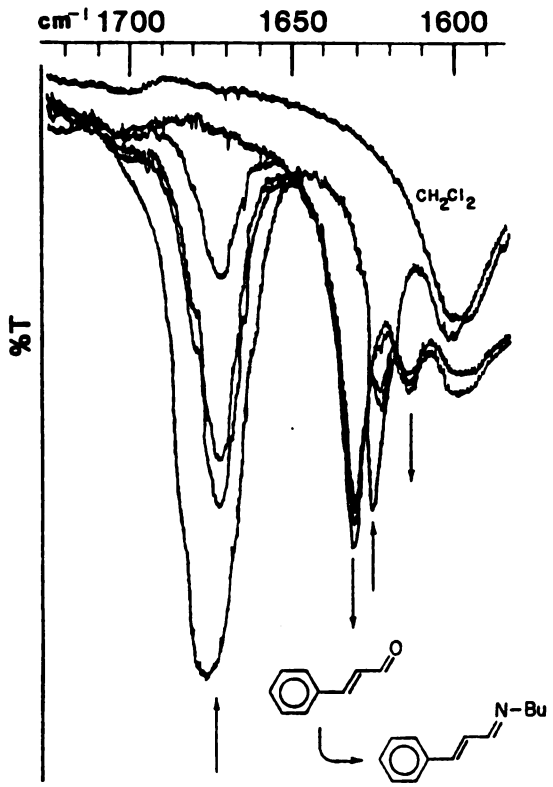

Figure R-1. Infrared spectra monitoring Schiff's base formation between cinnamaldehyde and n-butylamine in CH_2Cl_2. Arrows indicate spectral changes with time.